CHARACTERIZATION OF BASIC FUNCTIONS OF CULTURED HUMAN GASTRIC MYOFIBROBLASTS

Ph.D. THESIS

MATYAS CZEPAN M.D.

First Department of Medicine,
University of Szeged
Szeged, Hungary
2012

Table of contents

Articles related to the subject of the thesis 3
Abbreviations 4
I. Introduction 6
1. The role of myofibroblasts in the gastric apparatus 6
1.1 Physiology of myofibroblasts 6
1.2 The pathophysiological relevance of gastric myofibroblasts 6
2. Clinical aspects and importance of gastric cancer 8
2.1 Epidemiology, significance 8
2.2 Diagnosis and management of gastric cancer 9
II. Aims 10
III. Materials and methods 11
1. Humans involved in the study 11
2. Generation of cell cultures 11
3. Immunocytochemistry 12
4. Immunohistochemistry and morphology scoring 12
5. RT-PCR 13
6. Immunoblot analysis 14
7. Intracellular pH measurement and determination of buffering capacity 15
8. Migration and proliferation assays 16
9. Statistics 17
IV. Results 18
1. Morphology of the myofibroblasts 18
2. Myofibroblast cultures 19
3. Investigation of acid/base transporters with microfluorometry 20
3.1. Determination of the resting pH_i and buffering capacity of human gastric myofibroblasts (HGMs) 20
3.2 Exploring of the main acid /base transporters with different techniques 22
3.3 Effect of bioactive compounds on NHE activity 27
4. mRNA and protein expression of NHE1-3 29
5. Migration is stimulated by carbachol and IGF-II 31
6. IGF-II increases proliferation in an NHE1-dependent manner 32
V. Discussion 34
VI. Acknowledgements 38
VII. References 39

Articles related to the subject of the thesis

I.

Czepán M, Rakonczay Z Jr, Varró A, Steele I, Dimaline R, Lertkowit N, Lonovics J, Schnúr A, Biczó G, Geisz A, Lázár G, Simonka Z, Venglovecz V, Wittmann T, Hegyi P.

NHE1 activity contributes to migration and is necessary for proliferation of human gastric myofibroblasts.

Pflügers Archive – European Journal of Physiology. 2012 Mar;463(3):459-75. **IF: 4.463**

II.

Holmberg C, Quante M, Steele I, Kumar JD, Balabanova S, Duval C, **Czepán M**, Rakonczay Z Jr, Tiszlavicz L, Németh I, Lázár G, Simonka Z, Jenkins R, Hegyi P, Wang TC, Dockray GJ, Varró A.

Release of TGFβig-h3 by gastric myofibroblasts slows tumor growth and is decreased with cancer progression.

(Contribution: I hereby certify, that Mátyás Czepán in our work "Release of TGFβig-h3 by gastric myofibroblasts slows tumor growth and is decreased with cancer progression." established, isolated and maintained the myofibroblast cell lines we performed the experiments on. Besides, he greatly contributed to the patient data collection and to the follow-up of patients' survivals. His participation contributed to the acceptance of the article.

Prof. Dr. Andrea Varró, corresponding author)

Carcinogenesis. 2012 Aug;33(8):1553-62. **IF: 5.702**

Summarized impact factor: 10.165

Abbreviations

AE: anion exchanger;

ATM: adjacent tissue myofibroblast;

β_i: intrinsic buffering capacity; β_{total}: total buffering capacity; β_{HCO3^-}: buffering capacity in bicarbonate/carbon-dioxide containing solution

BCECF-AM: 2,7-biscarboxyethyl-5(6)-carboxyfluorescein-acetoxymethylester;

CAM: cancer associated myofibroblast;

DAPI: 4,6-diamidino-2-phenylindole;

DMEM: Dulbecco's Modified Eagle's Medium;

DMSO: dimethyl sulfoxide;

dNTP: deoxyribonucleotide-triphosphate;

EDTA: ethylenediamine tetra-acetic acid;

EdU: 5-ethynyl-2-deoxyuridine;

FITC: fluorescein isothiocyanate;

GAPDH: glyceraldehyde 3-phosphate dehydrogenase**;**

H_2DIDS: 4,4'-diisothiocyanatodihydrostilbene-2,2'-disulfonic acid;

HEPES: (4-(2-hydroxyethyl)-1-piperazine-ethanesulfonic acid;

HGM: human gastric myofibroblast;

HOE-642: 4-isopropyl-3-methylsulphonylbenzoyl-guanidin methanesulphonate, also known as cariporide;

IGFBP-5: insulin like growth factor binding protein 5;

IGF-II: insulin like growth factor II;

$J(B^-)$: base flux;

MMP: matrix metalloproteinase;

NBC: Na^+/HCO_3^- cotransporter;

NF-κB: nuclear factor kappa B;

NHE: Na^+/H^+ exchanger;

NTM: normal tissue myofibroblast;

PBS: phosphate buffered saline;

PP: proton pump;

RT: room temperature;

RT-PCR: reverse transcription polymerase chain reaction;

SMA: smooth-muscle actin.

Summary

Myofibroblasts play central roles in wound healing, deposition of the extracellular matrix and - via extensive neurohumoral communication - in the epithelial function and cancer development as well. Their functions depend on migration and proliferation within the subepithelial matrix, which results in boosted cellular metabolism. Upregulated metabolic pathways generate acidic metabolites which need to be excreted to maintain intracellular pH (pH_i). It has been reported that acid/base transporters have a great impact on cell function and they also may have specific contributions to cancer development. We isolated human gastric myofibroblasts (HGMs) from surgical specimens of 5 patients. Our data show that HGMs originating from gastric cancer are greatly increased in number, their morphology is distorted and the architecture is damaged compared to those originating from nomal tissue. Then we characterized **(**for the first time**)** the expression and functional activities of the Na^+/H^+ exchanger (NHE) isoforms 1, 2 and 3, and the functional activities of the Na^+/HCO_3^- cotransporter (NBC) and the anion exchanger (AE) in cultured HGMs using microfluorimetry, immunocytochemistry, RT-PCR and immunoblot analysis. We showed that NHE1-3, NBC and AE activities are present in HGMs and that NHE1 is the most active of the NHEs. In scratch wound assays we also demonstrated (using the selective NHE inhibitor HOE-642) that carbachol and IGF-II partly stimulate migration of HGMs in a NHE1-dependent manner. 5-ethynyl-2-deoxyuridine (EdU) incorporation assays revealed that IGF-II induces proliferation of HGMs, which is inhibited by HOE-642. The results indicate that NHE1 is necessary for IGF-II-induced proliferation of HGMs. Overall, we have characterized the pH_i regulatory mechanisms of HGMs. In addition, we demonstrated that NHE1 activity contributes to both IGF-II- and carbachol-stimulated migration and that it is obligatory for IGF-II-induced proliferation of HGMs.

I. Introduction

1. The role of myofibroblasts in the gastric apparatus

1.1 Physiology of myofibroblasts

Myofibroblasts, also known as activated fibroblasts, are dynamic, spindle-like cells sharing the functional characteristics of both fibrocytes and smooth muscle cells [27]. They are localized subepithelially in the lamina propria mucosae, where a 3D, mesh-like network is constructed from them. They secrete a broad spectrum of cytokines and extracellular matrix molecules during morphogenesis which contributes to the colonization of epithelial cells and proper polarization of the epithelial linage. After embryonic stage, they remain in the supepithelium and most of them transform back into normal resident connective tissue fibrocytes. When epithelial lesions occur, bioactive compounds from the wounded endothelial cells release macrophages which transform resident fibrocytes into activated fibroblasts or myofibroblasts. Most commonly the transforming factor is transforming growth factor beta-1 (TGF-β1) [2]. Myofibroblasts express alpha smooth muscle actin (α-SMA) and vimentin, which are specific histhopathological markers of these cells and are capable of secreting collagen types I-III. Recent studies have shown that local or bone-marrow derived mesenchymal stem cells can also transform into myfibroblasts in the granulation stage of tissue repair [38]. Myofibroblasts may also originate from epithelial-mesencyhmal transition. These cells actively migrate, proliferate, synthesize and deposit the extracellular matrix components in the wound. They establish the optimal micro-enviroment for other cells to populate the newly generated tissue. During remodelling, they secrete matrix metalloproteinases and their inhibitors and in resolution phase of healing they disappear by apoptosis or transform back into connective tissue fibroblasts or stem cells which can reside or move back to their home place.

1.2 The pathophysiological relevance of gastric myofibroblasts

Myofibroblasts are sparse in healthy tissue but are abundant in wounded tissue. As the inflammatory response advances in wounded tissue, different mixtures of bioactive compounds (such as growth factors, cytokines, chemokines and cyclo-

oxygenase products) are released by the injured mucosa, endothelial cells and even by the fibroblasts. This causes a regulatory cascade and transformation of the fibrocytes as it has been discussed above. Under pathophysiological conditions such as in case of a permanent noxa, the normal remodelling process is damaged. Chronic gastritis due to *Helicobacter pylori* infection has been extensively studied in recent decades and the connection between the pathogen and gastric cancer is now proven. Most investigations focused their research on epithelial cells and little is known about the connective tissue cells in tumors, though they are important in tumor expansion [45]. In gastric cancer the tumor stroma can make up to 80% of the whole tumor mass and the dominating cell type within are fibroblasts. Myofibroblasts take part in the chronic inflammation-adenoma-carcinoma sequence by altering the microenvironment around epithelial cells [9, 17, 31]. In case of *Helicobacter pylori* gastritis, gastric epithelial cells secrete matrix metalloproteinase-7 which cleaves myofibroblast-produced insulin-like growth factor binding protein-5 (IGFBP-5) thereby releasing insulin-like growth factor-II (IGF-II). IGF-II acts as a potent stimulant of both epithelial and myofibroblast proliferation, thus increasing the mass of the lesion [40]. If the inflammation resides long in the mucosa, there is a high risk of failure in DNA-repairing mechanisms and thereby the chance for metaplasia and dysplasia elevates. It seems that stromal cells are in permanent and complex communication with epithelial cells via the released bioactive agents. This communication generates an auto-activator mechanism that must be interrupted in order to succesfully treat the lesion.

In the tumor, the boosted metabolic pathways generate lots of acidic metabolites which are exported from the cells via various plasma membrane transporters (Na^+/H^+ exchangers, Na^+/HCO_3^- cotransporters, anion exchangers, proton pumps, etc.). As upregulated ion transporters excrete the excess protons from the cells, the cytoplasm becomes more alkaline, while the environment becomes more acidic. In recent years this phenomenon became a hallmark of cancer and provided the researchers a new, thermodynamic approach to cancer research. The reversed proton gradient may underlie the initiation and progression of the neoplastic process, which gives us new oppurtunities and new targets in cancer treatment [22]. Many authors have investigated the regulation of acid/base transporters and their role in migration and proliferation [41, 53]. Generally, they found that certain transporters are implicated in upregulated migration and proliferation, which highlights the importance of the above discussed proton gradient and the participating transporters. Acid/base transporters are well

characterized in gastric epithelial cells, but there is scarce information about the transporters of gastric myofibroblasts which sourround the malignant cells.

The alterations in the epithelial microenvironment in the evolution of cancer are poorly understood, yet they are of great importance [15]. Data indicate that myofibroblasts may be the pioneer cells at the site of distant invasion, called niche, thus aiding malignant cells in forming metastases [8]. Cancer-associated myofibroblasts (CAMs), a sub-class of myofibroblasts, are important stromal cells with distinct properties [3] and recent work indicates that differences in gene expression in the stromal compartment predict clinical outcome and response to therapy [18]. The changes on epigenetic level have also been detected in CAMs from gastric cancer compared with myofibroblasts derived from normal tissue myofibroblasts [30]. We also know that TGF-β1 levels in the tumor mass and myofibroblast numbers correlate with worse survival of gastric cancer [25].

2. Clinical aspects and importance of gastric cancer

2.1 Epidemiology, significance

Gastric cancer was first described in 3000 BC in hieroglyphic inscriptions and papyri from ancient Egypt. The first major statistical analysis of cancer incidence and mortality are from the mid 18th century, Verona showed that gastric cancer was the most common and lethal cancer in that era [57]. Gastric cancer is the second most common cause of cancer death after lung cancer and the fourth most common cancer in the world according to data collected by the World Health Organization (2003). Its death rate is approximately 800.000 per year worldwide and almost one million new cases show up yearly, accounting for about 8 % of new cancers [28]. Its incidence culminates in men around the age of 40. The male dominance (3 men to 1 woman) of the disease highlights a possible protective role of oestrogen. Gastric cancer is very frequent in developing countries, Japan, Korea, Chile, Finland and Iceland. Its ethnic distribution is known, it is more common in non-white races in the United States. Fortunately, the worldwide incidence of gastric cancer has dropped in the past few decades mainly due to the recognition of risk factors such as *Helicobacter pylori* and environmental factors. It is also noteworthy, that during the past few decades, it occurs in the younger and in the

older age groups more frequently, this may be caused by unknown new environmental factors related to industrial development [29].

Helicobacter pylori infection, particularly in coagulase-A positive cases, is proven to be the cause of most gastric cancers [24]. Some other risk factors are autoimmune atrophic gastritis, various genetic factors and dietary habits. Smoked foods, salted fish and meat, pickled vegetables, nitrates and nitrites in cured meats also increase the risk of developing gastric cancer. Protective factors include eating fresh fruits and vegetables that contain antioxidants and it is also known that gastric cancer is less common amongst people on a mediterranean diet [10].

An important and preventable cause of gastric cancer is smoking. It considerably increases the risk of developing gastric cancer; from 40% increased risk for current smokers to 82% increase for heavy smokers [4]. In smokers, gastric cancer develops more frequently in the upper part of stomach near the esophago-gastric junction. Excessive, regular alcohol consumption, which is also a risk factor, along with tobacco smoking increases the risk of developing other cancers as well [4]. A rare form of gastric cancer is the hereditary diffuse gastric cancer, in which the genetic factors are under investigation [4].

2.2 Diagnosis and management of gastric cancer

Unfortunately, stomach cancer is often asymptomatic in its early stages or it causes only non-specific symptoms like indigestion, loss of appetite, disgust of meat, abdominal discomfort, fatigue, bloating or weakness. These sings are commonly belittled by the patients, who often seek for medical attention only when more severe symptoms at the late stage occur as pain, nausea, vomiting, weight loss, dysphagia or black stool. At this stage gastric cancer is commonly untreatable.

Correct diagnosis is based on proper medical history, physical examination, laboratory tests (with tumor markers if possible), faecal occult blood test and imaging (endoscopy, endoscopic ultrasound, barium meal, computed tomography, positron emission tomography or even laparoscopy). Pre-requisite for early diagnosis is total upper gastrointestinal endoscopy, where not only the lesion can be visualised, but multiple biopsies can also be taken for accurate histological and immuno-histochemical assessment, which is crucial for adequate therapy. For clinical staging tomography is generally obligatory. Histologically, stomach cancer is overwhelmingly adenocarcinoma with approximately 90 % frequency [34]. It rarely originates from the mucosa

associated lymphoid tissue, called "MALToma" or neuro-endocrine carcinoid. In Hungary, we often use the Lauren histological classification, by which histology is classified as intestinal, diffuse or mixed type. The diffuse type is generally more aggressive, quickly invading the surrounding tissue and forming early lymphogen and haematogen metastases. A rare form of the disease is the linitis plastica, also known as morbus Brinton, which hardens the gastric wall throughout the whole organ. When mucus is retained in the cells, a cytoplasmically peripheral nucleus can be seen making signet-ring cells; this type of carcinoma is associated with very poor average survival.

Endoscopic mucosal resection or submucosal dissection is first to be chosen to remove early gastric cancer (clinical stage 0), when cancer cells are limited to the mucosa (carcinoma *in situ*). In any other cases (clinical stage I-IV) multimodality therapy must be chosen. Stage I gastric cancer, when malignant cells are limited to the stomach or 1 or 2 lymph nodes near the stomach wall, is resected (partial gastrectomy) with security zone and omental resection. Chemotherapy (often 5-fluorouracil or cisplatin, epirubicin, etoposide, oxaliplatin, capecitabine, irinotecan) may follow the stage I-II-III surgery [4]. In stage II, where cancer cells penetrate the gastric wall to the serosa and often reach a few lymph nodes, neoadjuvant radio/chemotherapy is combined with surgery showing good results. Stage III stomach cancer spreads to the neighbouring tissues, organs and distant lymph nodes; it is roughly treated like stage II but often there is no cure. Stage IV gastric cancer metastatizes to distant organs and parts of the body and often leaves opportunity only for palliative care. Antibodies against receptor tyrosine kinases were used to treat epidermal cancers and a few years ago their possible benefit in gastric cancer arose [6]. Recently a monoclonal antibody (trastuzumab) that interferes with the human epidermal growth factor receptor 2 was approved in Hungary for adenocarcinoma or gastroesophageal junction carcinoma in patients who have not been treated for metastatic cancer. It has been shown that not only the tumor cells but the bulging tumor stroma can also be targeted to suppress tumor growth [8]. However, these therapeutic efforts are far from human application.

II. Aims

Our primary objective was to characterize the acid/base transporters of cultured human gastric myofibroblasts and to search for a connection to cell function.

III. Materials and methods

1. Humans involved in the study

The study was approved by the Ethics Committee of the University of Szeged, Hungary (study number 12/2006). All patients gave infomed consent. Tissue specimens were collected intra-operatively from patients who underwent gastric tumor resection in the Department of Surgery, University of Szeged, Hungary. Samples were obtained at least 3-4 cm away from the tumor from macroscopically healthy antrum/corpus tissue and were transported immediately to the laboratory in ice-cold transport media for culturing. Two other specimens from multiple organ cadaver donors were obtained similarly. Patients details are found in *Table 1*.

Patient No.	Gender	Age	Diagnosis
1	female	71	gastric cancer
2	male	76	gastric cancer
3	male	66	gastric cancer
4	female	42	subarachnoidal haemorrhage
5	male	49	traumatic head-injury

Table 1. Patients' details

2. Generation of cell cultures

The specimens were washed and chopped into very small pieces and were then bathed in a shaking water bath at 37 °C for 15 min with 1mM dithiothreitol. After washing, the specimens were incubated for 30 min at 37 °C with 1mM ethylenediamine tetra-acetic acid (EDTA) four times. Specimens were cultured for 1-2 weeks in Roswell Park Memorial Institute (RPMI) medium supplemented with 10 % fetal bovine serum, 1 % penicillin-streptomycin and 2 % antibiotic-antimycotic solution. After the cells became confluent, they were trypsinized with 0.25 % trypsin-EDTA and were transferred into Dulbecco's Modified Eagle's Medium (DMEM) with 4mM L-glutamine containing 10 % fetal bovine serum, 1 % amino acid solution, 1 % penicillin-streptomycin and 2 % antibiotic-antimycotic solution. The medium was replaced every

48 h and the cells were passaged after reaching confluency up to passage 10. Cell cultures were incubated at 37 °C in a mixture of 5 % CO_2 and 95 % air. Cells were used between passages 3 and 10. All reagents for cell culture were purchased from Sigma Aldrich (Budapest, Hungary).

3. Immunocytochemistry

Myofibroblasts were seeded onto chamber slides and were allowed to adhere overnight. Cells were fixed using 4 % paraformaldehyde for 30 min and were washed twice with phosphate buffered saline (PBS, Invitrogen, Paisley, UK). Permeabilization was performed by incubation with a filtered, PBS-based solution containing 0.2 % Triton X-100 and 0.3 % protease-free bovine serum albumin for 30 min. Cells were then incubated with 10 % donkey serum in PBS for 30 min. After washing twice with PBS, primary antibodies were added to the chambers and the slides were incubated in moist atmosphere at 4 °C, overnight. The following primary antibodies were used: anti-α-SMA antibody raised in guinea pig (1:400), anti-vimentin antibody raised in mouse (1:400), anti-cytokeratin antibody raised in mouse (1:400), anti-desmin antibody raised in mouse (1:400, all four antibodies from Dako, Denmark), anti-NHE1, -NHE2, -NHE3 antibodies raised in goat (1:50, purchased from Santa Cruz Biotechnology, Santa Cruz, CA, USA). Primary antibodies were removed by a sequence of washes for 10 min each with 0.14 M NaCl, 0.5 M NaCl, 0.14 M NaCl dissolved in PBS. Slides were then incubated with secondary antibodies for 60 min in dark and moist conditions. The following secondary antibodies were used: fluorescein isothiocyanate (FITC)-conjugated anti-guinea pig secondary antibody [1:400, diluted in 10 mM 4-(2-hydroxyethyl)-1-piperazine-ethanesulfonic acid (HEPES), pH 7.5], Texas Red- or FITC-conjugated anti-mouse antibody (1:400), FITC-conjugated anti-goat secondary antibody (1:400). After hybridization, slides were washed three times with PBS and were covered with 4,6-diamidino-2-phenylindole (DAPI) containing Vectashield mounting medium (Vector Laboratories, Peterborough, UK), then cover-slipped.

4. Immunohistochemistry and morphology scoring

Resection specimens consecutively evaluated in the Department of Histopathology of the University of Szeged were routinely processed from formalin into

paraffin, sectioned at 4 um, stained with hematoxylin/eosin (HE), Giemsa technique, and periodic acid – Schiff technique/Alcian blue and immunostained for α-smooth-muscle actin (α-SMA), vimentin and desmin (LabVision, Fremont, CA). Antigen retrieval, tissue processing, and visualisation were conducted according to the manufacturers' instructions. For visualisation, high-affinity polymer (Envision; Dako) was used for 30 min. Sections were counterstained with hematoxylin. Myofibroblasts in normal and tumor samples were analysed semiquantitatively according to myofibroblast morphology (0 - normal, 1 - mildly distorted, 2 - severely distorted), architecture (0 – only in periglandular /subepithelial localization, 1 - not only in periglandular/subepithelial localisation, but in the interstitium elsewhere, 2 – severe architectural damage with meshwork-like myofibroblast appearance), and number (0 – normal, 1 – mildly increased, 2 – strongly increased). For the histopathological assessment, myofibroblasts were defined as stellate/spindle-shaped cells with consistent α-smooth-muscle actin α-SMA/vimentin co-expresssion. Smooth muscle fibers were excluded based on their characteristic morphology. Complementary desmin immunostainings were performed to distinguish smooth muscle cells from myofibroblasts in uncertain cases. Desmin immunostain exhibited pronounced expression in smooth muscle fibers but not in the myofibroblasts (results not shown).

5. RT-PCR

RNA was isolated from myofibroblast cultures using a Qiagen RNEasy Mini Kit (Qiagen House, Crawly, UK) according to the manufacturer's instructions; human kidney RNA was isolated from whole tissue from cadaver specimens utilizing TRIzol reagent. RNA was reverse transcribed to cDNA and RNA/primer annealing was performed with 0.5 µg oligo-dT primer at 65 °C for 5 min. After cooling, samples were reverse transcribed in a final reaction volume of 30 µl containing the annealed RNA/primer set, 5x AMV (avian myeloblastosis virus) buffer, 1.25 mM dNTP (deoxyribonucleotide-triphosphates) mix, 20 unit RNAse inhibitor and 15 unit AMV-RT (AMV-reverse transcriptase). Reactions were incubated at 42 °C for 1 h; enzymes were inactivated at 85 °C for 5 min. 1 µl of cDNA was used as template for each polymerase chain reaction (PCR) in a final volume of 25 µl, containing 10x master mix Taq-buffer, 10 nM dNTPs, 2.5 unit Taq-polymerase, and 1 µM NHE primer sets. The sequence of NHE primers are given in Table 3. PCR settings were as follows: denaturation at 95 °C

for 15 s, annealing at 60 °C for 15 s, extension at 72 °C for 45 s, 30 cycles. PCR products and DNA HyperLadderPlus (BioLine, Taunton, USA) were run on a 0.8 % agarose gel containing 0.005 % ethidium-bromide in Tris-buffered EDTA solution at 80V, then the gel was illuminated in a BioRad UV (ultraviolet) chamber and photographs were taken.

6. Immunoblot analysis

Protein extracts of myofibroblasts were prepared in RIPA (Radio-Immuno Precipitation Assay) buffer containing protease and phosphatase inhibitors and proteins resolved by sodium dodecyl sulphate – polyacrylamide gel electrophoresis) and processed for Western blotting as described previously [26]. Briefly, confluent cells were washed with PBS after removing the media and were then incubated with 100 mM EDTA for 15 min. After centrifugation (500 g, 8 min), the supernatant was gently removed and cells were lysed with radio-immuno precipitation assay (RIPA) buffer supplemented with 1% protease inhibitor cocktail (Calbiochem-Merck Chemicals, Darmstadt, Germany). Samples were vortexed and frozen in liquid nitrogen for a few seconds then centrifuged at 11,000 g for 10 min at 4 °C. The protein concentrations of supernatants containing whole cell protein lysates were determined by using Bradford's reagent. Samples were heat treated at 30 °C for 30 min and 100 μg protein was electrophoresed on 8% sodium dodecylsulfate-polyacrylamide gels according to the method of Laemmli using a Hoefer Mighty Small II instrument (Harvard Bioscience Inc., Massachusetts, USA). After separation, proteins were blotted to matching-sized nitrocellulose membrane for 60 min at 100 V. Membranes were blocked in 5% nonfat dry milk for 1 h, and were incubated with primary antibodies (1:100 for NHE) overnight at 4 °C on a rocker. The same NHE primary antibodies were used as for immunocytochemistry. Primary antibodies were removed by washing with Tris-Buffered Saline and Tween 20 (TBST) for 3x10 min. HRP-conjugated secondary antibodies (Dako, Denmark) were applied for 60 min at RT on a rocker. After 3x10 min TBST wash, the immunoreactive protein was visualized by enhanced chemiluminescence. Remaining antibodies were removed by washing with TBST, then anti-GAPDH (glyceraldehyde 3-phosphate dehydrogenase) antibody (Dako, Denmark) was added to the membrane for 60 min at RT. Secondary antibody (1:10,000) was also applied for 60 min at RT then signals were recorded as described earlier.

7. Intracellular pH measurement and determination of buffering capacity

All components were purchased from Sigma Aldrich (Budapest, Hunagry). Myofibrobalsts were seeded onto 24 mm diameter round glass coverslips in full media. They were allowed to recover for 24 h before experiments. Coverslips were then transferred into a perfusion chamber and mounted on an inverted microscope (Olympus, Budapest, Hungary). Cells were bathed in standard HEPES solution at 37 °C and were loaded with pH-sensitive fluorescent dye BCECF-AM (2 μM, Invitrogen, Paisley, UK) for 20 to 30 min. Thereafter, myofibroblasts were continuously perfused with solutions at a rate of 5 to 6 mL/min and pH_i was measured by using an imaging system (CellR; Olympus, Budapest, Hungary). Cells were excited at wavelengths of 490 nm and 440 nm, and the 490/440 fluorescence emission ratio was measured at 535 nm. One pH_i measurement was recorded per s. *In situ* calibration of the fluorescence signal was performed using the high K^+-nigericin technique as previously described [54]. Briefly, the pH of high K^+-HEPES solution supplemented with 10 μM nigericin was set to 6.8 or 7.4 at 37 °C, then cells loaded with BCECF and were superfused by these solutions and the 490/440 fluorescence ratio was recorded. Multiple-point calibrations, i.e. sequential pH measurements (with high K^+-HEPES-nigericin solutions ranging pH from 6.2 by 0.4 step to 8.2) were performed to confirm data accuracy. Linear projections were made from the steady-state fluorescence pH data during high K^+-HEPES-nigericin superfusion. Adaptation of projections to the resting fluorescence data of unknown pH_i in standard HEPES solution results in accurate resting pH_i. In order to characterize the acid/base transporters, we used ion-withdrawal technique, and ammonium pulse technique in HEPES- and HCO_3^-/CO_2-buffered solutions. Initial rates (first 30-60 s) of recovery from acidosis were calculated by linear regression. The intrinsic buffering capacity (β_i) of the cells was estimated by the NH_4^+ pre-pulse technique [52]. β_i refers to the ability of intrinsic cellular components (excluding the bicarbonate buffer system) to buffer changes of pH_i. Briefly, cells were exposed to various concentrations of NH_4Cl while Na^+ and HCO_3^- were omitted from the solution to block the Na^+-dependent pH regulatory mechanisms. β_i was estimated by the Henderson-Hasselbalch equation. The total buffering capacity (β_{total}) was calculated as $\beta_{total} = \beta_i + \beta_{HCO_3^-} = \beta_i + 2.3 \times [HCO_3^-]_i$, where $\beta_{HCO_3^-}$ is the buffering capacity of the HCO_3^-/CO_2 system and $[HCO_3]_i$ is the intracellular concentration of HCO_3^-. Transmembrane base flux [$J(B^-)$] was calculated

by using the equation $J(B^-)$ = dpH/dt x β_{total}. The β_{total} value used in the calculation of $J(B^-)$ was obtained from *Figure 3* by using the pH_i value at the start of the 30-s period over which dpH/dt was measured. Composition of solutions is found in *Table 2*.

	HEPES	HCO_3^-	NH_4Cl HEPES	NH_4Cl HCO_3^-	Cl^--free HEPES	Cl^--free HCO_3^-	Cl^--free NH_4Cl/ HEPES	Cl^--free NH_4Cl/ HCO_3^-	Na^+-free HEPES	Na^+-free HCO_3^-	Na^+-free NH_4Cl/ HEPES	Na^+-free NH_4Cl/ HCO_3^-	High K^+ HEPES
NaCl	130	115	110	95									5
KCl	5	5	5	5					5	5	5	5	130
Na-HEPES	10	25	10										10
$CaCl_2$	1	1	1	1					1	1	1	1	1
$MgCl_2$	1	1	1	1					1	1	1	1	1
Glucose	10	10	10	10	10	10	10	10	10	10	10	10	10
NH_4Cl			20	20							20	20	
$NaHCO_3$						25		25					
HEPES					10		10		10		10		
Na-gluconate					140	115	120	95					
K_2-sulfate					2.5	2.5	2.5	2.5					
Ca-gluconate					6	6	6	6					
Mg-gluconate					1	1	1	1					
NH_4-sulfate						20		20					
NMDG									140	115	120	95	
Atropine										0.01	0.01	0.01	
Choline-HCO_3										25	25	25	

Table 2. Composition of solutions
Values are concentrations in mM.

8. Migration and proliferation assays

Scratch wound assays were performed to monitor migration as described previously [44]. Briefly, cells were seeded onto six-well plates and were allowed to adhere overnight in full media. On the following day, the confluent monolayer was gently scratched using a P2 tip. Only the wells containing even-sided and sharp-edged wounds were used for experiments. After gentle washing for three times with serum-free media, wounds were measured and photographed under inverted light microscope. Reagents were then added to the wells in serum-free media in all experiments, and plates were incubated in a CO_2 incubator at 37 °C for 24 h. Migration was evaluated by counting the cells in the same area of the wound after 12 and 24 h.

For the proliferation assay myofibroblasts were seeded onto cover glasses. After overnight recovery, cells were synchronized by incubation for 30 h in serum-free media. Thereafter, 10 μM 5-ethynyl-2-deoxyuridine (EdU; Alexa Fluor 488 Imaging Kit, Invitrogen, Oregon, USA) was added to the cells for overnight incubation with or without treatment. After incubation, the manufacturer's protocol was applied to fix and permeabilize the cells and to detect EdU incorporation. We used DAPI to detect nuclear

staining. The proliferation rate was calculated by normalizing the number of EdU positive cells to the DAPI-stained cells in 10 fields at 20x magnification.

9. Statistics

Results are expressed as mean ± standard error of the mean (SEM), unless stated otherwise. Student's t-test or ANOVA, with post hoc testing, was used as appropriate to determine statistical significance of results. Results were considered significant at $p<0.05$.

IV. Results

1. Morphology of the myofibroblasts

We histologically processed the same gastric samples from which we took our specimens to investigate myofibroblast morphology. We showed increased number of myofibroblasts, disordered cell morphology and damaged cyto-architecture in the samples from gastric cancer compared to the normal tissue (*Figure 1*).

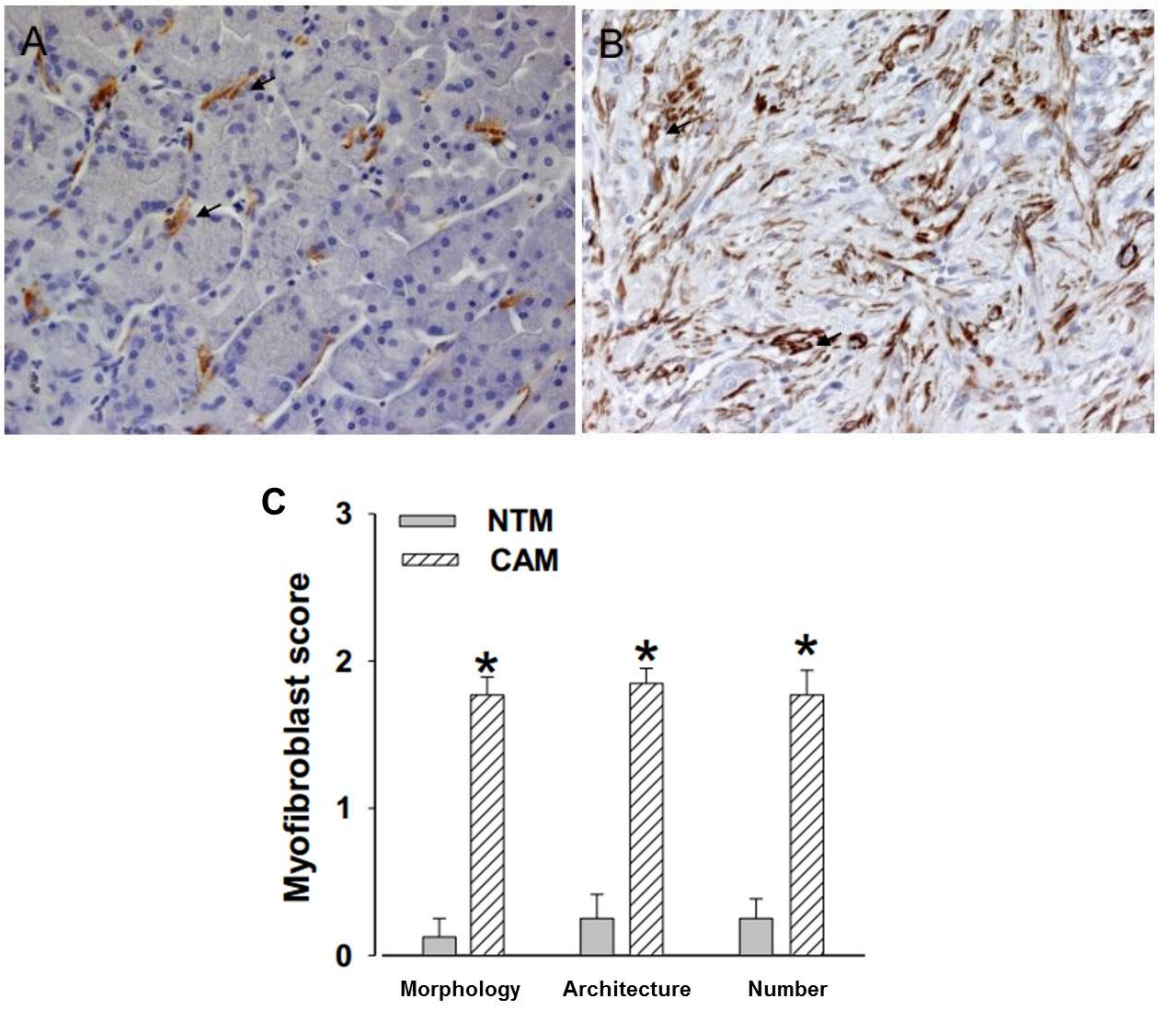

*Figure 1. Increased number and disordered myofibroblast morphology in human gastric cancer specimen. A) Immunohistochemical localization of α-SMA in normal tissue. B) Increased numbers and disordered myofibroblasts were seen in a gastric tumor. C) Quantification of myofibroblast morphology, architecture and number in cancer and normal tissue, * $p<0.05$, $n=5$ (modified from Holmberg C. et al., with permission).*

2. Myofibroblast cultures

In order to monitor purity of our cell cultures, we stained the cells for myofibroblast and epithelial cell markers. Cells showed positive staining for α-SMA and vimentin but not for cytokeratin and desmin, which are characteristics of myofibroblasts (*Figure 2*). The purity of myofibroblast cell cultures was ~100 %. As positive controls for cytokeratin and desmin antibodies, we used CAPAN-1 (human pancreas adenocarcinoma cell line) cells and cultured human high grade pancreatic neuroendocrine carcinoma cells, respectively. In both cases of desmin and cytokeratin stanings, appropriate localization was demonstrated (*Figure 2*).

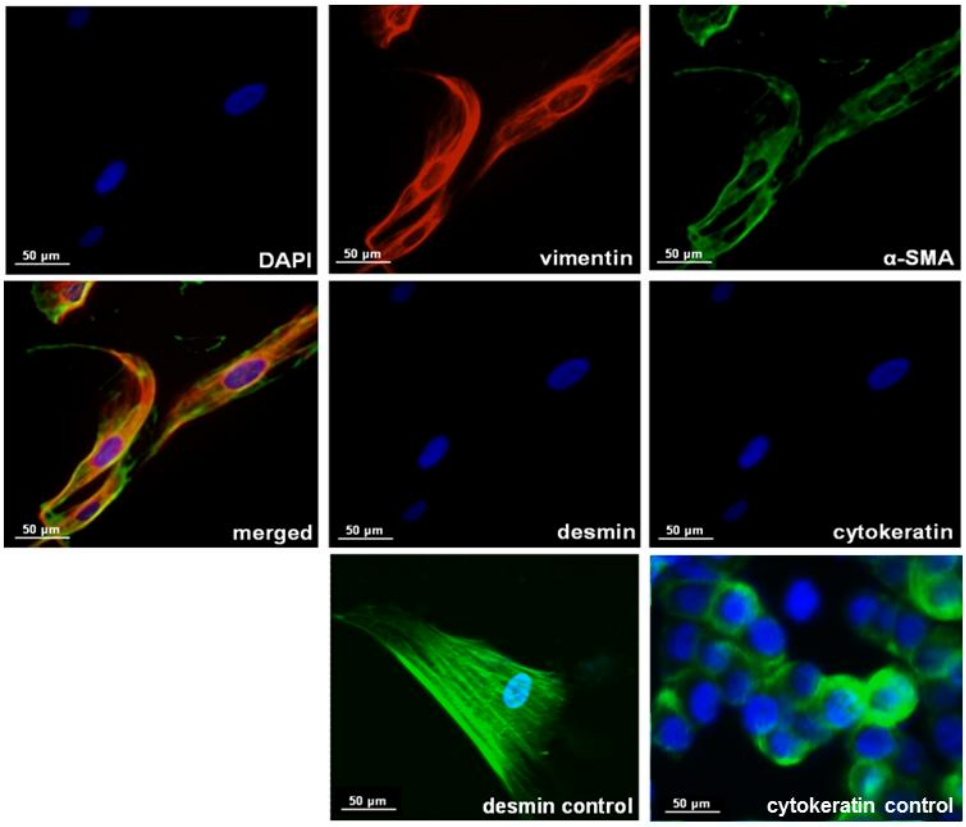

Figure 2. Cells isolated from human gastric samples were grown on chamber slides and were subjected to immunocytochemical analysis of vimentin and α-smooth-muscle actin (α-SMA) expression as specific markers of myofibroblasts. Cytokeratin and desmin antibodies were used for detecting epithelial and muscle cells respectively. Nuclei were counterstained with DAPI (blue). Vimentin (red) and α-SMA (green) verified the presence of myofibroblasts, whereas no epithelial or smooth muscle cells were detected (n=5). Control stainings were performed to test the desmin and cytokeratin antibodies. Cultured cancer cells (from human high grade pancreatic neuroendocrine carcinoma) were used as positive control (n=1) for desmin (green staining). To test the cytokeratin antibody, control staining (n=1) was performed on CAPAN-1 human pancreatic adenocarcinoma cell line. Green staining shows cytokeratin, blue staining shows DAPI.

3. Investigation of acid/base transporters with microfluorometry

First we compared the functional measurements of acid/base transporters from cancer associated myofibroblasts (CAM) and normal myofibroblasts and we set out to explore possible functional differences. During the pilot microflurometric experiments, CAMs exhibited properties that made them very difficult to handle technically. Due to uninformative or technically failed experiments, there were lots of repeats with very low cost-effectiveness. Moreover, when evalutaing the primary results, we experienced that the CAM dataset was highly variable and no conlcusion can be drawn from it. Therefore, after multiple consultations within our research group, we decided to let go of the opportunity of comparison in fluorometric measurements and continue the study with the acid/base characterization of normal myofibroblasts. In these experiments, we defined them as human gastric myofibroblasts or HGMs (N numbers are given as follows: n=number of patients/number of independent experiments per patient).

3.1. Determination of the resting pH_i and buffering capacity of human gastric myofibroblasts (HGMs)

The multiple-point calibration technique utilizing high K^+-HEPES/nigericin solution was used to determine the resting pH_i of HGMs. Representative pictures of the design of microflurometric experiments, thermal coloured image and measurement curves are shown on *Figure 3*. Our experiments showed that the resting pH_i of HGMs in standard HEPES solution was 7.09 ± 0.02 (*Figure 3*).

A

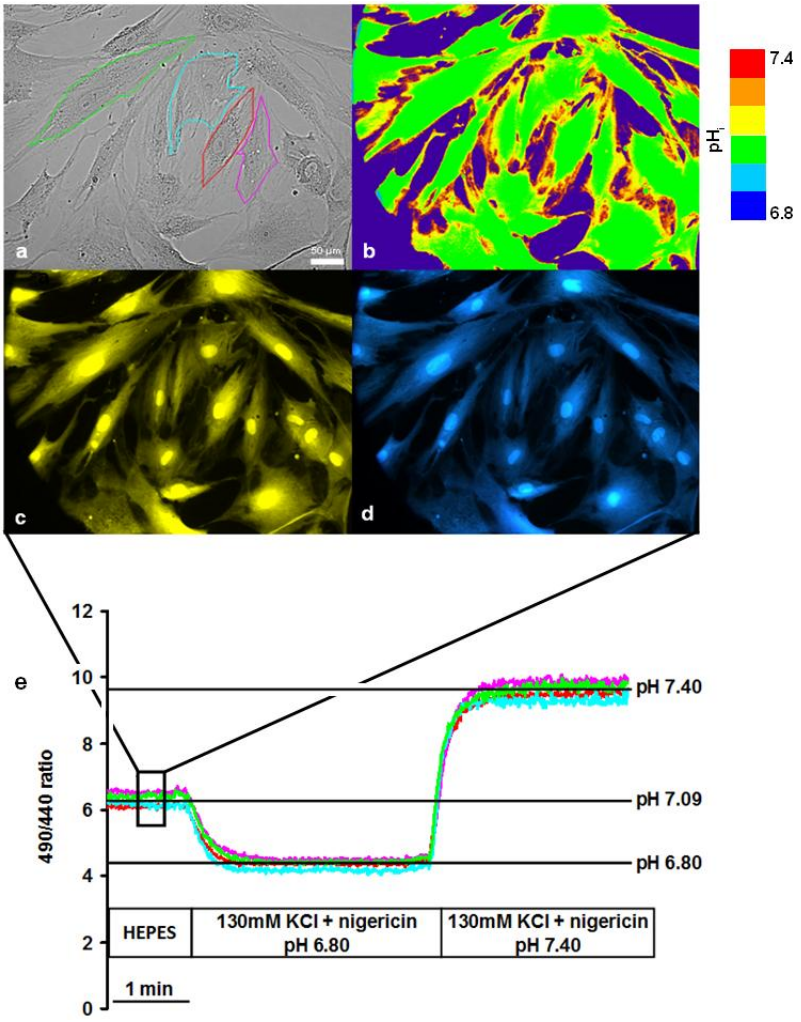
a
b
c
d
e
50 µm
7.4
6.8
pH$_i$
12
10
8
6
4
2
0
490/440 ratio
pH 7.40
pH 7.09
pH 6.80
HEPES
130mM KCl + nigericin
pH 6.80
130mM KCl + nigericin
pH 7.40
1 min

B

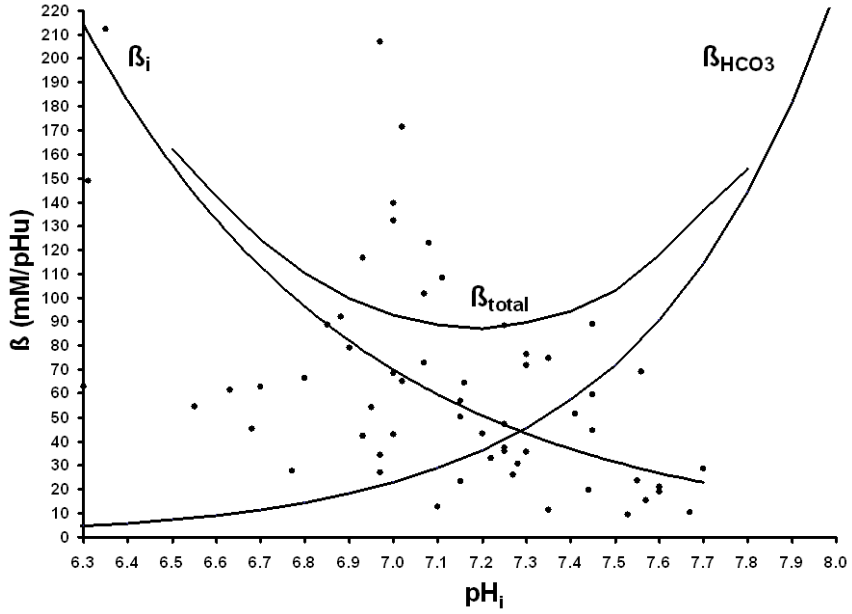
ß$_i$
ß$_{HCO3}$
ß$_{total}$
ß (mM/pHu)
pH$_i$
220
210
200
190
180
170
160
150
140
130
120
110
100
90
80
70
60
50
40
30
20
10
0
6.3
6.4
6.5
6.6
6.7
6.8
6.9
7.0
7.1
7.2
7.3
7.4
7.5
7.6
7.7
7.8
7.9
8.0

Figure 3. (see previous page) The resting pH_i of gastric myofibroblasts and measurement of buffering capacity (A) Human gastric myofibroblasts (HGMs, 100,000) were seeded onto cover glass to form monolayers. Cells were allowed to recover for 24 hours and were then loaded with 2 μM BCECF-AM. (a) Phase contrast image of myofibroblasts is shown. Four to seven cells as regions of interests (ROIs) were marked. (b) Thermal-adjusted image is shown to demonstrate homogenous BCECF dye distribution. Cells were excited at wavelengths of 490 nm (c) and 440 nm (d). (e) The 490:440 fluorescence emission ratio was measured at 535 nm. Cells were exposed to continuous perfusion with nigericin/high K^+-HEPES solutions of pH 6.80 and 7.40. The resting pH_i was calculated by multiple-point calibration (n=5/5-6). The figure shows a representative calibration curve; the mean resting pH_i in standard HEPES solution was 7.09 ± 0.02. (B) The buffering capacity of HGMs was determined by exposing the cells to various concentrations of NH_4Cl while Na^+ and HCO_3^- were omitted from the solution to block Na^+-dependent pH regulatory mechanisms. The intrinsic buffering capacity (β_i) at different pH_i (●, n = 85) was estimated by the Henderson-Hasselbalch equation. Regression analysis was performed using the curve-fitting protocol in Excel. The total buffering capacity (β_{total}) was calculated as $\beta_{total} = \beta_i\ \beta_{HCO_3}^- = \beta_i + 2.3 \times [HCO_3^-]_i$, where $\beta_{HCO_3}^-$ is the buffering capacity of the HCO_3^-/CO_2 system and $[HCO_3]_i$ is the intracellular concentration of HCO_3^-.

3.2 Exploring of the main acid /base transporters with different techniques

Next we tried to identify the functionally active acid/base transporters expressed on the plasma membrane of HGMs. Na^+-withdrawal from the standard HEPES solution caused strong reversible acidification suggesting the presence of an active Na^+-dependent H^+-efflux mechanism (*Figure 4A*). Switching the standard HEPES solution to standard HCO_3^-/CO_2 solution caused rapid intracellular acidification, most probably due to CO_2 diffusion into the cells. Thereafter, a small pH_i recovery was observed suggesting a HCO_3^--influx and/or H^+-efflux mechanism (*Figure 4B*). In order to determine the Na^+-dependency of this HCO_3^--influx/H^+-efflux mechanism, the same experiment was performed in Na^+-free conditions (*Figure 4C*). Since no recovery was found in the presence of HCO_3^-/CO_2 in Na^+-free solution, we can assume that the HCO_3^--influx/H^+-efflux mechanism in HGMs is Na^+-dependent. These results indicate that HGMs express functionally active NHE and/or NBC. Next we tested whether HGMs contain functionally active anion exchangers (AE). Cl^--removal from the standard HCO_3^-/CO_2 solution caused reversible alkalization suggesting the presence of a Cl^--dependent HCO_3^--efflux mechanism (*Figure 4D*). Importantly, omitting HCO_3^- from the extracellular solution in combination with Cl^--removal resulted in no significant change in pH_i (*Figure 4E*). This indicates that HGMs express functionally active AE.

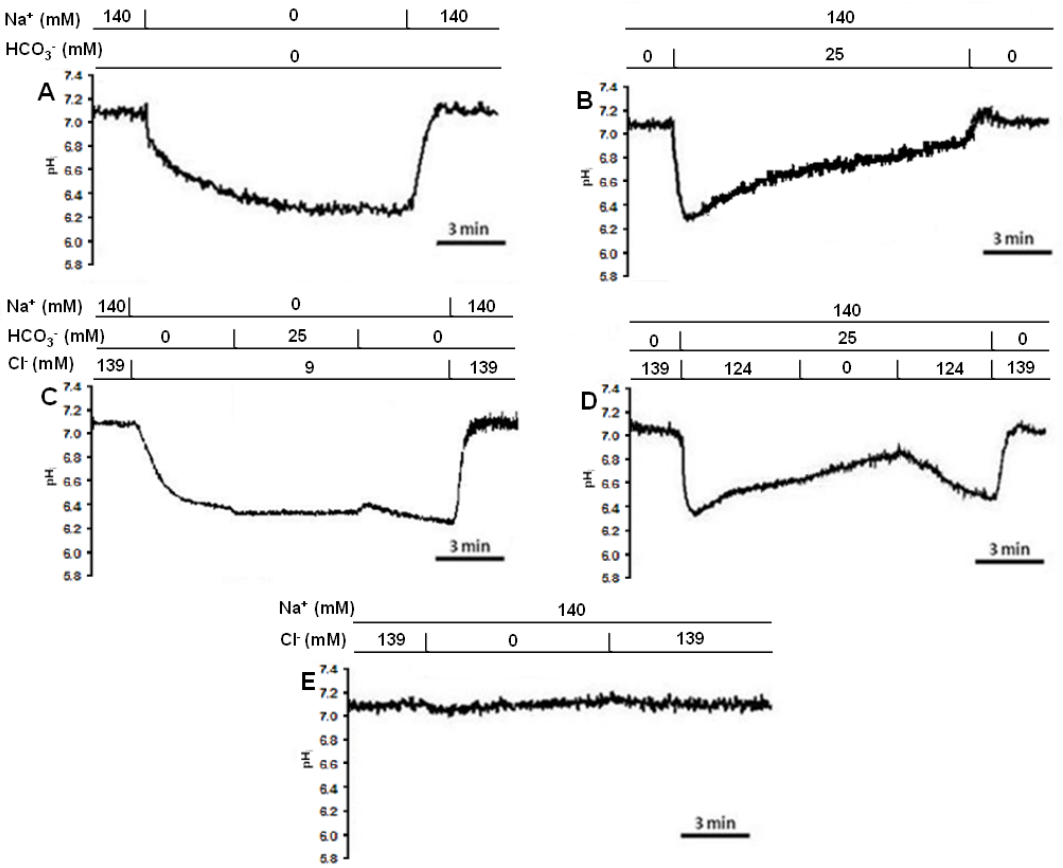

Figure 4. Na^+-dependent HCO_3^--influx and Cl^--dependent HCO_3^--efflux mechanisms are present in HGMs. Representative pH_i curves of HGMs are shown. (A) The sudden removal of extracellular Na^+ from the standard HEPES solution caused rapid acidification, which was reversed by the re-addition of the ion. (B) Administration of HCO_3^-/CO_2-buffered solution after standard HEPES solution caused acidification of pH_i followed by alkalization (HCO_3^--influx). (C) Switching from Na^+-free HEPES solution to Na^+-free HCO_3^-/CO_2-buffered solution caused acidification, but no pH_i recovery was seen. (D) In HCO_3^-/CO_2-buffered solution, Cl^--removal resulted in alkalization of pH_i followed by a complete recovery after re-addition of Cl^-. (E) Cl^--removal from the standard HEPES solution did not significantly alter the pH_i (n=5/5-6).

To confirm the findings, the activities of acid/base transporters were also investigated by the ammonium pulse technique. Exposure of HGMs to 20 mM NH_4Cl induced an immediate rise in pH_i due to the rapid entry of the lipophylic base NH_3 into the cells, which binds intracellular protons generating NH_4^+ and causing alkalization. The recovery from this alkali load is promoted by AEs in the presence of HCO_3^- and Cl^- in the extracellular solution. The recovery from alkali load was much steeper in the presence of HCO_3^-/CO_2 compared with the absence of HCO_3^-/CO_2 *(Figure 5A, first vs. third curve).* It is worth mentioning that the slow uptake of NH_4^+ via the NBC is also a prerequisite for the acid loading. After the removal of NH_4Cl, NH_3 diffuses out of the

cell, therefore facilitating the dissociation of intracellular NH_4^+ to H^+ and NH_3, which rapidly decreases pH_i. Thereafter, the pH_i starts to recover after this acidification owing to activation of pH_i regulatory mechanisms namely NHE, NBC and proton pumps (PP). In the absence of extracellular HCO_3^- and in the presence of Na^+, the recovery from acidosis reflects the activities of NHE and PP *(Figure 5A, first curve)*. However, the lack of recovery in the absence of Na^+ excludes functionally active PPs in HGMs *(Figure 5A, second curve)*. The addition of HCO_3^- to the extracellular solution strongly increases the pH_i recovery from acidosis *(Figure 5A, third curve)*. Since there is no pH_i recovery from acidosis in Na^+- and HCO_3^--free solution *(Figure 5A, fourth curve)*, it is assumed that the HCO_3^--influx mechanism is most probably accomplished by the Na^+-dependent NBC. Therefore, we tested the effects of the NBC inhibitor H_2DIDS (0.5 mM) and the NHE1 and NHE2 inhibitor HOE-642 (50 µM) on the recovery rates during and following an acid load in HCO_3^-/CO_2 buffered solution *(Figure 5C)*. We calculated $J(B^-)$ from these and from the above mentioned experiments *(Figure 5B and D)* and found that NBC inhibition greatly reduced pH_i recovery after acid load (20.54 ± 1.76 vs. 7.99 ± 0.39 mM B^-/min) revealing high transporter activity. 50 µM HOE-642 further decreased the recovery rate from acidosis (7.99 ± 0.39 vs. 3.91 ± 0.41 mM B^-/min) indicating high NHE1 and NHE2 activities. Simultaneously applying the two inhibitors resulted in very slow recovery (0.98 ± 0.09 mM B^-/min). Without HCO_3^-/CO_2 buffering in standard HEPES solution, cells showed much slower recovery than with bicarbonate buffering (13.36 ± 0.41 vs. 20.54 ± 1.76 mM B^-/min, respectively). As seen on *Figures 5B/5D*, eliminating Na^+ from the extracellular solution inhibited the cells to recover from an acid load in both HCO_3^-/CO_2-buffered solution and in standard HEPES solution.

A

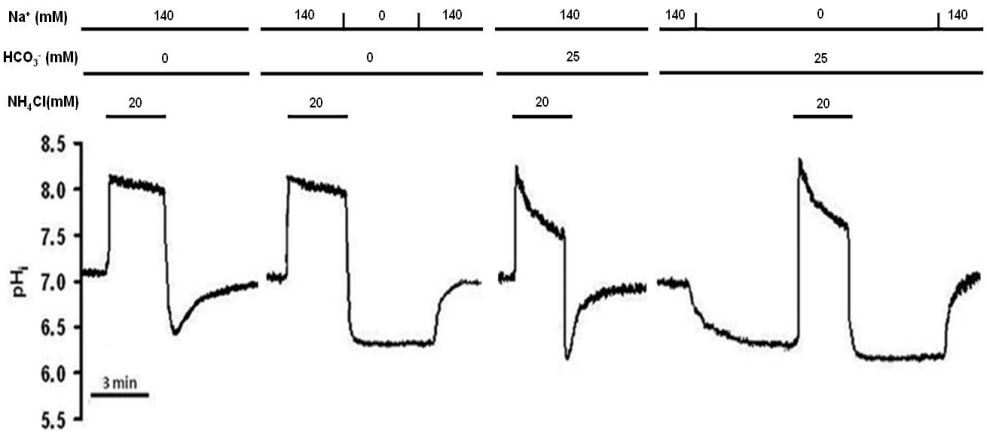

B

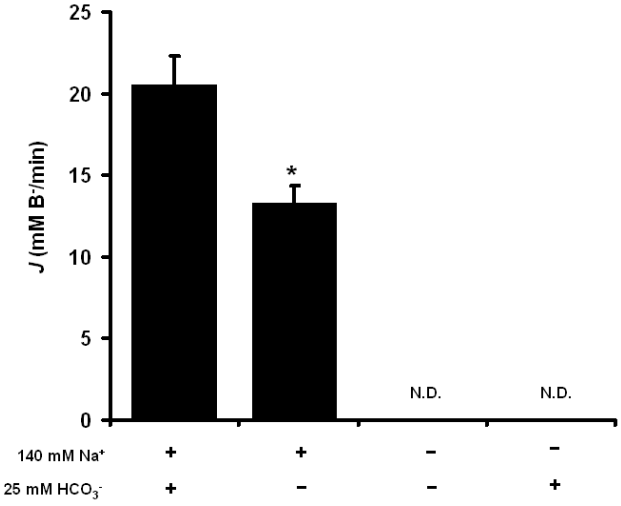
25
20
15
10
5
0
J (mM B⁻/min)
*
N.D.
N.D.
140 mM Na⁺ + + – –
25 mM HCO3⁻ + – – +

C

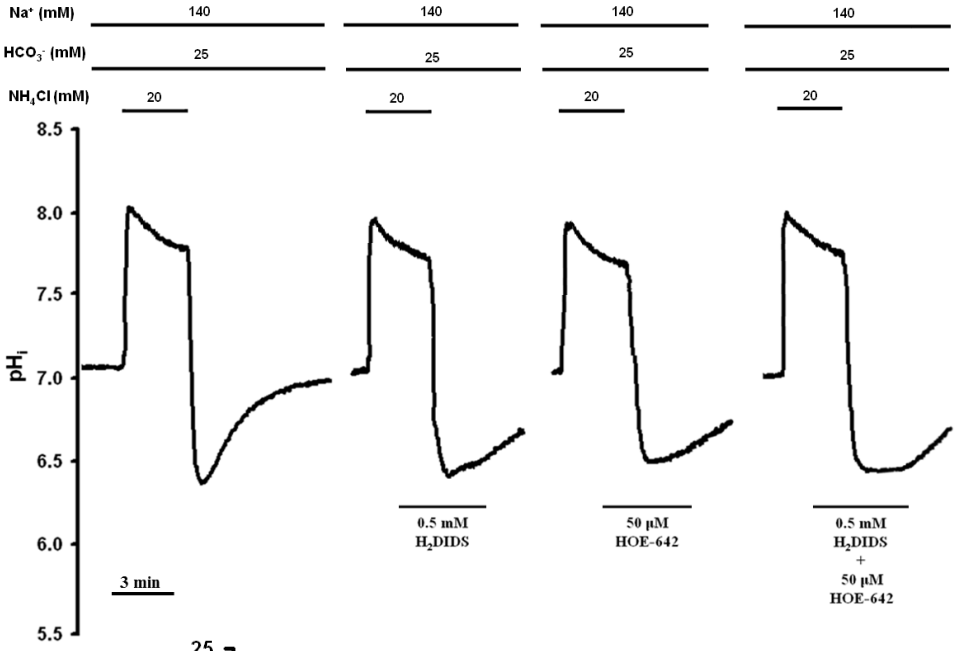
Na⁺ (mM) 140 140 140 140
HCO3⁻ (mM) 25 25 25 25
NH4Cl (mM) 20 20 20 20
8.5
8.0
7.5
7.0
6.5
6.0
5.5
pHi
3 min
0.5 mM H2DIDS
50 µM HOE-642
0.5 mM H2DIDS + 50 µM HOE-642

D

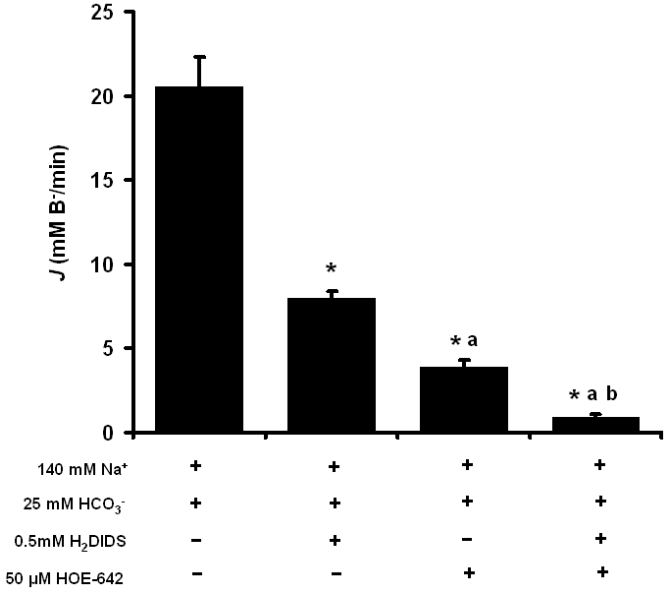
25
20
15
10
5
0
J (mM B⁻/min)
*
* a
* a b
140 mM Na⁺ + + + +
25 mM HCO3⁻ + + + +
0.5mM H2DIDS – + – +
50 µM HOE-642 – – + +

*Figure 5. (see previous pages 24 and 25) Na^+-dependent H^+-efflux and Na^+-dependent $HCO3^-$-influx were detected in HGMs. (A) Representative pH_i traces of HGMs are shown. Cells were exposed to 20 mM NH_4Cl in HEPES-buffered solution for 3 minutes. After the acid load, recovery of pH_i could be observed. However, the administration of Na^+-free HEPES solution after the ammonium pulse inhibited pH_i recovery after the acid load. The same technique was applied in HCO_3^-/CO_2-buffered solution. Note that the initial phase of the pH_i recovery during the ammonium pulse is quicker than in HEPES solution and the recovery phase after the acid load is much steeper. Also in Na^+-free HCO_3^-/CO_2-buffered solution, no recovery could be seen after the ammonium pulse. (B) The bar chart shows the summary data of base fluxes ($J(B^-)$) after recoveries from acid load. Values are shown as means ± SEM (n=5/10-12). *: $p<0.05$ vs. 25 mM $HCO3^-$. (C) Inhibition of Na^+/ HCO_3^-- co-transporter (NBC) with 0.5 mM H_2DIDS and/or inhibition of NHE1-2 with 50 μM HOE-642 during acid load in HCO_3^-/CO_2-buffered solution is shown. (D) The rates of ecovery from acid load were determined and $J(B^-)$s were calculated from the experiments shown above. Absolute values are displayed for comparison (n=5/1-2); values are shown as means ± SEM. *: $p<0.05$ vs. 25 mM HCO_3^-; a: $p<0.05$ vs. 25 mM HCO_3^- + 0.5 mM H_2DIDS; b: $p<0.05$ vs. 25 mM HCO_3^- + 50 μM HOE-642.*

Next, we focused our attention on characterizing the NHE isoforms expressed on the plasma membrane of HGMs with functional measurements. The HGMs were acid-loaded by exposure to a 3-min-pulse of 20 mM NH_4Cl in HEPES solution followed by a 5-min-exposure to Na^+-free HEPES solution *(Figure 6A)*. Since neither Na^+ nor HCO_3^- was present in the extracellular solution, acid/base transporters were inhibited and the pH_i stayed at a stable acidic level. NHE activity was induced by the re-addition of extracellular Na^+ and the activity of NHEs was determined by measuring the initial rates of pH_i recovery over the first 60 sec (60 data points). The activities of the different NHE isoforms were determined by using the isoform selective NHE inhibitor HOE-642 (cariporide). At 1 μM HOE642 inhibits NHE1 whereas at 50 μM it inhibits both NHE1 and NHE2, but not NHE3. Our data indicate that NHE1 is responsible for about 85% of the Na^+/H^+ exchange activity, whereas NHE2 activity is around 10 % and the remaining NHE activity is approximately 5 % (*Figure 6B*). Of course, we cannot exclude the possible involvement of other NHEs. However, even if they were expressed, they would only have marginal influence on H^+-efflux.

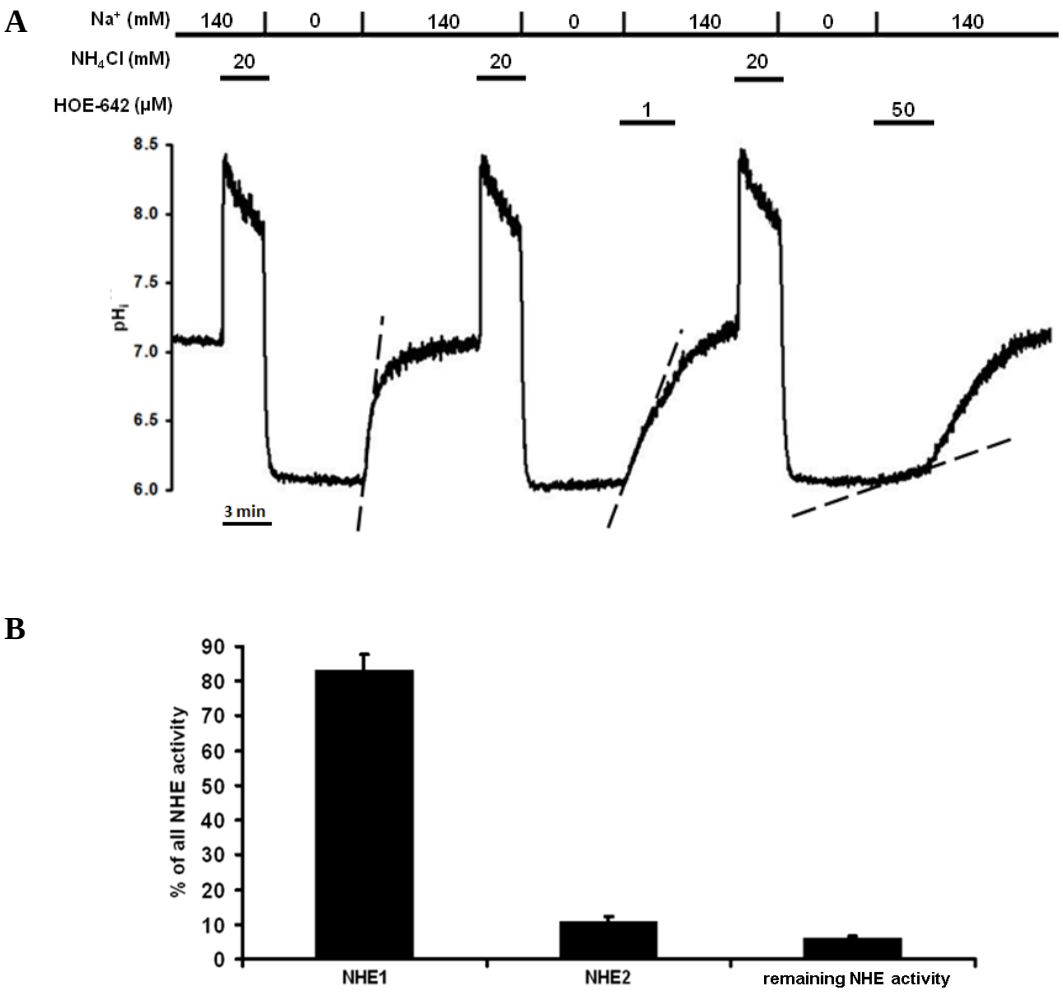

Figure 6. Identification of NHE isoforms by microfluorometry. (A) Representative pH_i traces of HGMs are shown. Cells were loaded with acid by using the ammonium pulse technique. After Na^+-withdrawal, the isoform-selective NHE inhibitor HOE-642 was administered in 1 µM (inhibits NHE1) or 50 µM (inhibits NHE1 and NHE2) concentration, together with re-addition of Na^+. The initial rates of pH_i recovery during HOE-642 administration was calculated by linear regression analysis to determine the activities of NHE isoforms. (B) The bar chart demonstrates that NHE1 is responsible for 83±5%, NHE2 for 11±1% and other isoforms for 4.5±0.8% of all Na^+/H^+ exchange activity. Data are shown as means ± SEM (n=5/5-6).

3.3 Effect of bioactive compounds on NHE activity

We next investigated the effects of IGF-II and carbachol on the activities of NHEs (*Figure 7*). Importantly, both IGF-II and carbachol dose-dependently stimulated NHE activity. Carbachol concentrations were tested within the range of 1-1000 µM. 10

μM carbachol had the greatest effect on NHE activity. 100 ng/ml IGF-II was more effective than 10 ng/ml in increasing NHE activity.

A

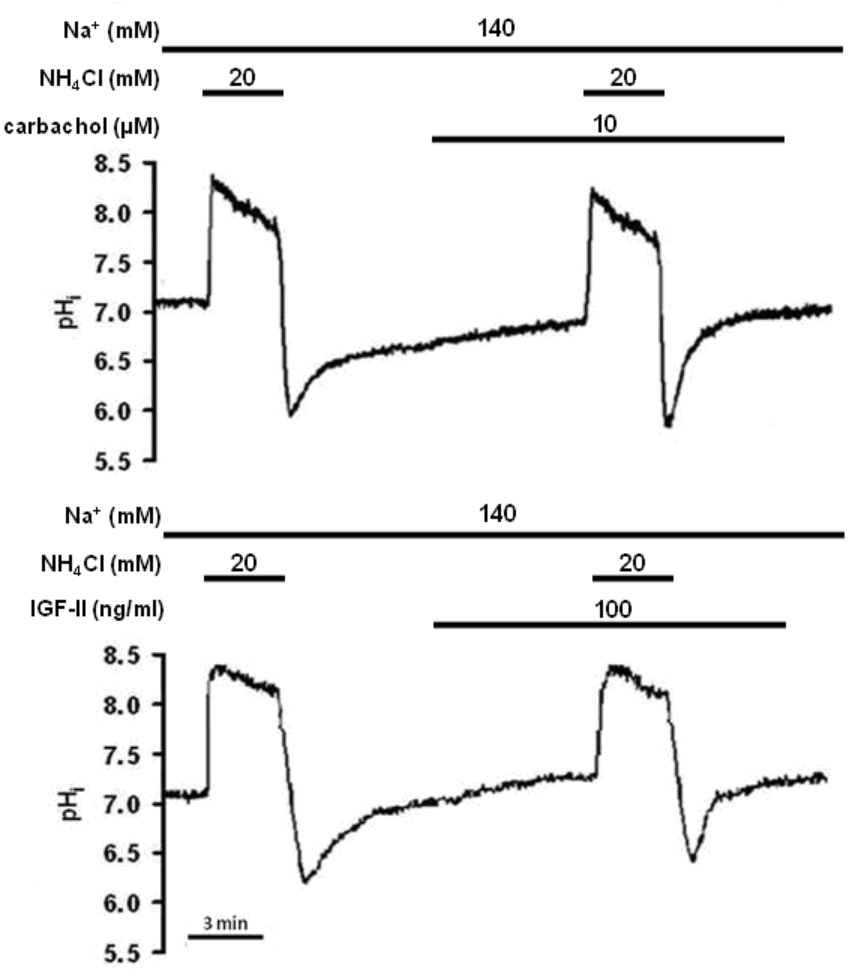

B

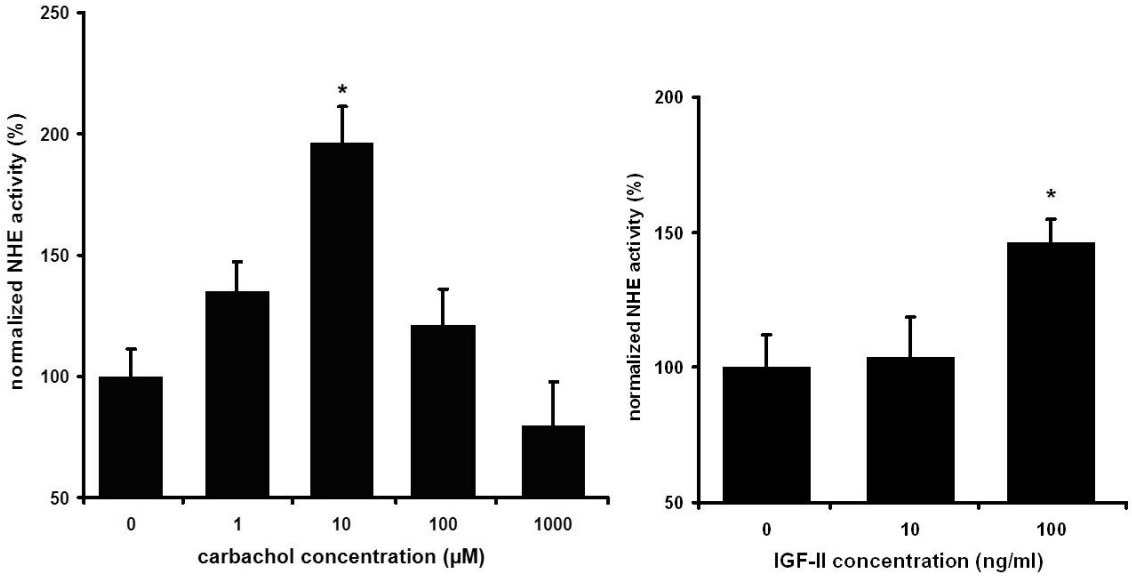

*Figure 7. (see previous page) The effects of carbachol and IGF-II on NHE activity. (A) Representative pH_i traces of HGMs are shown. We tested different carbachol and IGF-II concentrations on NHE activity using the ammonium pulse technique. The figure shows the effects of 10 μM carbachol and 100 ng/ml IGF-II treatment. Note that the changes in the rates of pH_i recovery from acidosis during treatment is much higher compared to the recovery rates without IGF-II or carbachol treatment. (B) The bar diagrams show the summary data obtained from the above mentioned experiments. Administration of 10 μM carbachol and 100 ng/ml IGF-II significantly increased NHE activity. Values are normalized to the basal NHE activity. Data are shown as means ± SEM (n=5/5-6). *: $p<0.05$ vs. 0 μM.*

4. mRNA and protein expression of NHE1-3

Based on results of the functional measurements, we investigated the presence of NHE transporters at the mRNA and protein levels. RT-PCR confirmed the expression of NHE1, NHE2 and NHE3 (*Figure 8A*). We also analysed the expression of NHE isoforms in HGMs by Western blot. We found that NHE1 is present in HGMs, but we were unable to show NHE2 and NHE3 expression. Positive controls (human kidney) confirmed that the antibodies used for these studies recognize specific proteins (*Figure 8B*). We speculate that NHE2 and NHE3 protein abundance was low in our lysates, below the limit of detection. Using immunocytochemistry, we demonstrated NHE1-3 localization to the plasma membrane of HGMs (*Figure 8C*).

A

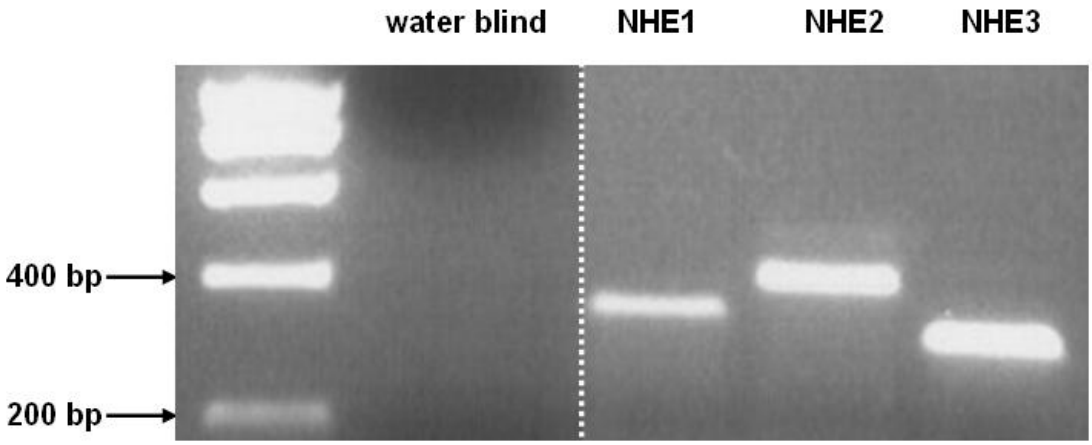

B

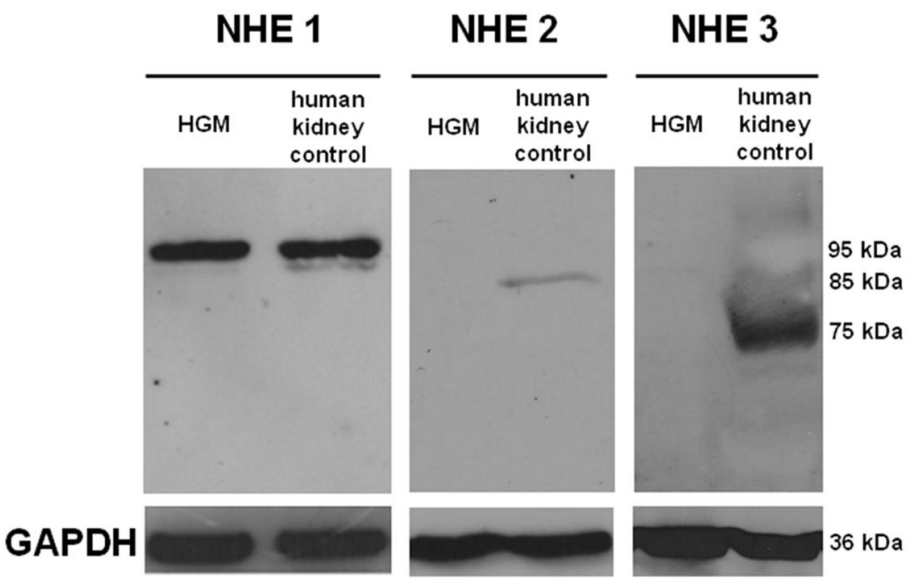

C

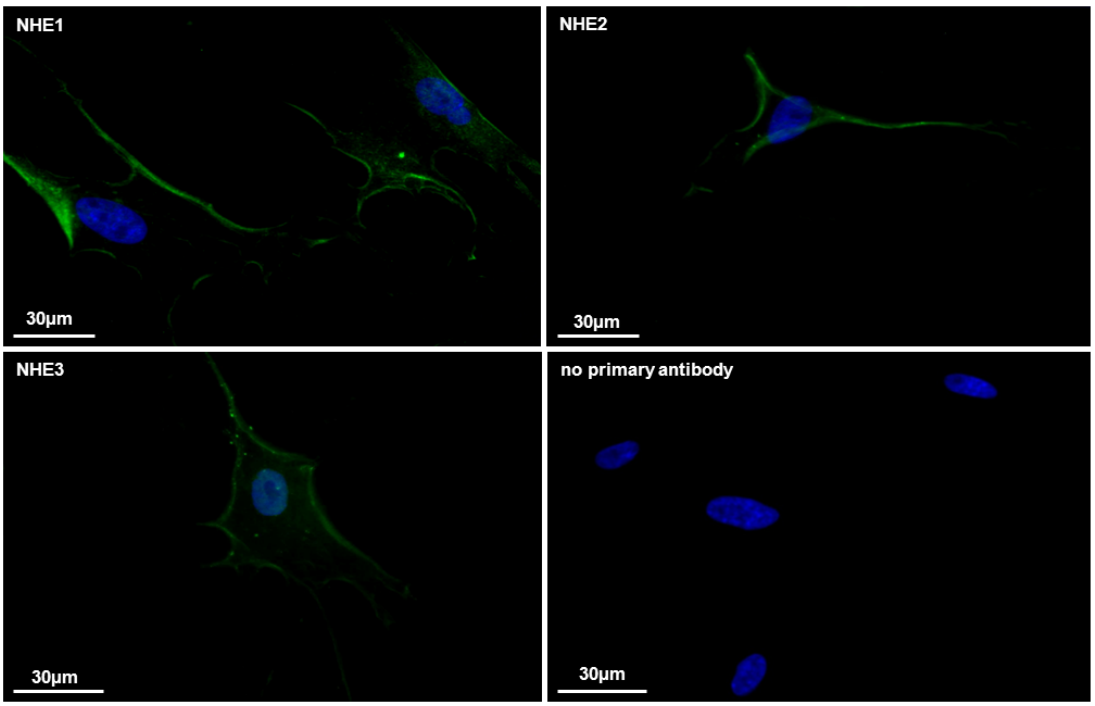

Figure 8. (see previous page) mRNA and protein expression of NHE isoforms in HGMs. (A) Reverse transcription PCR confirmed the expression of NHE1-3 isoforms (n=3/6-7). Expected PCR product sizes: NHE1: 341 bp, NHE2: 407 bp, NHE3: 299 bp. In water blind we used water as template. (B) Immunoblot analysis showing different NHE isoforms in HGMs and human kidney controls. Protein sizes are as follows: NHE1: 95 kDa, NHE2: 85 kDa, NHE3: 75 kDa, GAPDH: 36 kDa (n=4-5/3-10). (C) NHE1, NHE2 and NHE3 were identified by immunocytochemistry in the plasma membrane of HGMs. Nuclei were counterstained with DAPI (blue staining). No specific staining was detected when the primary antibody was omitted (n=3/1-2).

5. Migration is stimulated by carbachol and IGF-II

Next, we investigated the effects of carbachol and IGF-II on cell migration and the role of NHE1 in migration of HGMs using the scratch wound assay. We found that both 100 ng/ml IGF-II and 10 µM carbachol stimulates the migration of HGMs (*Figure 9)*. Inhibition of NHE1 by HOE-642 had no effect on unstimulated cell migration, but it significantly inhibited both carbachol- and IGF-II-stimulated migration (by 29±7 % and 33±8 %, respectively).

A

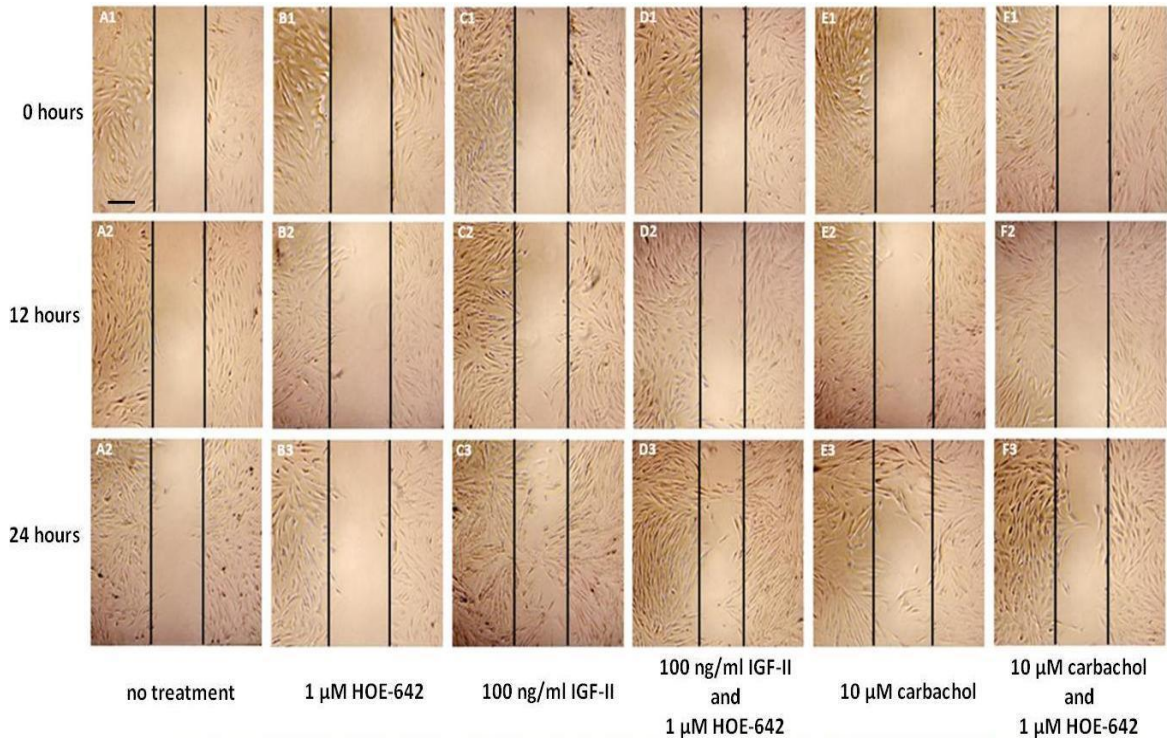

B

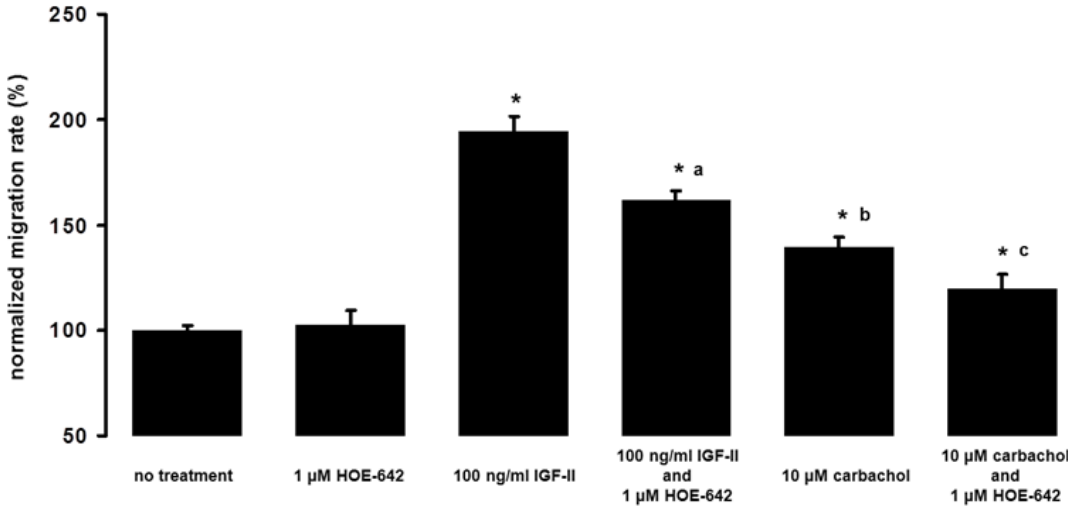

*Figure 9. Carbachol and IGF-II treatment increased migration rates of HGMs in a NHE1-dependent manner. (A) 100,000 HGMs were cultured in six-well plates. After reaching confluency, the monolayer was wounded by a P2 tip along an oriented line in the middle of the well and detached cells were removed by washing with serum-free media. Only wounds with sharp and even edges were used for experiments. Reagents were added to the wells in serum-free media and the plate was incubated for 24 hours at 37 °C, 5 % CO_2. Images were taken at 0, 12 and 24 hours from representative areas. Cells were treated with or without 10 μM carbachol or 100 ng/ml IGF-II, and/or 1 μM HOE-642 and cells which migrated into the wound were counted at 12 and 24 hours. The scale bar on the first picture represents 100 μm. (B) The bar chart shows the migration rates normalized to the basal rate at 24 hours. Values are shown as means ± SEM, n=5/1-3, *: p<0.05 vs. no treatment; a: p<0.05 vs 100 ng/ml IGF-II, c: p<0.05 vs 10 μM carbachol. Picture columns differ by treatment (see markers A-F on picures).*

6. IGF-II increases proliferation in an NHE1-dependent manner

Finally, we tested the effects of HOE-642, IGF-II and carbachol on HGM proliferation. EdU incorporation assays showed that 100 ng/ml IGF-II increased cell proliferation over two-fold. Carbachol and/or HOE-642 did not affect proliferation. However, NHE1 inhibition by 1 μM HOE-642 completely blocked the stimulatory effect of IGF-II on cell proliferation (*Figure 10*).

Our paralell work regarding thesis issue (related article II) shows that proliferation of HGMs from specimens of gastric cancer (CAMs) is geratly enhanced by IGF-II stimulation compared to healthy tissue. Those data demostrate that the proteome and secretome of normal myofibroblasts and CAMs are different by Metacore analyses. The differences are exaggerated in CAMs from patients with short survival. Dominant changes are mostly at the level of ECM (extracelluar matrix) proteins, cytoskeletal re-arrengement and actin filaments.

By focusing on CAM secretomes we have identified an unexpected role for myofibroblasts in restraining tumor migration and proliferation in early disease through secretion of a certain ECM molecule, TGFβig-h3, which not only inhibits proliferation and migration of myofibroblasts and gastric cancer cells, but also restrains tumor growth *in vivo* in xenograft experiments. This molecule is down-regulated in CAMs enabling more aggresive expansion and better response to IGF-II. We demonstrate, that TGFβig-h3 is highly decreased in CAMs originating from patients with poor survival. Depression of TGFβig-h3 secretion by myofibroblasts occurs with tumor progression and could provide as a unique functional biomarker for stromal cell properties in cancer. Moreover, it may also be possible to develop novel therapeutic strategies based on the

observation that stromal cell-stimulated tumor growth *in vivo* is prevented by restoration of TGFβig-h3.

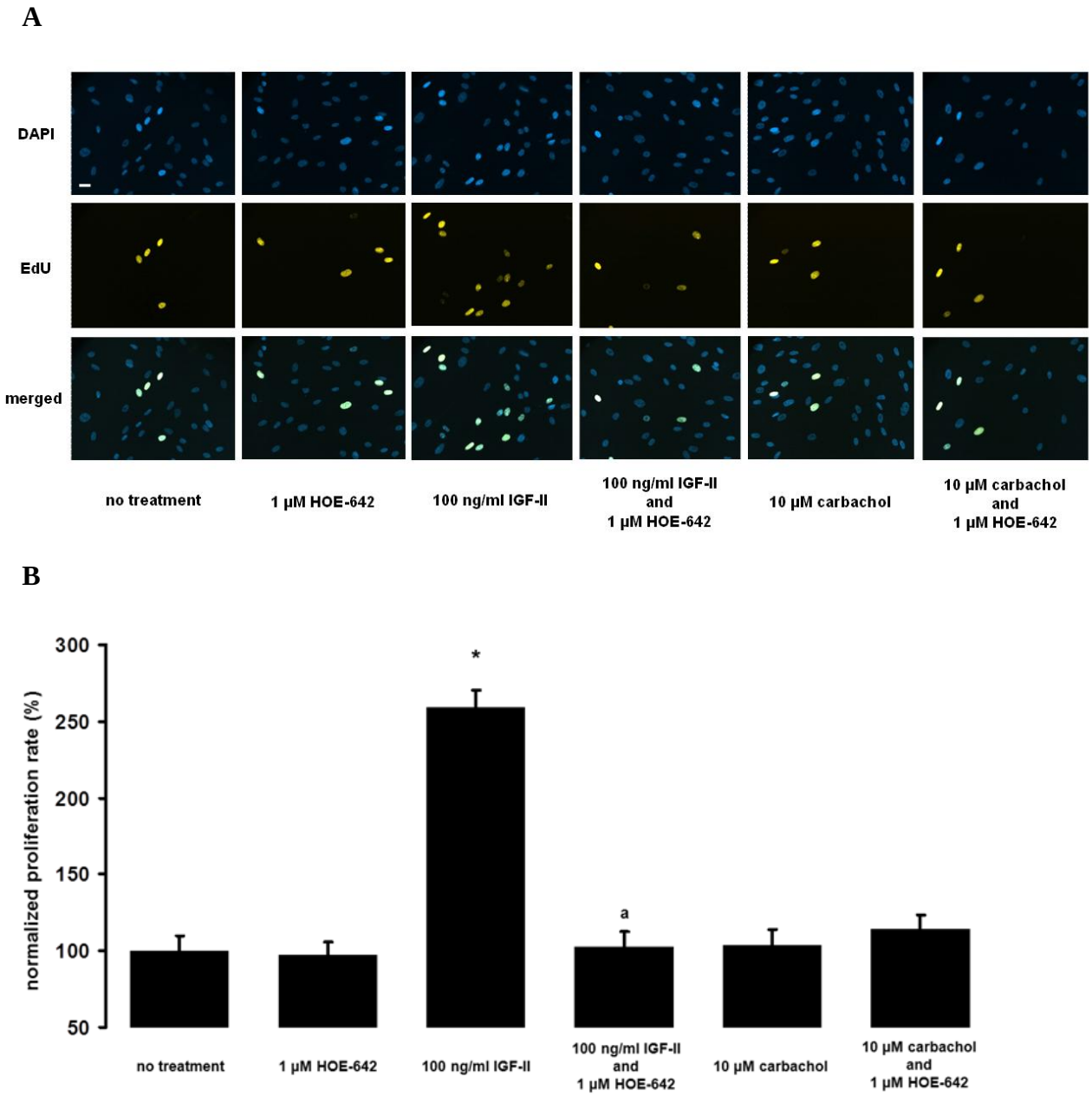

*Figure 10. IGF-II stimulates the proliferation of HGMs in a NHE1-dependent manner. (A) Representative images showing EdU-localisation after treatment with 1 µM HOE-642, 100 ng/ml IGF-II and/or 10 µM carbachol compared to control. 1 µM HOE-642 did not affect proliferation either on its own, or in a combination with 10 µM carbachol. 100 ng/ml IGF-II increased the rate of proliferation. Furthermore, the inhibition of NHE1 suppressed the IGF-II stimulatory response. Nuclei were counterstained with DAPI (blue staining). The scale bar on the first picture represents 50 µm. (B) The bar chart shows the proliferation rates of (A) normalized to the basal proliferation rate; *: $p<0.05$, a: $p<0.05$ vs 100 ng/ml IGF-II (n=5/1-2).*

V. Discussion

We have characterized the pH_i regulatory mechanisms of HGMs for the first time. The data demonstrate that NHE1 activity contributes to IGF-II- and carbachol-stimulated migration and that it is obligatory for IGF-II-induced proliferation.

In theory, it is possible that cultured myofibroblasts might be unstable, however we have found at least 10 culture passages to have both the functional properties and molecular profiles to be stable. So it is possible to perform both functional and molecular biology studies.

The resting pH_i of HGMs (7.09 ± 0.02) is similar to that observed in fibroblasts [13, 32, 46] and smooth muscle cells [58]. Myofibroblasts displayed three main acid/base transporters, namely NBC, AE, and NHE. These are also the main mechanisms regulating pH_i in fibroblasts [13, 35] and in smooth muscle cells [16]. Thus, AE decreases, whereas NBC and NHE increase pH_i. Due to the inaccurate comparison of pH/dt values between transpoter acitivities and because these values estimate rather than measure activity, we determined buffering capacity [$J(B^-)$] of HGMs in HCO_3^--free and HCO_3^--containing solution. $J(B^-)$ calculations revealed high NBC and high NHE activities which are the main transporters aiding recovery from an acid load in HGMs. In the present study we also focused on the roles of NHEs because large amounts of data collected showed that NHEs coupled through signal transduction or simply by altering pH dynamics have great impact on cell function. Most studies focused on tumor cells, despite the well known contribution of stromal cells to cancer development. Stromal cells have been largely neglected and so, information on these matters concerning them is scarce.

10 μM carbachol strongly stimulated NHE activity of HGMs. It has been shown that carbachol also increases NHE (and AE) activity in lacrimal gland epithelia [55] and in rabbit parietal cells [5]. In the latter study, carbachol strongly increased NHE activity and its effect were completely blocked by 1 μM HOE-642 suggesting the involvement of NHE1. Atropine or intracellular Ca^{2+}-chelation inhibited the activation of NHE indicating a typical muscarinic receptor effect with a Ca^{2+}-dependent signalling pathway [55, 48]. In the latter publications, the authors suggested that Ca^{2+}-dependent stimulation causes a selective activation of NHE1, whereas cAMP-dependent stimulation with forskolin activated NHE1, NHE2, and more strongly NHE4. In HCO_3^-

/CO_2 containing solution the pH_i did not change, indicating that activation of NHE and AE are primarily volume regulatory mechanisms. They speculated that the physiological significance of secretagogue-induced NHE activity may be related to volume and not to pH_i regulation during acid secretion of rabbit parietal cells [5]. It seems that in our work both NHE and NBC have a cardinal role in counter-regulating pH_i against acid load. They promote pH_i recovery after acid load even more effectively during carbachol treatment in HCO_3^--containing solution. We did not detect any change in cell volume during our experiments. In humans these transporters might have a more prominent pH_i regulating role, rather than a volume regulating role in response to cholinerg agonists.

IGF-II (which has been shown to stimulate migration and proliferation of many cell types including myofibroblasts [40, 50],) also stimulates NHE activity. It is known that IGF-II exerts its effects through the tyrosine kinase receptor IGF-IR and it is also well known that NHE1 acitivity is mainly regulated by phosphorylation. *Meima et al.* reported that IGF-IR activates Ser/Thr kinases in the Akt signalling pathway and increases myofibroblast migration, growth and NHE activity by phosphorylating intracellular NHE regulatory domains thus enhancing transporter activity [41]. The distal region of the cytoplasmic tail of NHE corresponding to amino acids 700-815, is enriched in serine and threonin residues that are phosphorylated by different protein kinases in response to hormones and/or growth factors [49]. It has also been suggested that Ser/Thr kinases not only stimulate NHE1 activity, but also increase NHE1 promoter transcription [7]. Extracellular signal-regulated kinase 1/2 regulates gene expression via the mitogen-activated protein kinase cascade [43] after NHE1 phosphorylation/activation through $p90^{RSK}$ (a downstream substrate of ERK1/2) [52]. $p90^{RSK}$ directly phosphorylates NHE1 at position 703 (Ser) in vascular smooth muscle cells after growth hormone treatment; the exchanger activity was found to be increased [52]. Another important factor in the regulation of NHE is protein 14-3-3, which binds to position 703 (Ser) after its phosphorylation and also limits dephosphorylation by protein phosphatases [37]. Additional Ser/Thr phosphorylation sites have been recently identified in the ERK pathway, but their importance must be confirmed [39].

Our experiments demonstrate that reagents increasing NHE activity also increase HGM migration and proliferation. So the question arises whether NHE inhibition may inhibit cell migration and proliferation. The effects of parasympathomimetics on cell migration are conflicting, though they are thought to stimulate NHE activity in general. In HaCaT cells, carbachol did not alter single random cell locomotion compared to non-

treated cultures [42]. Epidermal keratinocytes showed enhanced migration after long-term muscarinic stimulation with acetylcholine in an agarose gel outgrowth system [20] whereas carbachol treatment arrested wound healing in epidermal keratinocytes [12]. Besides the differences between species and tissues, it seems that various muscarinic receptors can mediate different migration responses even in the same cell [56]. Our experiments clearly showed that 10 μM carbachol stimulated migration of HGMs, at least partly in an NHE1-dependent manner, but higher or lower doses had no further effect on migration (data not shown). It is known that protein kinase C (PKC) might mediate M3 receptor signals causing PLC to cleave membrane phospholipids. Phosphatidylinositol 4,5-bisphosphate is cleaved into diacyl glycerol and inositol trisphosphate (IP3) which is released into the cytosol and binds to IP3 receptors localised at the endoplasmic reticulum (or sarcoplasmic reticulum) causing consequent increase of the cytosolic calcium concentration and a cascade of activity including locomotion of contractile cells [1]. M3 receptors, through phospholipase C, may also activate PI3K/Akt cascade. In the context of gastric cancer, it is worth mentioning that apoptosis can be suppressed through the PI3K/Akt/mTOR pathway allowing vigorous proliferation and better survival [60]. PKC also modulates gene regulation via nuclear factor-κB and by joining Raf/MAPK cascade. It has been shown recently that PKC may phosphorylate the potent activation transcription factor-2, which controls c-Jun-mediated activation of transcription [59]. The observed increase in migration in our studies suggests, however, a permissive or supporting role of NHE1 in enabling migratory mechanisms to take effect in response to bioactive compounds. Others have found that not only NHE1 activity, but also intact NHE1 protein structure is required for locomotion, since mutations/modifications of protein structure or inhibition of the exchanger activity also inhibit migration [14]. Notably, NHE1 is a scaffolding-organizing protein functioning as a transmembrane signal transducer for various agents modulating cell volume, cell migration and growth through NHE1 activity [36]. This may be a part of an answer to how NHE organizes cell function. Muscarinic agonists have also been shown to evoke differential effects on proliferation depending on the type of the muscarinic receptor [56]. We found that the M3 agonist carbachol does not induce proliferation of HGMs.

IGF-II stimulates the proliferation of many cell types, including myofibroblasts [21, 40]. NHE1 may act as an organizer of different cell growth inducing signals through modulation of transporter activity via receptor tyrosine kinases and joint

pathways. *Denker et al.* reported that NHE1 protein contains an intracellular esrin/radixin/moesin (ERM) motif close to the plasma membrane, which anchors the protein to the subcortical actin filament network and serves as a host to actin polymerization. In a wound healing assay, migration was impaired when mutations disrupted the ERM site. Not only ERM site mutations, but also mutations of the transporter sequence (resulting in diminished NHE1 activity), impair de-adhesion resulting in failure to retract lamellipodia [36]. Besides this membrane anchoring, NHE1 is important in regulating cell volume and local pH at changing membrane sites of a moving cell; it is known that in fibroblasts NHE1 is most abundant at the rear and front pole of a spatially polarized migrating cell [14].

We showed that inhibition of NHE1 blocks migration and proliferation of HGMs. Since stromal cells play an important role in cancer initiation and progression [48, 8, 43], our results may have both physiological and therapeutic relevance. It is well documented that proliferation is reduced by NHE1 inhibition in human cancer cells [23, 47]. However, it is also possible that intracellular alkalization simply promotes or permits proliferative responses because as the pH_i becomes more alkaline, cellular metabolism becomes more rapid mainly due to the more effective energy producing mechanisms [23]. For example, in tumor cells, acid/base conditions are of particular importance because cancer cells share an aberrant intracellular alkalization which facilitates their malignant behavior whereas the microenvironment becomes more acidic [11]. Nevertheless, as mentioned before, NHE1 is highly regulated by phosphorylation and Akt kinases which increase its activity while also stimulating proliferation at the same time [19, 41, 51].

In conclusion, we have demonstrated that HGMs express functionally active NHE, NBC and AE transporters which regulate pH_i. Furthermore, we have shown that NHE1 contributes to IGF-II- and carbachol-stimulated migration, and that it is obligatory for IGF-II-induced proliferation.

Additionally, we demonstrated in our related work, that HGMs secrete TGFβig-h3 that restrain tumor growth *in vivo* and this function is damaged in CAMs.

VI. Acknowledgements

I would like to thank all of the people who have helped and inspired me during my doctoral study.

I am grateful to **Prof. Dr. Tibor Wittmann**, Head of the First Department of Medicine and to **Prof. Dr. András Varró**, the Head of Department of Pharmacology and Pharmacotherapy, who gave me the opportunity to work in their Departments.

I would like to thank my **supervisors Prof. Dr. Péter Hegyi** and **Dr. Zoltán Rakonczay Jr.** for their support, understanding, encouraging and personal guidance. I appreciate all their contributions of time, ideas, and funding to make my Ph.D. experience productive and stimulating.

I also would like to thank **the pathologists, Dr. László Tiszlavicz and Dr. István Németh** at the Department of Pathology and **Prof. Dr. György Lázár** Head of Department of Surgery, and the surgeons **Dr. Zsolt Simonka, Dr. László Varga, Dr. Pál Szenohradszky** at the Department of Surgery for collecting tissue samples. I also would like to thank **the transplant team** of the Department of Surgery for their help and specimen collection.

I am deeply grateful to **Prof. Dr. Andrea Varró, Prof. Dr. Graham Dockray** and **Prof. Dr. Rod Dimaline** and their **research team** at the Liverpool University, UK for the opportunity of a Ph.D. scholarship, for their outstanding collaboration and guidance in molecular biology experiments.

Nevertheless, I would like to thank the **assistants and students of the Cell Biology Research Laboratory at the First Department of Medicine** for their continuous help in preparing my experiments.

My special thank goes to our assistant, **Erzsébet Zoltánné Fuksz** whose continuous attention and care established the proper conditions of our tissue culture laboratory.

VII. References

1. Alberts B, Alexander J, Julian L, Martin R, Keith R, Peter W. Molecular Biology of the Cell, Fourth Edition, Garland Science, New York, US, 2002
2. Alexandratou E, Dido Y, Panagiotis H, Dimitris K and Spyros L. Human fibroblast alterations induced by low power laser irradiation at the single cell level using confocal microscopy. Photochem Photobiol Sci 2002;8:547-552.
3. Allinen M, Beroukhim R, Cai L, Brennan C, Lahti-Domenici J, Huang H, Porter D, Hu M, Chin L, Richardson A, Schnitt S, Sellers WR, Polyak K. Molecular characterization of the tumor microenvironment in breast cancer. Cancer Cell 2004;6:17-32.
4. American Cancer Society statement, 2010.
5. Bachmann O, Reichelt D, Tuo B, Manns MP and Seidler U. Carbachol increases Na+-HCO3- cotransport activity in murine colonic crypts in a M3-, Ca2+/calmodulin-, and PKC-dependent manner. Am J Physiol Gastrointest Liver Physiol 2006;291:G650-657.
6. Becker JC, Muller-Tidow C, Serve H, Domschke W, Pohle T. Role of receptor tyrosine kinases in gastric cancer: new targets for a selective therapy. World J Gastroenterol. 2006;12(21):3297-305.
7. Besson P, Fernandez-Rachubinski F, Yang W and Fliegel L. Regulation of Na+/H+ exchanger gene expression: mitogenic stimulation increases NHE1 promoter activity. Am J Physiol 1998;274:C831-839.
8. Bhowmick NA, Neilson EG, Moses HL. Stromal fibroblasts in cancer initiation and progression. Nature 2004;432:332-337.
9. Bissell MJ, Hines WC. Why don't we get more cancer? A proposed role of the microenvironment in restraining cancer progression. Nat Med 2011;17:320-9.
10. Buckland G, Agudo A, Lujan L, Jakszyn P, Bueno-De-Mesquita HB, Palli D, Boeing H, Carneiro F, Krogh V. Adherence to a Mediterranean diet and risk of gastric adenocarcinoma within the European Prospective Investigation into Cancer and Nutrition (EPIC) cohort study. Am J Clin Nut 2009;91(2): 381–9
11. Cardone RA, Casavola V and Reshkin SJ. The role of disturbed pH dynamics and the Na+/H+ exchanger in metastasis. Nature Reviews. Cancer 2005;5:786-795.

12. Chernyavsky AI, Arredondo J, Wess J, Karlsson E and Grando SA. Novel signaling pathways mediating reciprocal control of keratinocyte migration and wound epithelialization through M3 and M4 muscarinic receptors. J Cell Biol 2004;166: 261-272.

13. Davies JE, Ng LL, Kofoed-Enevoldsen A, Li LK, Earle KA, Trevisan R and Viberti G. Intracellular pH and Na+/H+ antiport activity of cultured skin fibroblasts from diabetics. Kidney Int 1994;42:1184-1190.

14. Denker SP and Barber DL. Cell migration requires both ion translocation and cytoskeletal anchoring by the Na-H exchanger NHE1. J Cell Biol 2002;159:1087-1096.

15. Desmouliere A, Guyot C, Gabbiani G. The stroma reaction myofibroblast: a key player in the control of tumor cell behavior. Int J Dev Biol 2004;48:509-17.

16. Duquette RA and Wray S. pH regulation and buffering power in gastric smooth muscle. Eur J Physiol 2001;442:459-466.

17. Erez N, Truitt M, Olson P, Arron ST, Hanahan D. Cancer-Associated Fibroblasts Are Activated in Incipient Neoplasia to Orchestrate Tumor-Promoting Inflammation in an NF-kappaB-Dependent Manner. Cancer Cell 2010;17:135-147.

18. Farmer P, Bonnefoi H, Anderle P, Cameron D, Wirapati P, Becette V, André S, Piccart M, Campone M, Brain E, Macgrogan G, Petit T, Jassem J, Bibeau F, Blot E, Bogaerts J, Aguet M, Bergh J, Iggo R, Delorenzi M. A stroma-related gene signature predicts resistance to neoadjuvant chemotherapy in breast cancer. Nat Med 2009;15:68-74.

19. Goss GG, Woodside M, Wakabayashi S, Pouyssegur J, Waddell T, Downey GP and Grinstein S. ATP dependence of NHE-1, the ubiquitous isoform of the Na+/H+ antiporter. Analysis of phosphorylation and subcellular localization. J Biol Chem 1994;269:8741-8748.

20. Grando SA, Crosby AM, Zelickson BD and Dahl MW. Agarose gel keratinocyte outgrowth system as a model of skin re-epithelization: requirement of endogenous acetylcholine for outgrowth initiation. J Invest Dermatol 1999;101:804-810.

21. Grotendorst GR, Rahmanie H and Duncan MR. Combinatorial signaling pathways determine fibroblast proliferation and myofibroblast differentiation. FASEB 2004;18:469-479.

22. Harguindey S, Arranz JL, Wahl ML, Orive G, Reshkin SJ. Proton transport inhibitors as potentially selective anticancer drugs. Anticancer Res. 2009;29(6):2127-36.

23. Harguindey S, Orive G, Pedraz JL, Paradiso A and Reshkin SJ. The role of pH dynamics and the Na+/H+ antiporter in the etiopathogenesis and treatment of cancer. Two faces of the same coin--one single nature. Biochim Biophys Acta 2005;1756:1-24.

24. Hatakeyama, M. & Higashi, H. Helicobacter pylori CagA: a new paradigm for bacterial carcinogenesis. Cancer Sci 2005; 96: 835–843.

25. Hawinkels LJ, Verspaget HW, van Duijn W, van der Zon JM, Zuidwijk K, Kubben FJ, Verheijen JH, Hommes DW, Lamers CB, Sier CF. Tissue level, activation and cellular localisation of TGF-beta1 and association with survival in gastric cancer patients. Br J Cancer. 2007;97(3):398-404.

26. Hemers E, Duval C, McCaig C, Handley M, Dockray GJ, Varro A. Insulin-like growth factor binding protein-5 is a target of matrix metalloproteinase-7: implications for epithelial-mesenchymal signaling. Cancer Res 2005;65:7363-9

27. Hinz B, Phan SH, Thannickal VJ, Galli A, Bochaton-Piallat M-L and Gabbiani G. The myofibroblast: one function, multiple origins. Am J Pathol 2007;170:1807-1816.

28. Jemal A, Bray F, Center MM, et al. Global cancer statistics. CA Cancer J Clin 2011; 61:69.

29. Jemal A, Siegel R, Ward E, et al. Cancer statistics, 2006. CA Cancer J Clin 2006; 56:106.

30. Jiang L, Gonda TA, Gamble MV, Salas M, Seshan V, Tu S. Global hypomethylation of genomic DNA in cancer-associated myofibroblasts. Cancer Res 2008;68:9900-8.

31. Kalluri R. Fibroblasts in cancer. Nat Rev Cancer 2006;6:392-401.

32. Kapus A, Grinstein S, Wasan S, Kandasamy R and Orlowski J. Functional characterization of three isoforms of the Na+/H+ exchanger stably expressed in Chinese hamster ovary cells. ATP dependence, osmotic sensitivity, and role in cell proliferation. J Biol Chem 1994;269:23544-23552.

33. Koliakos G, Paletas K and Kaloyianni M. NHE-1: a molecular target for signalling and cell matrix interactions. Connect Tissue Res 2008;49:157-161.

34. Kumar; et al. Pathologic Basis of Disease (8th ed, 2010.). Saunders Elsevier. p. 784.

35. L'Allemain G, Paris S and Pouysségur J. Role of a Na+-dependent Cl-/HCO3- exchange in regulation of intracellular pH in fibroblasts. J Bioll Chem 1985;260:4877-4883.

36. Lagana A, Vadnais J, Le PU, Nguyen TN, Laprade R, Nabi IR and Noël J. Regulation of the formation of tumor cell pseudopodia by the Na(+)/H(+) exchanger NHE1. J Cell Sci 2000;113:3649-3662.

37. Lehoux S, Ji A, Florian JA and Berk BC. 14-3-3 Binding to Na+/H+ exchanger isoform-1 is associated with serum-dependent activation of Na+/H+ exchange. J Biol Chem 2001;276:15794-15800.

38. Ludovic M, Nicolas V, Fabrice B, Bernard C, Ian A D, Desmoulière A. The myofibroblast, multiple origins for major roles in normal and pathological tissue repair. Fibrogen Tis Rep 2012;5:S5

39. Malo ME and Fliegel L. Physiological role and regulation of the Na+/H+ exchanger. Can J Physiol Pharmacol 2006;84:1081-1095.

40. McCaig C, Duval C, Hemers E, Steele I, Pritchard DM, Przemeck S, Dimaline R, Ahmed S, Bodger K, Kerrigan DD, Wang TC, Dockray GJ and Varro A. The role of matrix metalloproteinase-7 in redefining the gastric microenvironment in response to Helicobacter pylori. Gastroent 2006;130:1754-1763.

41. Meima ME, Webb BA, Witkowska HE and Barber DL. The odium-hydrogen exchanger NHE1 is an Akt substrate necessary for actin filament reorganization by growth factors. J Biol Chem 2009, 284:26666-26675.

42. Metzger M, Just L, Boss A and Drews U. Identification and functional characterization of the muscarinic receptor M3 in the human keratinocyte cell line HaCaT. Cells, Tissues, Organs 2005;180:96-105.

43. Moor AN and Fliegel L. Protein kinase-mediated regulation of the Na(+)/H(+) exchanger in the rat myocardium by mitogen-activated protein kinase-dependent pathways. J Biol Chem 1999;274:22985-22992.

44. Noble A, Towne C, Chopin L, Leavesley D and Upton Z. Insulin-like growth factor-II bound to vitronectin enhances MCF-7 breast cancer cell migration. Endocrinology 2003;144:2417-2424.

45. Orimo A, Gupta PB, Sgroi DC, renzana-Seisdedos F, Delaunay T, Naeem R. Stromal fibroblasts present in invasive human breast carcinomas promote tumor

growth and angiogenesis through elevated SDF-1/CXCL12 secretion. Cell 2005;121:335-48.

46. Perona R, Portillo F, Giraldez F and Serrano R. Transformation and pH homeostasis of fibroblasts expressing yeast H(+)-ATPase containing site-directed mutations. Mol Cell Biol 1990;10:4110-4115.

47. Ritter M, Fuerst J, Wöll E, Chwatal S, Gschwentner M, Lang F, Deetjen P and Paulmichl M. Na(+)/H(+)exchangers: linking osmotic dysequilibrium to modified cell function. Cell Phys Biochem 2001;11:1-18.

48. Rozengurt E, Guha S, Sinnett-Smith J. Gastrointestinal peptide signalling in health and disease. Eur J Surg Suppl. 2002;(587):23-38.

49. Sardet C, Fafournoux P and Pouysségur J. Alpha-thrombin, epidermal growth factor, and okadaic acid activate the Na+/H+ exchanger, NHE-1, by phosphorylating a set of common sites. J Biol Chem 1991;266:19166-19171.

50. Schmid C. Insulin-like growth factors. Cell Biol Int 1995;19:445-457.

51. Slepkov ER, Rainey JK, Sykes BD and Fliegel L. Structural and functional analysis of the Na+/H+ exchanger. Biochem J 2007;401:623-633.

52. Takahashi E, Abe J, Gallis B, Aebersold R, Spring DJ, Krebs EG and Berk BC. p90(RSK) is a serum-stimulated Na+/H+ exchanger isoform-1 kinase. Regulatory phosphorylation of serine 703 of Na+/H+ exchanger isoform-1. J Biol Chem 1990;274:20206-20214.

53. Taves J, Rastedt D, Canine J, Mork D, Wallert MA and Provost JJ. Sodium hydrogen exchanger and phospholipase D are required for alpha1-adrenergic receptor stimulation of metalloproteinase-9 and cellular invasion in CCL39 fibroblasts. Arch Biochem Biophys 2008, 477:60-66.

54. Thomas JA, Buchsbaum RN, Zimniak A and Racker E. Intracellular pH measurements in Ehrlich ascites tumor cells utilizing spectroscopic probes generated in situ. Biochemistry 1979;18:2210-2218.

55. Tóth-Molnár E, Venglovecz V, Ózsvári B, Rakonczay Z, Varró A, Papp JG, Tóth A, Lonovics J, Takács T, Ignáth I, Iványi B and Hegyi P. New experimental method to study acid/base transporters and their regulation in lacrimal gland ductal epithelia. Inv Opht Vis Sci 2007;48:3746-3755.

56. Wessler I and Kirkpatrick CJ. Acetylcholine beyond neurons: the non-neuronal cholinergic system in humans. Brit J Pharmacol 2008;154:1558-1571.

57. Wolters Kluwer-UpToDate database, 2012

58. Wray S. Smooth muscle intracellular pH: measurement, regulation, and function. Am J Physiol. Cellular Physiology 1998;254:C213-225.

59. Yamasaki T, Takahashi A, Pan J,Yamaguchi N and Yokoyama KK. Phosphorylation of Activation Transcription Factor-2 at Serine 121 by Protein Kinase C Controls c-Jun-mediated Activation of Transcription. J Biol Chem 2009;284:8567-8581.

60. Yap TA, Garrett MD, Walton MI, Raynaud F, de Bono J S and Workman P. Targeting the PI3K-AKT-mTOR pathway: progress, pitfalls, and promises. Curr Opin Pharmacol 2008;8:393-412.

Articles related to the subject of the thesis

I.

Pflugers Arch - Eur J Physiol (2012) 463:459–475
DOI 10.1007/s00424-011-1059-6

SIGNALING AND CELL PHYSIOLOGY

NHE1 activity contributes to migration and is necessary for proliferation of human gastric myofibroblasts

Mátyás Czepán · Zoltán Rakonczay Jr. · Andrea Varró · Islay Steele · Rod Dimaline · Nantaporn Lertkowit · János Lonovics · Andrea Schnúr · György Biczó · Andrea Geisz · György Lázár · Zsolt Simonka · Viktória Venglovecz · Tibor Wittmann · Péter Hegyi

Received: 31 March 2011 / Revised: 31 October 2011 / Accepted: 2 November 2011 / Published online: 6 December 2011
© Springer-Verlag 2011

Abstract Myofibroblasts play central roles in wound healing, deposition of the extracellular matrix and epithelial function. Their functions depend on migration and proliferation within the subepithelial matrix, which results in accelerated cellular metabolism. Upregulated metabolic pathways generate protons which need to be excreted to maintain intracellular pH (pH_i). We isolated human gastric myofibroblasts (HGMs) from surgical specimens of five patients. Then we characterized, for the first time, the expression and functional activities of the Na^+/H^+ exchanger (NHE) isoforms 1, 2 and 3, and the functional activities of the Na^+/HCO_3^- cotransporter (NBC) and the anion exchanger (AE) in cultured HGMs using microfluorimetry, immunocytochemistry, reverse transcription polymerase chain reaction and immunoblot analysis. We showed that NHE1–3, NBC and AE activities are present in HGMs and that NHE1 is the most active of the NHEs. In scratch wound assays we also demonstrated (using the selective NHE inhibitor HOE-642) that carbachol and insulin like growth factor II (IGF-II) partly stimulate migration of HGMs in a NHE1-dependent manner. EdU incorporation assays revealed that IGF-II induces proliferation of HGMs which is inhibited by HOE-642. The results indicate that NHE1 is necessary for IGF-II-induced proliferation response of HGMs. Overall, we have characterized the pH_i regulatory mechanisms of HGMs. In addition, we demonstrated that NHE1 activity contributes to both IGF-II- and carbachol-stimulated migration and that it is obligatory for IGF-II-induced proliferation of HGMs.

Keywords Fibroblast · Na^+/H^+ exchange · Gastrointestinal tract · Human

Abbreviations

AE	Anion exchanger
AMV	Avian myeloblastosis virus
AMV-RT	Avian myeloblastosis virus reverse transcriptase
BCECF-AM	2,7-Biscarboxyethyl-5(6)-carboxyfluorescein-acetoxymethylester
DAG	Diacyl-glicerol
DAPI	4,6-Diamidino-2-phenylindole
DMEM	Dulbecco's Modified Eagle's Medium

Specific author contributions György Lázár, Zsolt Simonka, Tibor Wittmann and János Lonovics were involved in patient selection and sample collection; Zoltán Rakonczay Jr., Viktória Venglovecz and Péter Hegyi were involved in tissue culturing and microfluorometric experiments; Andrea Varró, Rod Dimaline, Islay Steele, Nantaporn Lertkowit, Andrea Schnúr, György Biczó and Andrea Geisz performed molecular biology experiments and biological assay experiments. Mátyás Czepán was involved in all of the above mentioned experiments and drafted the manuscript. Péter Hegyi designed and supervised the project, the experiments and the manuscript. Mátyás Czepán spent 3 months in Liverpool as part of the project funded by the NIH and NIHR.

M. Czepán · Z. Rakonczay Jr. · J. Lonovics · A. Schnúr · G. Biczó · A. Geisz · T. Wittmann · P. Hegyi (✉)
First Department of Medicine, University of Szeged,
6720 Korányi fasor 8-10,
Szeged, Hungary
e-mail: hegyi.peter@med.u-szeged.hu

G. Lázár · Z. Simonka
Department of Surgery, University of Szeged,
Szeged, Hungary

V. Venglovecz
Department of Pharmacology and Pharmacotherapy,
University of Szeged,
Szeged, Hungary

A. Varró · I. Steele · R. Dimaline · N. Lertkowit
Department of Physiology, University of Liverpool,
Liverpool, UK

DMSO	Dimethyl sulfoxide
dNTP	Deoxyribonucleotide-triphosphate
EDTA	Ethylenediamine tetra-acetic acid
EdU	5-Ethynyl-2-deoxyuridine
ER	Endoplasmic reticulum
FITC	Fluorescein isothiocyanate
GAPDH	Glyceraldehyde 3-phosphate dehydrogenase
H_2DIDS	4,4′-Diisothiocyanatodihydrostilbene-2, 2′-disulfonic acid
HaCaT cells	Human adult low calcium temperature keratinocytes
HEPES	(4-(2-Hydroxyethyl)-1-piperazine-ethanesulfonic acid
HGM	Human gastric myofibroblast
HOE-642	4-Isopropyl-3-methylsulphonylbenzoyl-guanidin methanesulphonate also known as cariporide
IGF-II	Insulin like growth factor II
IP_3	Inositol 1,4,5-trisphosphate
$J(B^-)$	Base flux
NBC	Na^+/HCO_3^- cotransporter
NF-κB	Nuclear factor kappa B
NHE	Na^+/H^+ exchanger
NMDG	N-metil D-glucamine
PBS	Phosphate buffered saline
pH_i	Intracellular pH
PIP_2	Phosphatidylinositol 4,5-bisphosphate
PKC	Protein kinase C
PLC	Phospholipase C
PP	Proton pump
RPMI	Roswell Park Memorial Institute
RT	Room temperature
RT-PCR	Reverse transcription polymerase chain reaction
SEM	Standard error of mean
SMA	Smooth muscle actin
SR	Sarcoplasmic reticulum

Introduction

Myofibroblasts, also known as activated fibroblasts, are dynamic, spindle-like cells sharing the functional characteristics of both fibrocytes and smooth muscle cells [24]. They are crucial for the production of extracellular matrix and for morphogenesis [42]; moreover, they take part in inflammatory processes related to tissue repair and in the chronic inflammation–adenoma–carcinoma sequence by secreting a broad spectrum of cytokines thereby altering the microenvironment around epithelial cells [23, 41]. To accomplish their functions, myofibroblasts migrate and proliferate in the subepithelial compartment, generating acidic metabolites and consequently protons in the cytosol [21]. Protons are removed from cells mainly by acid/base transporters located on the plasma membrane [7], thus maintaining isoionic intracellular conditions.

Although many authors have investigated the regulation of acid/base transporters and their role in migration and proliferation of epithelial cells [16, 31, 39, 45] or fibroblasts [10, 11, 48, 57], no information is available concerning the effects of acid/base transporter activities on migration and proliferation of gastric myofibroblasts.

One of the main proton extrusion mechanisms is sodium/hydrogen exchange through the Na^+/H^+ exchangers (NHEs), which are members of a transporter family comprising of ten isoforms [32, 44]. It has been demonstrated that NHE1 functions not only as a cation exchanger, but also as a modulator of intracellular signalling thereby regulating motility in different animal species including mouse [53], rat [14], dog [30], guinea pig [57] and human cells including leukocytes [49], melanoma cells [55] and hepatoma cells [67]. NHE1 activity was found to be necessary for proliferation of brain-derived pericytes [25], fibroblasts [26], lymphocytes [60] and vascular smooth muscle cells [65]. Furthermore, inhibition of NHE1 activity significantly reduces proliferation rates in vascular smooth muscle cells [65].

It has been demonstrated that gastric epithelial cells secrete matrix metalloproteinase-7 which cleaves myofibroblast-produced insulin-like growth factor binding protein-5 thereby releasing insulin-like growth factor-II (IGF-II). IGF-II acts as a potent stimulant of both epithelial and myofibroblast proliferation [36]. The muscarinic acetylcholine receptor type 3 (M3) agonist carbachol has been shown to increase NHE activity in rabbit parietal cells [3] and in guinea pig pancreatic ductal epithelial cells [59]. Many inhibitors of NHE activity have been described as a consequence of intensive research on amiloride derivatives to develop isoform-specific NHE inhibitors for use in cardiovascular care. 4-Isopropyl-3-methylsulphonylbenzoyl-guanidin methanesulphonate (HOE-642), also known as cariporide, is one of the most effective compounds, which can dose-dependently inhibit specific NHE isoforms [47].

The aim of this study was to characterize the acid/base transporters of human gastric myofibroblasts (HGMs), focusing on the possible roles of NHE1 in cell migration and proliferation.

Materials and methods

Chemicals and solutions

Chemicals and solutions used for cell culture were purchased from Sigma-Aldrich (Budapest, Hungary). All reagents for

immunocytochemistry, unless indicated otherwise, were purchased from Jackson ImmunoResearch Laboratories (West Grove, PA, USA). Chemicals and reagents for polymerase chain reaction (PCR), unless indicated otherwise, were obtained from Promega (Southampton, UK). All primers were purchased from Eurogentec (Southampton, UK).

HOE-642 (cariporide) was kindly donated by Sanofi-Aventis (Frankfurt, Germany). 2,7-Biscarboxyethyl-5(6)-carboxyfluorescein-acetoxymethylester (BCECF-AM) and HOE-642 were dissolved in dimethyl sulfoxide. The composition of solutions used for the measurements of intracellular pH (pH_i) is given in Table 1. 4-(2-Hydroxyethyl)-1-piperazine-ethanesulfonic acid (HEPES) solutions were titrated to pH 7.4 at 37°C using either NaOH or HCl. HCO_3^--buffered solutions were gassed with 95% O_2 and 5% CO_2 at 37°C.

Ethics

The study was approved by the Ethics Committee of the University of Szeged, Hungary. All surgical patients gave informed consent.

Patients, isolation and culture of HGMs

Tissue specimens from patients undergoing gastric tumour resection in the Department of Surgery, University of Szeged, Hungary were obtained intraoperatively at least 3–4 cm away from the tumour and were transported immediately to the laboratory in ice-cold media for culturing (n=3). Two other specimens from multiple organ cadaver donors were obtained similarly. Patient details can be found in Table 2. Histopathology confirmed that all specimens were normal gastric tissue samples. The isolation of HGMs was performed using a previously described method [27]. Briefly, the specimens were washed and chopped into very small pieces and were then bathed in a shaking water bath at 37°C for 15 min with 1 mM dithiothreitol. After washing, the specimens were incubated for 30 min at 37°C with 1 mM ethylenediamine tetra-acetic acid (EDTA) four times. Specimens were cultured for 1–2 weeks in Roswell Park Memorial Institute (RPMI) medium supplemented with 10% fetal bovine serum, 1% penicillin–streptomycin and 2% antibiotic–antimycotic solution. After the cells became confluent, they were trypsinized with 0.25% trypsin-EDTA and were transferred into Dulbecco's Modified Eagle's Medium (DMEM) with 4 mM L-glutamine containing 10% fetal bovine serum, 1% amino acid solution, 1% penicillin–streptomycin and 2% antibiotic–antimycotic solution. The medium was replaced every 48 h and the cells were passaged after reaching confluency up to

Table 2 Patients' details

Patient no.	Gender	Age	Diagnosis
1	Female	71	Gastric cancer
2	Male	76	Gastric cancer
3	Male	66	Gastric cancer
4	Female	42	Subarachnoidal haemorrhage
5	Male	49	Traumatic head injury

Table 1 Composition of solutions. Values are in millimolar concentrations

	HEPES	HCO_3^-	NH_4Cl HEPES	NH_4Cl HCO_3^-	Cl^--free HEPES	Cl^--free HCO_3^-	Cl^--free NH_4Cl/ HEPES	Cl^--free NH_4Cl/ HCO_3^-	Na^+-free HEPES	Na^+-free HCO_3^-	Na^+-free NH_4Cl/ HEPES	Na^+-free NH_4Cl/ HCO_3^-	High K^+-HEPES
NaCl	130	115	110	95									5
KCl	5	5	5	5					5	5	5	5	130
Na-HEPES	10	25	10										10
$CaCl_2$	1	1	1	1					1	1	1	1	1
$MgCl_2$	1	1	1	1					1	1	1	1	1
Glucose	10	10	10	10	10	10	10	10	10	10	10	10	10
NH_4Cl			20	20							20	20	
$NaHCO_3$						25		25					
HEPES					10		10		10		10		
Na-gluconate					140	115	120	95					
K_2-sulfate					2.5	2.5	2.5	2.5					
Ca-gluconate					6	6	6	6					
Mg-gluconate					1	1	1	1					
NH_4-sulfate						20		20					
NMDG									140	115	120	95	
Atropine										0.01	0.01	0.01	
Choline-HCO_3										25	25	25	

passage 10. Cell cultures were continually incubated at 37°C in a mixture of 5% CO_2 and 95% air.

Immunocytochemistry

Twelve thousand HGMs were seeded onto chamber slides and were allowed to adhere overnight. Cells were fixed using 4% paraformaldehyde for 30 min and were washed twice with phosphate buffered saline (PBS, Invitrogen, Paisley, UK). Permeabilization was performed by incubation with a filtered, PBS-based solution containing 0.2% Triton X-100 and 0.3% protease-free bovine serum albumin for 30 min. Cells were then incubated with 10% donkey serum in PBS for 30 min. After washing twice with PBS, primary antibodies were added to the chambers and the slides were incubated in moist atmosphere at 4°C, overnight. The following primary antibodies were used: anti-α-smooth muscle actin (α-SMA) antibody raised in guinea pig (1:400), anti-vimentin antibody raised in mouse (1:400), anti-cytokeratin antibody raised in mouse (1:400), anti-desmin antibody raised in mouse (1:400, all four antibodies from Dako, Denmark) and anti-NHE1, -NHE2 and -NHE3 antibodies raised in goat (1:50, purchased from Santa Cruz Biotechnology, Santa Cruz, CA, USA). Primary antibodies were removed by a sequence of washes for 10 min each with 0.14, 0.5 and 0.14 M NaCl dissolved in PBS, respectively. Slides were then incubated with secondary antibodies for 60 min in dark and moist conditions. The following secondary antibodies were used: fluorescein isothiocyanate (FITC)-conjugated anti-guinea pig secondary antibody [1:400, diluted in 10 mM HEPES, pH 7.5], Texas Red- and FITC-conjugated anti-mouse antibody (1:400) and FITC-conjugated anti-goat secondary antibody (1:400). After hybridization, slides were washed three times with PBS and were covered with 4,6-diamidino-2-phenylindole (DAPI) containing Vectashield mounting medium (Vector Laboratories, Peterborough, UK), then cover slipped.

Intracellular pH measurement

One hundred thousand HGMs were seeded onto 24-mm-diameter round glass coverslips in full media. They were allowed to recover for 24 h before experiments. Coverslips were then transferred into a perfusion chamber and mounted on an inverted microscope (Olympus, Budapest, Hungary). Cells were bathed in HEPES solution at 37°C and were loaded with 2 μM pH-sensitive fluorescent dye BCECF-AM (Invitrogen, Paisley, UK) for 20 to 30 min. Thereafter, myofibroblasts were continuously perfused with solutions at a rate of 5 to 6 ml/min and pH_i was measured by using an imaging system (CellR; Olympus, Budapest, Hungary). Cells were excited at wavelengths of 490 nm and 440 nm, and the 490/440 fluorescence emission ratio was measured at 535 nm. One pH_i measurement was recorded per second.

In situ calibration of the fluorescence signal was performed using the high K^+-nigericin technique as previously described [22, 58]. The pH of high K^+–HEPES solution supplemented with 10 μM nigericin was set to 6.8 or 7.4 at 37°C, then cells loaded with BCECF were superfused by these solutions and the 490/440 fluorescence ratio was recorded. Multiple-point calibrations, i.e. sequential BCECF pH measurements (with high K^+–HEPES–nigericin solutions ranging pH from 6.2 by 0.4 step to 8.2) were performed to confirm data accuracy. Linear projections were made from the steady-state fluorescence pH data during high K^+-nigericin superfusion with known pH. Adaptation of projections to the resting fluorescence data of unknown pH_i in standard HEPES solution results in accurate resting pH_i.

In order to characterize the acid/base transporters, we used ion-withdrawal technique, and ammonium pulse technique in HEPES- and HCO_3^-/CO_2-buffered solutions. Initial rates (first 30–60 s) of recovery from acidosis were calculated by linear regression.

Determination of buffering capacity and calculation of base fluxes

The intrinsic buffering capacity (β_i) of HGMs was estimated by the NH_4^+ pre-pulse technique [62]. β_i refers to the ability of intrinsic cellular components (excluding the bicarbonate buffer system) to buffer changes of pH_i. Briefly, HGMs were exposed to various concentrations of NH_4Cl while Na^+ and HCO_3^- were omitted from the solution to block the Na^+-dependent pH regulatory mechanisms. β_i was estimated by the Henderson–Hasselbalch equation. The total buffering capacity (β_{total}) was calculated as $\beta_{total}=\beta_i+\beta_{HCO3^-}=\beta_i+2.3\times[HCO_3^-]_i$, where β_{HCO3^-} is the buffering capacity of the HCO_3^-/CO_2 system and $[HCO_3]_i$ is the intracellular concentration of HCO_3^-. Transmembrane base flux [$J(B^-)$] was calculated by using the equation $J(B^-)=dpH/dt\times\beta_{total}$. The β_{total} value used in the calculation of $J(B^-)$ was obtained from Fig. 2b by using the pH_i value at the start of the 30-s period over which dpH/dt was measured.

Reverse transcription polymerase chain reaction

RNA was isolated from myofibroblast cultures using a Qiagen RNEasy Mini Kit (Qiagen House, Crawly, UK) according to the manufacturer's instructions; human kidney RNA was isolated from whole tissue from surgical specimens utilizing TRIzol reagent. RNA was reverse transcribed to cDNA and RNA/primer annealing was performed with 0.5 μg oligo-dT primer at 65°C for 5 min. After cooling, samples were reverse transcribed in a final reaction volume of 30 μl containing the annealed RNA/primer set, 5× AMV (avian

myeloblastosis virus) buffer, 1.25 mM dNTP (deoxyribonucleotide-triphosphates) mix, 20 unit RNAse inhibitor and 15 unit AMV-RT (AMV-reverse transcriptase). Reactions were incubated at 42°C for 1 h; enzymes were inactivated at 85°C for 5 min. cDNA (1 μl) was used as template for each PCR in a final volume of 25 μl, containing 10× master mix Taq-buffer, 10 nM dNTPs, 2.5 unit Taq-polymerase and 1 μM NHE primer sets. The sequence of NHE primers is given in Table 3. PCR settings were as follows: denaturation at 95°C for 15 s, annealing at 60°C for 15 s, extension at 72°C for 45 s, 30 cycles. PCR products and DNA HyperLadderPlus (BioLine, Taunton, USA) were run on a 0.8% agarose gel containing 0.005% ethidium bromide in Tris-buffered EDTA solution at 80 V, then the gel was illuminated in a BioRad UV (ultraviolet) chamber and photographs were taken.

Immunoblot analysis

Confluent cells (3,000,000 cells at least) were washed with PBS after removing the media and were then incubated with 100 mM EDTA for 15 min. After centrifugation (500×*g*, 8 min), the supernatant was gently removed and was lysed with RIPA (radio-immuno precipitation assay) buffer supplemented with 1% protease inhibitor cocktail (Calbiochem-Merck Chemicals, Darmstadt, Germany). Samples were vortexed and frozen in liquid nitrogen for a few seconds then centrifuged at 11,000×*g* for 10 min at 4°C. The protein concentrations of supernatants containing whole cell protein lysates were determined by using Bradford's reagent. Samples were heat treated at 30°C for 30 min and 100 μg protein was electrophoresed on 8% sodium dodecylsulfate-polyacrylamide gels according to the method of Laemmli using a Hoefer Mighty Small II instrument (Harvard Bioscience Inc., Massachusetts, USA). After separation, proteins were blotted to matching-sized nitrocellulose membrane for 60 min at 100 V. Membranes were blocked in 5% nonfat dry milk for 1 h and were incubated with primary antibodies (1:100 for NHE) overnight at 4°C on a rocker. The same NHE primary antibodies were used as for immunocytochemistry. Primary antibodies were removed by washing with TBST for 3× 10 min. HRP-conjugated secondary antibodies (Dako, Denmark) were applied for 60 min at RT on a rocker. After 3×10 min TBST wash, the immunoreactive protein was visualized by enhanced chemiluminescence. Remaining antibodies were removed by washing with TBST, then anti-glyceraldehyde 3-phosphate dehydrogenase antibody (Dako, Denmark) was added to the membrane for 60 min at RT. Secondary antibody (1:10,000) was also applied for 60 min at RT then signals were recorded as described earlier.

Table 3 NHE primer sequences

Primer name	Sequence (5' - 3')
NHE1 forward	CCT-CTC-TGG-GTG-GAG-AAG-CT
NHE1 reverse	CCC-AGG-AAC-GAC-ACA-GAA-AG
NHE2 forward	CCA-TGG-AAC-CAC-TGG-GCA-AC
NHE2 reverse	TGC-AGG-GGG-AGA-CTT-CTC-AT
NHE3 forward	TCC-AAG-TCG-ACC-AAG-CTG-GG
NHE3 reverse	AAG-GCC-TCG-TCC-GGA-GAA-AA

Migration assays

HGMs (125,000 cells) were seeded onto six-well plates and allowed to adhere overnight in full media. On the following day, the confluent monolayer was gently scratched using a P2 tip. Only the wells containing even-sided and sharp-edged wounds were used for experiments. After gentle washing for three times with serum-free media, wounds were measured and photographed under inverted light microscope. Reagents were then added to the wells in serum-free media in all of the experiments and plates were incubated in CO_2 incubator at 37°C for 24 h. Migration was evaluated by counting the cells in the same area of the wound after 12 and 24 h as reported earlier [43].

Proliferation assays

Myofibroblasts (50,000 cells) were seeded onto cover glasses. After overnight incubation, HGMs were synchronized by incubation for 30 h in serum-free media. Thereafter, 10 μM 5-ethynyl-2-deoxyuridine (EdU; Alexa Fluor 488 Imaging Kit, Invitrogen, Oregon, USA; for further details, see reference [50]) was added to the cells for overnight incubation with or without treatment. After incubation, the manufacturer's protocol was applied to fix and permeabilize the cells and to detect EdU incorporation. We used DAPI to detect nuclear staining. The proliferation rate was calculated by normalizing the number of EdU positive cells to the DAPI-stained cells in 10 fields at 20x magnification.

Statistical analysis

Values are expressed as means±standard error of mean (SEM). Statistical analyses were performed using non-parametric Kruskal–Wallis tests with post-hoc Wilcoxon tests for pairwise comparisons and Bonferroni correction to test post-hoc significance. $p<0.05$ was accepted as significant. n numbers are given as follows: n = number of patients/number of independent experiments per patient.

Results

Identification of myofibroblasts

Cells showed positive staining for α-SMA and vimentin but not for cytokeratin and desmin, which are characteristics of myofibroblasts (Fig. 1). The purity of the HGM cell cultures was ~100%. As positive controls for cytokeratin and desmin antibodies, we used CAPAN-1 (human pancreatic adenocarcinoma cell line) cells and cultured human high grade pancreatic neuroendocrine carcinoma cells, respectively. In both cases, appropriate localisation was demonstrated (Fig. 1).

Determination of the resting pH_i of HGMs

The multiple-point calibration technique utilizing high K^+–HEPES/nigericin solution was used to determine the resting pH_i of HGMs. Our experiments showed that the resting pH_i of HGMs in HEPES solution was 7.09±0.02 (Fig. 2).

Characterization of the acid/base transporters of HGMs

Next we tried to identify the functionally active acid/base transporters expressed on the plasma membrane of HGMs. Na^+ withdrawal from the standard HEPES solution

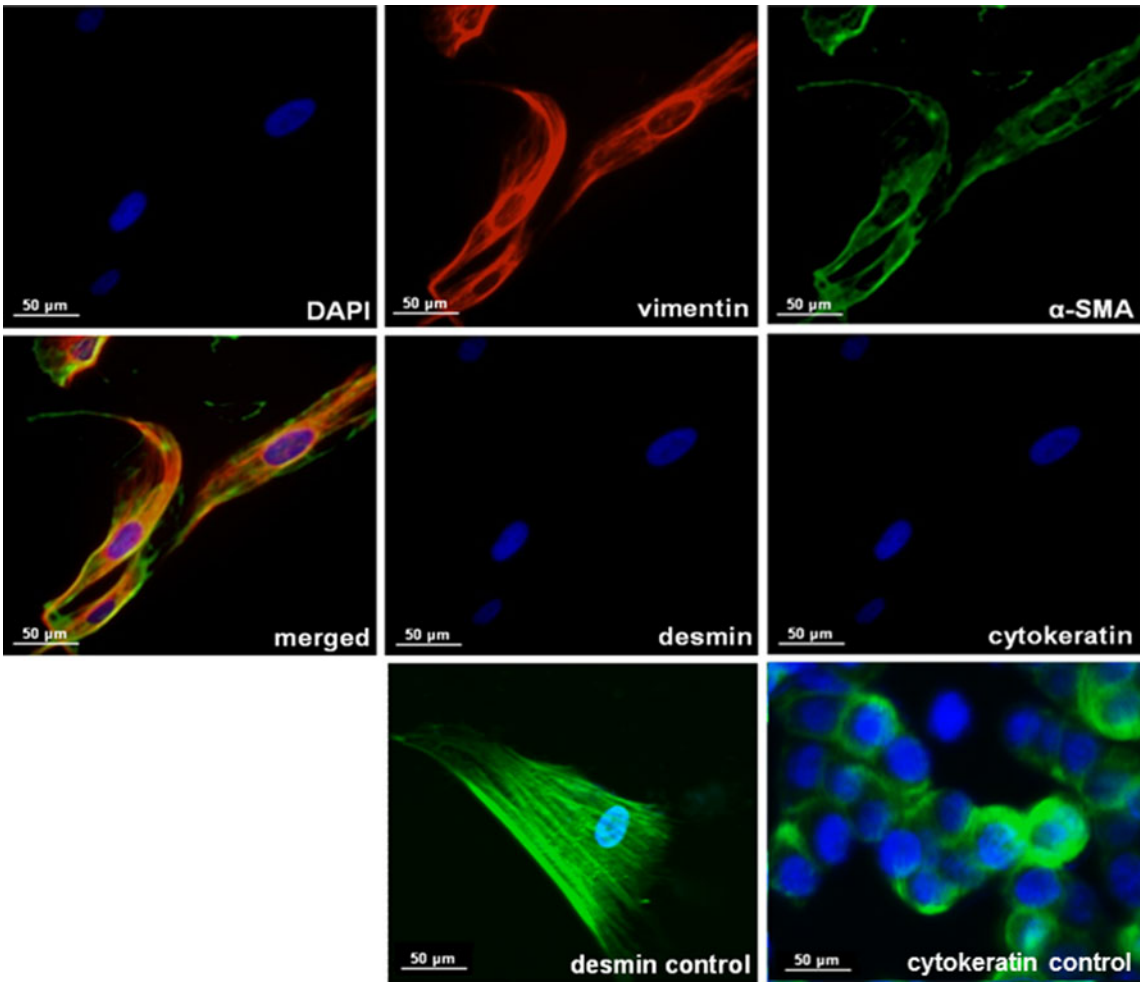

Fig. 1 Immunocytochemical identification of cell cultures. Cells isolated from human gastric samples were grown on chamber slides and were subjected to immunocytochemical analysis of vimentin and α-smooth muscle actin (α-SMA) expression as specific markers of myofibroblasts. Cytokeratin and desmin antibodies were used for detecting epithelial and muscle cells, respectively. Nuclei were counterstained with DAPI (*blue*). Vimentin (*red*) and α-SMA (*green*) verified the presence of myofibroblasts, whereas no epithelial or smooth muscle cells were detected (n=5/1–2). Control stainings were performed to test the desmin and cytokeratin antibodies. Cultured cancer cells (from human high grade pancreatic neuroendocrine carcinoma) were used as positive controls for desmin (*green staining*, n=1). To test the cytokeratin antibody, control staining was performed on CAPAN-1 (human pancreatic adenocarcinoma cell line) cells. *Green staining* shows cytokeratin; *blue staining* shows DAPI (n=1)

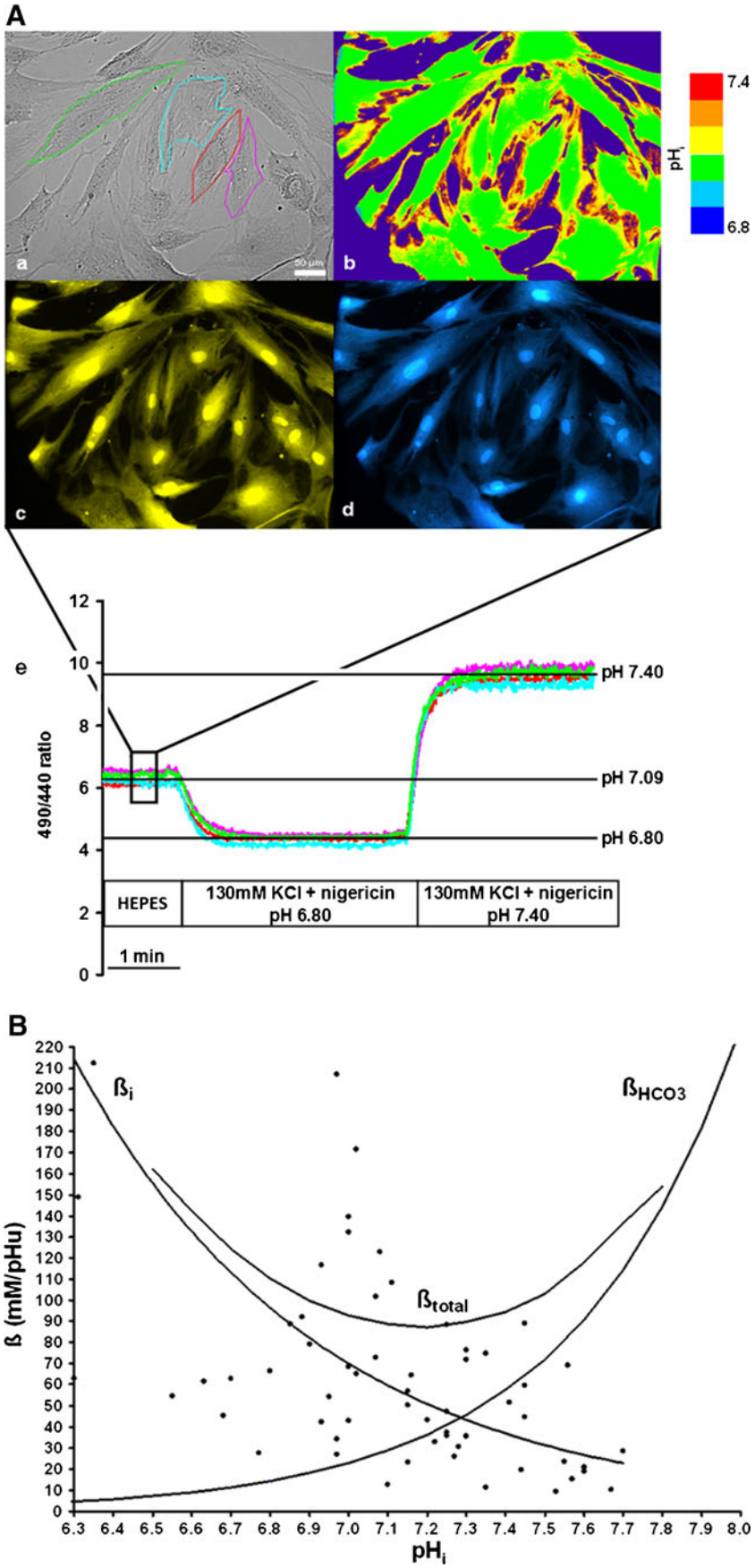

Fig. 2 The resting pH_i of gastric myofibroblasts and measurement of buffering capacity. **A** Human gastric myofibroblasts (HGMs, 100,000) were seeded onto cover glass to form monolayers. Cells were allowed to recover for 24 h. **a** Phase contrast image of myofibroblasts is shown. Four to seven cells as regions of interests (ROIs) were marked. **b** Thermal-adjusted image is shown to demonstrate homogenous BCECF dye distribution. Color coding shows the pH_i; **c** 490 and **d** 440 nm fluorescent images are also shown. **e** Cells were excited at wavelengths of 490 and 440 nm after loading the cells with the pH-sensitive fluorescent dye 2 μM BCECF-AM, and the 490:440 fluorescence emission ratio was measured at 535 nm. Cells were exposed to continuous perfusion with nigericin/high K^+–HEPES solutions of pH 6.80 and 7.40. The resting pH_i was calculated by multiple-point calibration (n=5/5–6). The figure shows a representative calibration curve; the mean resting pH_i in standard HEPES solution was 7.09±0.02. **B** The buffering capacity of HGMs was determined by exposing the cells to various concentrations of NH_4Cl while Na^+ and HCO_3^- were omitted from the solution to block Na^+-dependent pH regulatory mechanisms. The intrinsic buffering capacity (β_i) at different pH_i (*black circle*, n=85) was estimated by the Henderson–Hasselbalch equation. Regression analysis was performed using the curve-fitting protocol in Excel. The total buffering capacity (β_{total}) was calculated as $\beta_{total}=\beta_i+\beta HCO_3^-=\beta_i+2.3\times[HCO_3^-]_i$, where βHCO_3^- is the buffering capacity of the HCO_3^-/CO_2 system and $[HCO_3]_i$ is the intracellular concentration of HCO_3^-

caused strong reversible acidification suggesting the presence of an active Na^+-dependent H^+ efflux mechanism (Fig. 3a).

Switching the standard HEPES solution to standard HCO_3^-/CO_2 solution caused rapid intracellular acidification, most probably due to CO_2 diffusion into the cells. Thereafter, a small pH_i recovery was observed suggesting a HCO_3^- influx and/or H^+ efflux mechanism (Fig. 3b). In order to determine the Na^+ dependency of this HCO_3^- influx/H^+ efflux mechanism, the same experiment was performed in Na^+-free conditions (Fig. 3c). Since no recovery was found in the presence of HCO_3^-/CO_2 in Na^+-free solution, we can assume that the HCO_3^- influx/H^+ efflux mechanism in HGMs is Na^+-dependent. These results indicate that HGMs express functionally active NHE and/or NBC.

Next we tested whether HGMs contain functionally active anion exchangers (AE). Cl^- removal from the standard HCO_3^-/CO_2 solution caused reversible alkalization suggesting the presence of a Cl^--dependent HCO_3^- efflux mechanism (Fig. 3d). Importantly, omitting HCO_3^- from the extracellular solution in combination with Cl^- removal resulted in no significant change in pH_i (Fig. 3e). This indicates that HGMs express functionally active AE.

To confirm these findings, the activities of acid/base transporters were also investigated by the ammonium pulse technique. Exposure of HGMs to 20 mM NH_4Cl induced an immediate rise in pH_i due to the rapid entry of the lipophilic base, NH_3, into the cells, which binds intracellular protons generating NH_4^+ and causing alkalization. The recovery from this alkali load is promoted by AEs in the

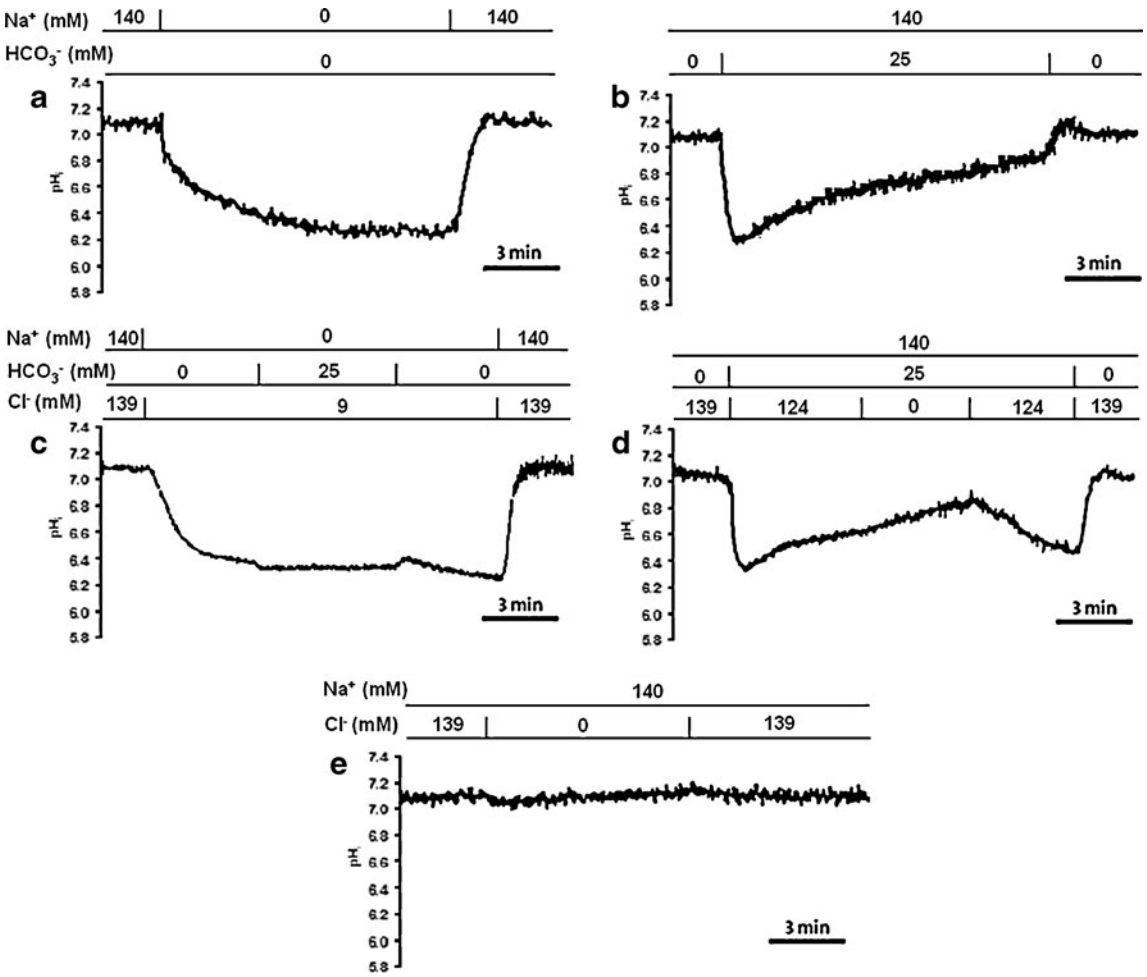

Fig. 3 Na^+-dependent HCO_3^- influx and Cl^--dependent HCO_3^- efflux mechanisms are present in HGMs. Representative pH_i curves of HGMs are shown. **a** The sudden removal of extracellular Na^+ from the standard HEPES solution caused rapid acidification, which was reversed by the re-addition of the ion. **b** Administration of HCO_3^-/CO_2-buffered solution after standard HEPES solution caused acidification of pH_i followed by alkalization (HCO_3^- influx). **c** Switching from Na^+-free HEPES solution to Na^+-free HCO_3^-/CO_2-buffered solution caused acidification, but no pH_i recovery was seen. **d** In HCO_3^-/CO_2-buffered solution, Cl^- removal resulted in alkalization of pH_i followed by a complete recovery after re-addition of Cl^-. **e** Cl^- removal from the standard HEPES solution did not alter significantly the pH_i, and it reached again the resting value before re-addition of Cl^- (n=5/5–6)

presence of HCO_3^- and Cl^- in the extracellular solution. In support of this, the recovery from alkali load was much steeper in the presence of HCO_3^-/CO_2 (Fig. 4c, d) compared with the absence (Fig. 4a, b) of HCO_3^-/CO_2. It is worth mentioning that the slow uptake of NH_4^+ is also a prerequisite for the acid loading. After the removal of NH_4Cl, NH_3 diffuses out of the cell, therefore facilitating the dissociation of intracellular NH_4^+ to H^+ and NH_3, which rapidly decreases pH_i. Thereafter, the pH_i starts to recover after this acidification owing to activation of pH_i regulatory mechanisms namely the NHE, NBC and proton pumps (PP; Fig. 4c). In the absence of extracellular HCO_3^- and in the presence of Na^+, the recovery from acidosis reflects the activity of NHE and PP (Fig. 4a). However, the lack of recovery in the absence of Na^+ excludes functionally active PP in HGMs (Fig. 4b). The addition of HCO_3^- to the extracellular solution strongly increases the pH_i recovery from acidosis (Fig. 4c). Since there is no pH_i recovery from acidosis in Na^+- and HCO_3^--free solution (Fig. 4d), it is assumed that the HCO_3^- influx mechanism is most probably accomplished by the Na^+-dependent NBC. Therefore, we tested the effects of the NBC inhibitor H_2DIDS in 0.5 mM concentration and the NHE1 and NHE2 inhibitor HOE-642 at 50 μM on the recovery rates during and following an acid load in HCO_3^-/CO_2-buffered solution (Fig. 4). We calculated $J(B^-)$ from these and from the above experiments (Fig. 4) and found that NBC inhibition greatly reduced pH_i recovery after acid load

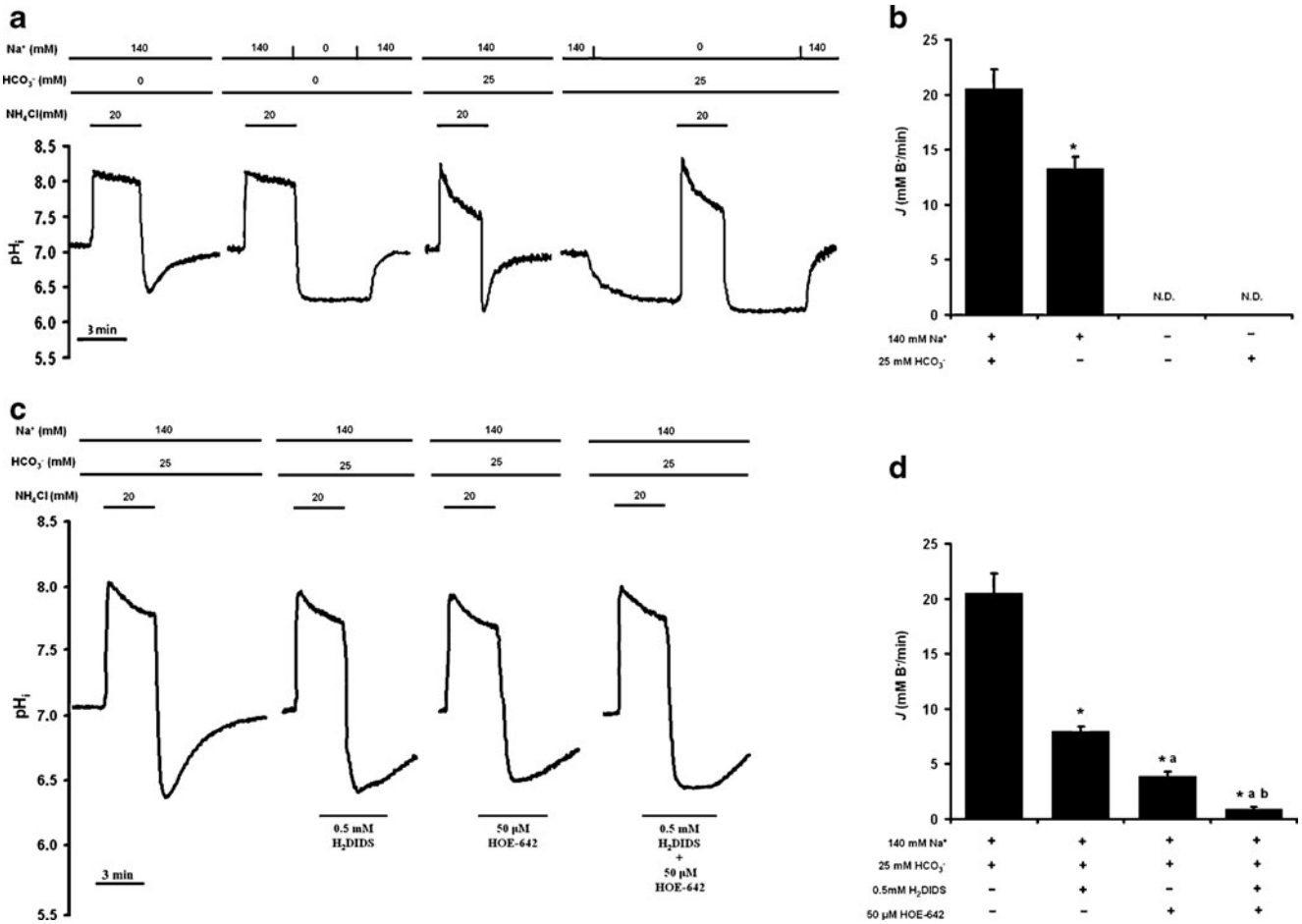

Fig. 4 Na^+-dependent H^+ efflux and Na^+-dependent HCO_3^- influx were detected in HGMs **a** Representative pH_i curves of HGMs are shown. Cells were exposed to 20 mM NH_4Cl pulse in HEPES-buffered solution for 3 min. After the acid load, recovery of pH_i could be observed. However, the administration of Na^+-free HEPES solution after the ammonium pulse inhibited pH_i recovery after the acid load. The same technique was applied in HCO_3^-/CO_2-buffered solution. Note that the initial phase of the pH_i recovery during the ammonium pulse is quicker than in HEPES solution and the recovery phase after the acid load is much steeper. Also in Na^+-free HCO_3^-/CO_2-buffered solution, no recovery could be seen after the ammonium pulse. **b** The *bar chart* shows the summary data of base fluxes after recoveries from acid load. Values are shown as means±SEM (n=5/10–12). *p<0.05 vs. 25 mM HCO_3^-. **c** Inhibition of Na^+/HCO_3^- co-transporter (NBC) with 0.5 mM H_2DIDS and/or inhibition of NHE1–2 with 50 μM HOE-642 during acid load in HCO_3^-/CO_2-buffered solution is shown. **d** The rates of recovery from acid load were determined and base fluxes were calculated from the experiments shown above. Absolute values are displayed for comparison (n=5/1–2); values are shown as means±SEM. *p<0.05 vs. 140 mM Na^+, 25 mM HCO_3^-; **a** p<0.05 vs. 25 mM HCO_3^-+0.5 mM H_2DIDS; **b** p<0.05 vs. 25 mM HCO_3^-+50 μM HOE-642

(20.54±1.76 vs. 7.99±0.39 mM B^-/min) revealing high transporter activity. 50 μM HOE-642 further decreased the recovery rate from acidosis (7.99±0.39 vs. 3.91±0.41 mM B^-/min) indicating high NHE1 and NHE2 activities. Simultaneous administration of the two inhibitors resulted in very slow recovery (0.98±0.09 mM B^-/min). Without HCO_3^-/CO_2 buffering in standard HEPES solution, cells showed much slower recovery than with bicarbonate buffering (13.36±0.41 vs. 20.54±1.76 mM B^-/min). As seen on Fig. 4b, d, eliminating Na^+ from the extracellular solution inhibited the cells to recover from an acid load in both HCO_3^-/CO_2-buffered solution and in standard HEPES solution.

Next, we focused our attention on characterizing the NHE isoforms expressed on the plasma membrane of HGMs. The HGMs were acid-loaded by exposure to a 3-min pulse of 20 mM NH_4Cl in HEPES solution followed by a 5-min exposure to Na^+-free HEPES solution (Fig. 5a). Since neither Na^+ nor HCO_3^- was present in the extracellular solution, acid/base transporters were inhibited and the pH_i was adjusted to a stable acidic level. NHE activity was induced by the re-addition of extracellular Na^+ and the activity of NHEs was determined by measuring the initial rates of pH_i recovery over the first 60 s (60 data points). The activities of the different NHE isoforms were determined by using the isoform selective NHE inhibitor HOE-642 (cariporide). At 1 μM HOE642 inhibits NHE1 whereas at 50 μM it inhibits both NHE1 and NHE2, but not NHE3 [69].

Our data indicate that NHE1 is responsible for about 85% of the Na^+/H^+ exchange activity, whereas NHE2 activity is around 10% and the remaining NHE activity is approximately 5% (Fig. 5b). Of course, we cannot exclude the possibility of the involvement of other NHEs. However, even if they were expressed, they would only have marginal influence on H^+ efflux.

mRNA and protein expression of NHE1-3 in HGMs

Based on results of the functional measurements, we investigated the presence of NHE transporters at the mRNA and protein levels. Reverse transcription polymerase chain reaction confirmed the expression of NHE1, NHE2 and NHE3 (Fig. 5c). We also analysed the expression of NHE isoforms in HGMs by Western blot. We found that NHE1 is present in HGMs, but we were unable to show NHE2 and NHE3 expression. Positive controls (human kidney) confirmed that the antibodies used for these studies were fit for purpose (Fig. 5d). We speculate that NHE2 and NHE3 protein abundance is low in our lysates so below the limit of detection. Using immunocytochemistry, we demonstrated NHE1-3 localisation to the plasma membrane of HGMs (Fig. 5e).

IGF-II and carbachol increases NHE activity

We then investigated the effects of IGF-II and carbachol on the activities of NHEs. Importantly, both IGF-II and carbachol dose-dependently stimulated NHE activity. Carbachol concentrations were tested in range of 1–1,000 μM. Carbachol (10 μM) had the greatest effect on NHE activity. 100 ng/ml IGF-II was more effective than 10 ng/ml in increasing NHE activity (Fig. 6).

Migration of HGMs is stimulated by carbachol and IGF-II

Next, we investigated the effects of carbachol and IGF-II on cell migration and the role of NHE1 in migration of HGMs using scratch wound assay. We found that both 100 ng/ml IGF-II and 10 μM carbachol stimulate the migration of HGMs (Fig. 7*)*. Inhibition of NHE1 by HOE-642 had no effect on unstimulated cell migration, but it significantly inhibited both carbachol- and IGF-II-stimulated migration (by 29±7% and 33±8%, respectively).

IGF-II increases proliferation in an NHE1-dependent manner

Finally, we tested the effects of HOE-642, IGF-II and carbachol on HGM proliferation. EdU incorporation assays showed that 100 ng/ml IGF-II increased cell proliferation over two-fold. Carbachol and/or HOE-642 did not affect proliferation. However, NHE1 inhibition by 1 μM HOE-642 completely blocked the stimulatory effect of IGF-II on cell proliferation (Fig. 8).

Discussion

In this study, we have characterized the pH_i regulatory mechanisms of HGMs for the first time. The data demonstrate that NHE1 activity contributes to IGF-II- and carbachol-stimulated migration and that it is obligatory for IGF-II-induced proliferation of HGMs.

The resting pH_i of HGMs, 7.09±0.02, is similar to that in fibroblasts [12, 28, 46] and smooth muscle cells [64]. Myofibroblasts displayed three main acid/base transporters, namely NBC, AE and NHE. These are also the main mechanisms regulating pH_i in fibroblasts [2, 12, 29] and in smooth muscle cells [15]. Thus, AE decreases, whereas, NBC and NHE increase pH_i. $J(B^-)$ calculations revealed high NBC and high NHE activities which are the main transporters aiding recovery from an acid load in HGMs. In the present study we chose to focus on the roles of NHEs.

Carbachol (10 μM) strongly stimulated NHE activity of HGMs. It has been shown that carbachol also increases NHE (and AE) activity in lacrimal gland epithelia [59] and in rabbit

parietal cells [3]. In the latter study, carbachol strongly increased NHE activity and its effect was completely blocked by 1 μM HOE-642 suggesting the involvement of NHE1. Atropine or intracellular Ca^{2+} chelation inhibited the activation of NHE indicating a typical muscarinic receptor effect with a Ca^{2+}-dependent signalling pathway [4, 59]. In the

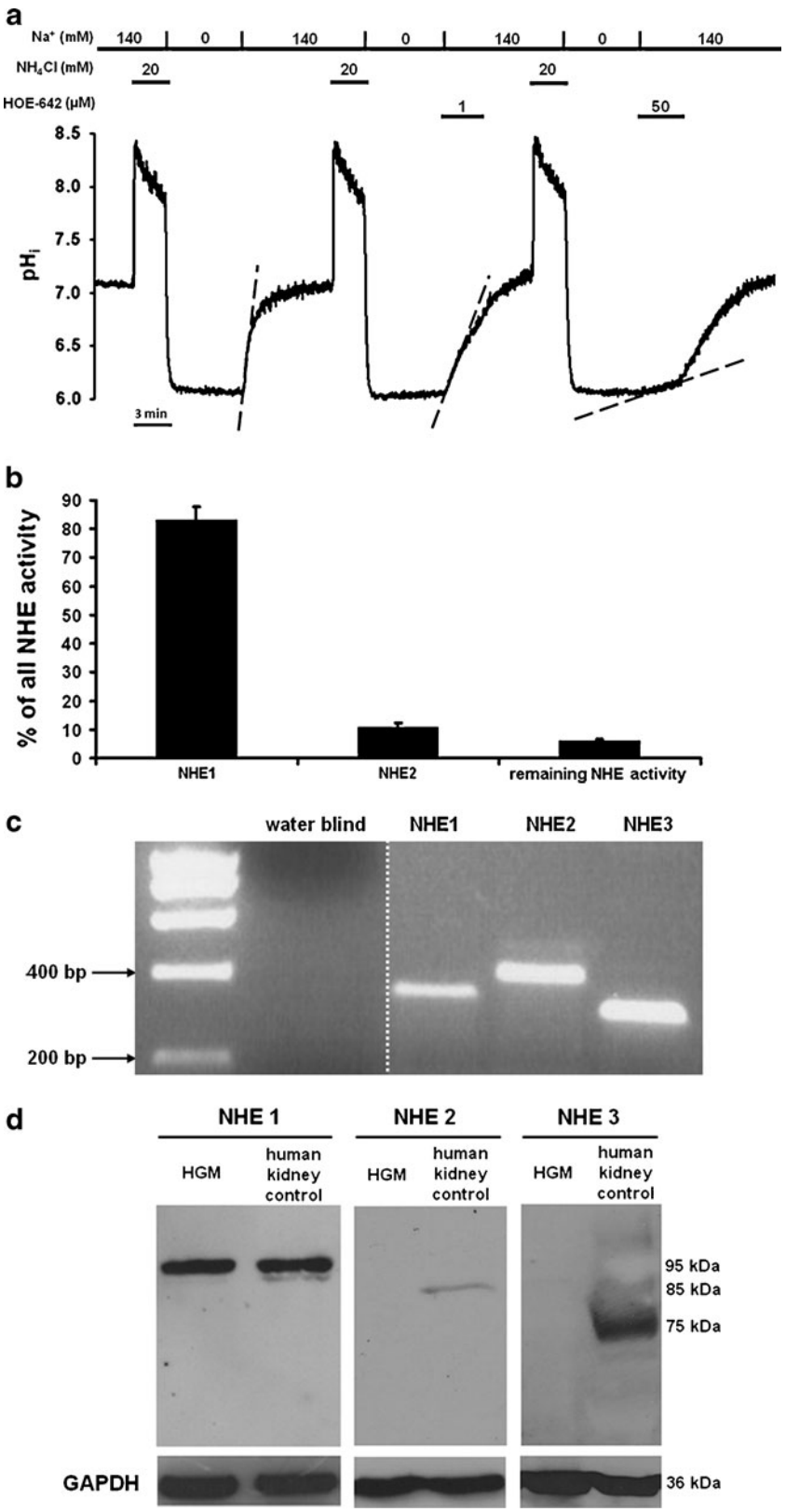

Fig. 5 Identification of NHE isoforms. **a** Representative pH_i curves of HGMs are shown. Cells were loaded with acid by using the ammonium pulse technique. After Na^+ withdrawal, the isoform-selective NHE inhibitor HOE-642 was administered in 1 μM (inhibits NHE1) or 50 μM (inhibits NHE1 and NHE2) concentration, together with re-addition of Na^+. The initial rates of the pH_i recovery during HOE-642 administration were calculated by linear regression analysis to determine the activity of NHE isoforms. **b** The *bar chart* demonstrates that NHE1 is responsible for 83 ±5%, NHE2 for 11±1% and other isoforms for 4.5±0.8% of all Na^+/H^+ exchange activity. Data are shown as means±SEM (n=5/5–6). **c** Reverse transcription PCR confirmed the expression of NHE1–3 isoforms (n=3/6–7). Expected PCR product sizes are as follows: NHE1, 341 bp; NHE2, 407 bp; NHE3, 299 bp. In water blind, we used water as template. **d** Immunoblot analysis showing different NHE isoforms in HGMs and human kidney controls. Protein sizes are as follows: NHE1, 95 kDa; NHE2, 85 kDa; NHE3, 75 kDa; GAPDH, 36 kDa (n=4–5/3–10). **e** NHE1, NHE2 and NHE3 were identified by immunocytochemistry in the plasma membrane of HGMs. Nuclei were counterstained with DAPI (*blue staining*). No specific staining was detected when the primary antibody was omitted (n=3/1–2)

Fig. 5 (continued)

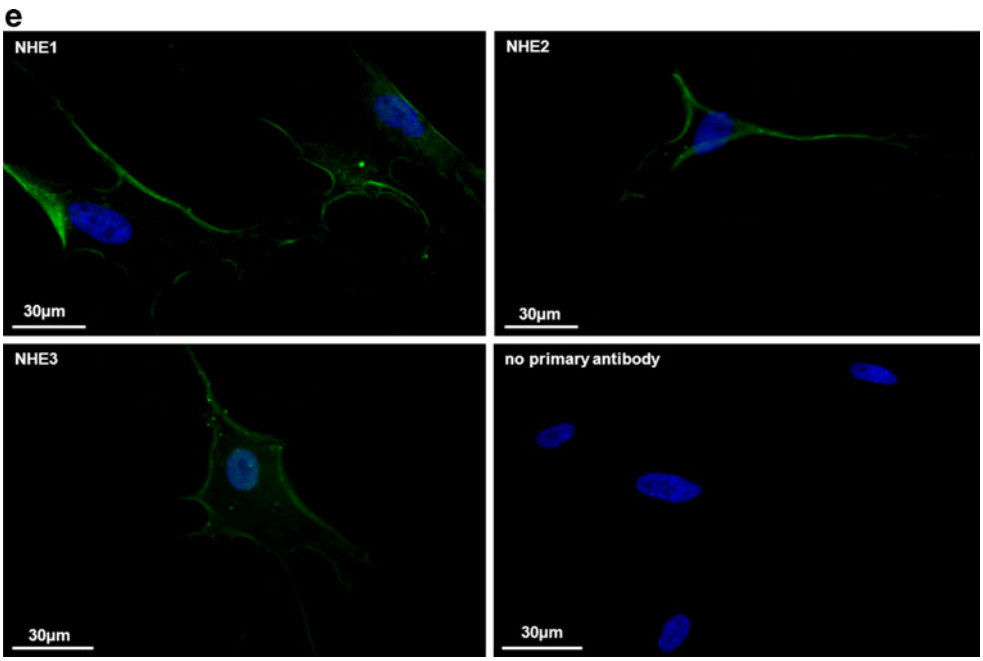

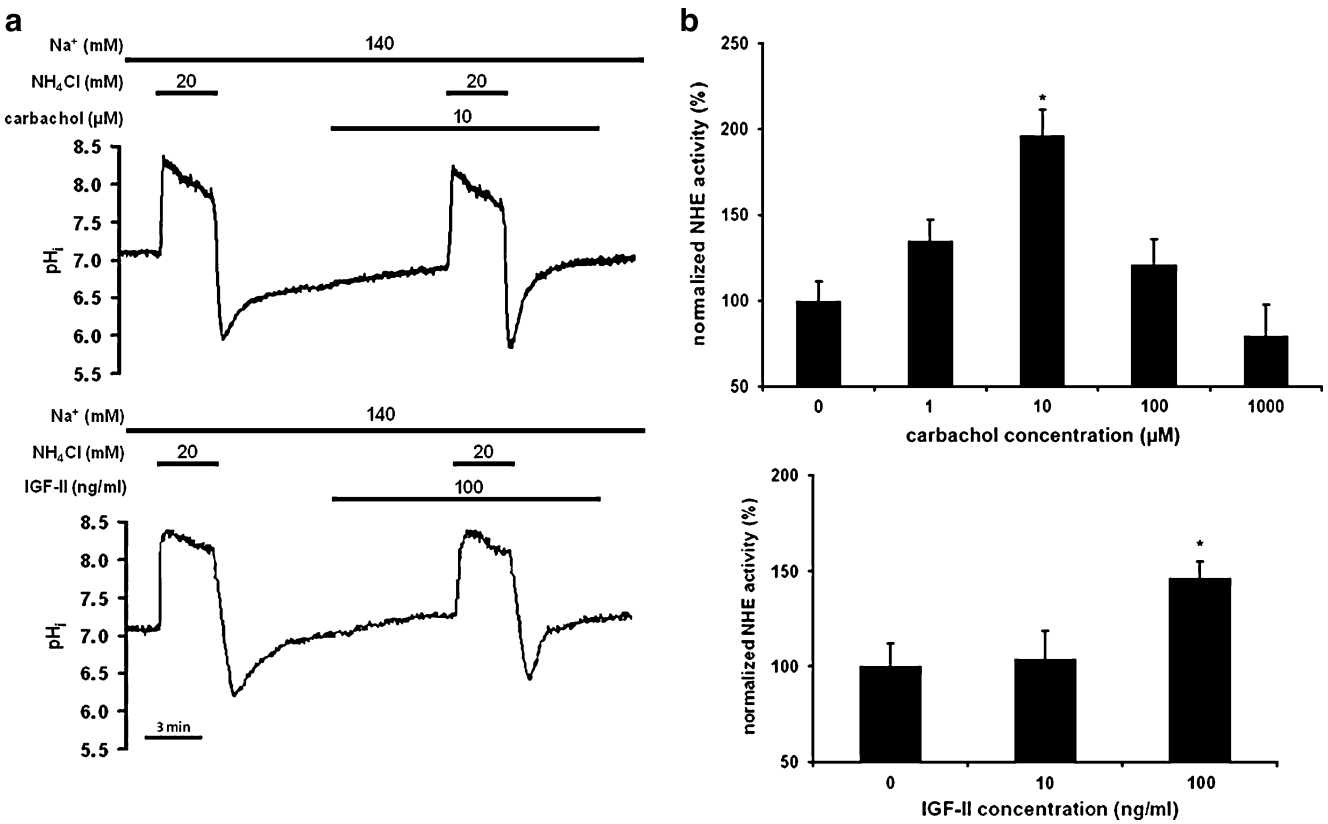

Fig. 6 The effects of carbachol and IGF-II on NHE activity. **a** Representative pH_i curves of HGMs are shown. We tested different carbachol and IGF-II concentrations on NHE activity using the ammonium pulse technique. The figure shows the effects of 10 µM carbachol and 100 ng/ml IGF-II treatment. Note that the changes in the rates of pH_i recovery from acidosis during treatment are much higher compared with the recovery rates without IGF-II or carbachol treatment. **b** The *bar diagram* shows the summary data obtained from the above mentioned experiments. Administration of 10 µM carbachol and 100 ng/ml IGF-II significantly increased NHE activity. Values are normalized to the basal NHE activity. Data are shown as means±SEM (n=5/5–6). *p<0.05 vs. 0 µM or 0 ng/ml

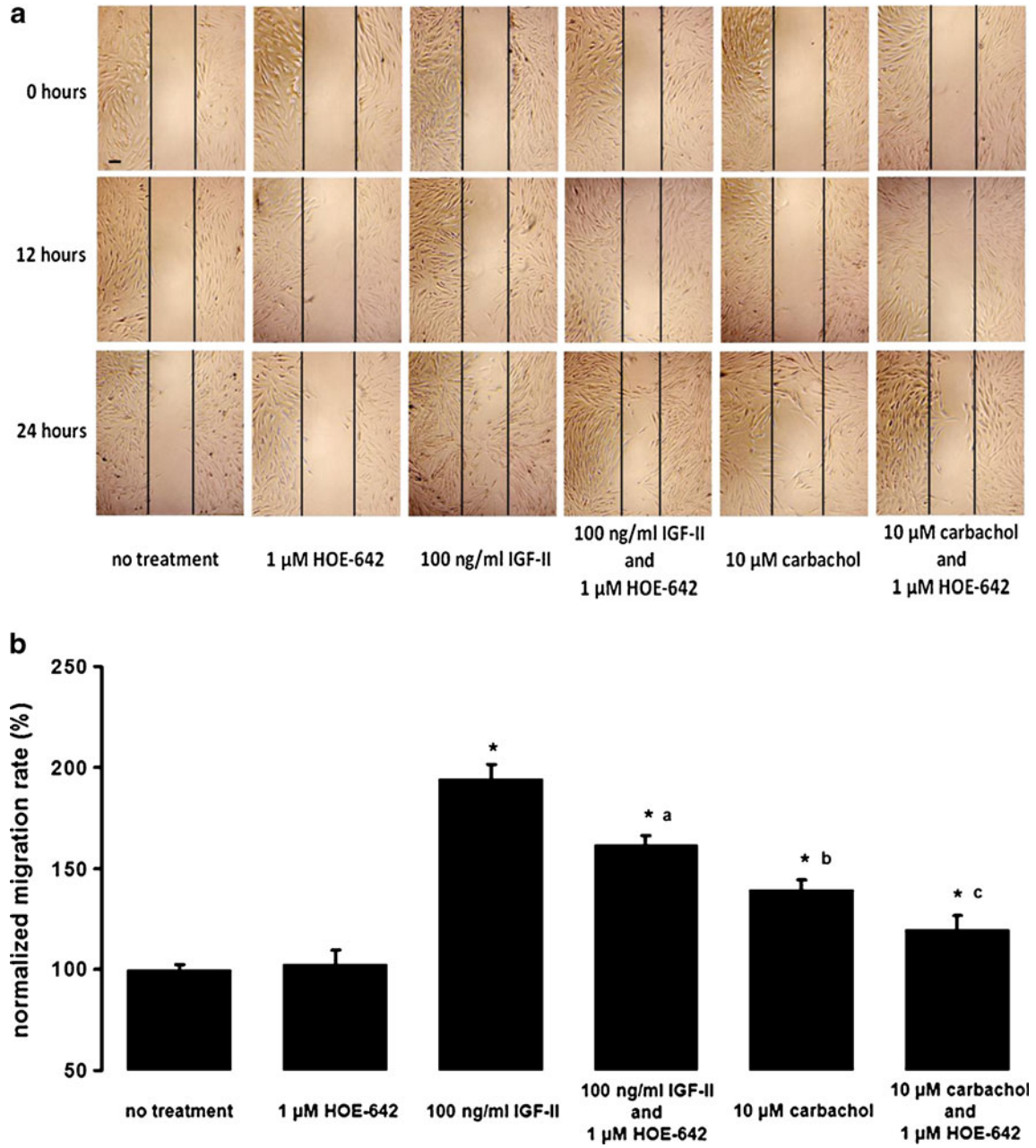

Fig. 7 Carbachol and IGF-II treatment increased migration rates of HGMs in a NHE1-dependent manner. **a** HGMs (100,000) were cultured in six-well plates. After reaching confluency, the monolayer was wounded by a P2 tip along an oriented line in the middle of the well and detached cells were removed by washing with serum-free media. Only wounds with sharp and even edges were used for experiments. Reagents were added to the wells in serum-free media and the plate was incubated for 24 h at 37°C, 5% CO_2. Images were taken at 0, 12 and 24 h from representative areas. Cells were treated with or without 10 µM carbachol or 100 ng/ml IGF-II, and/or 1 µM HOE-642 and cells which migrated into the wound were counted at 12 and 24 h. The *scale bar* on the first picture represents 100 µm. **b** The *bar chart* shows the migration rates normalized to the basal rate at 24 h. Values are shown as means±SEM, $n=5/1–3$; *$p<0.05$ vs. no treatment, *a* $p<0.05$ vs 100 ng/ml IGF-II, *b* $p<0.05$ vs 100 ng/ml IGF-II and 1 µM HOE-642, *c* $p<0.05$ vs 10 µM carbachol

latter publications, the authors suggested that Ca^{2+}-dependent stimulation causes a selective activation of NHE1, whereas cAMP-dependent stimulation with forskolin-activated NHE1, NHE2 and more strongly NHE4. In HCO_3^--containing solution, pH_i did not change indicating that activation of NHE and AE is primarily volume regulatory mechanisms, and they speculated that the physiological significance of secretagogue-induced NHE activity may be related to volume and not to pH_i regulation during acid secretion of rabbit parietal cells [3].

IGF-II, which has been shown to stimulate migration and proliferation of many cell types including myofibroblasts

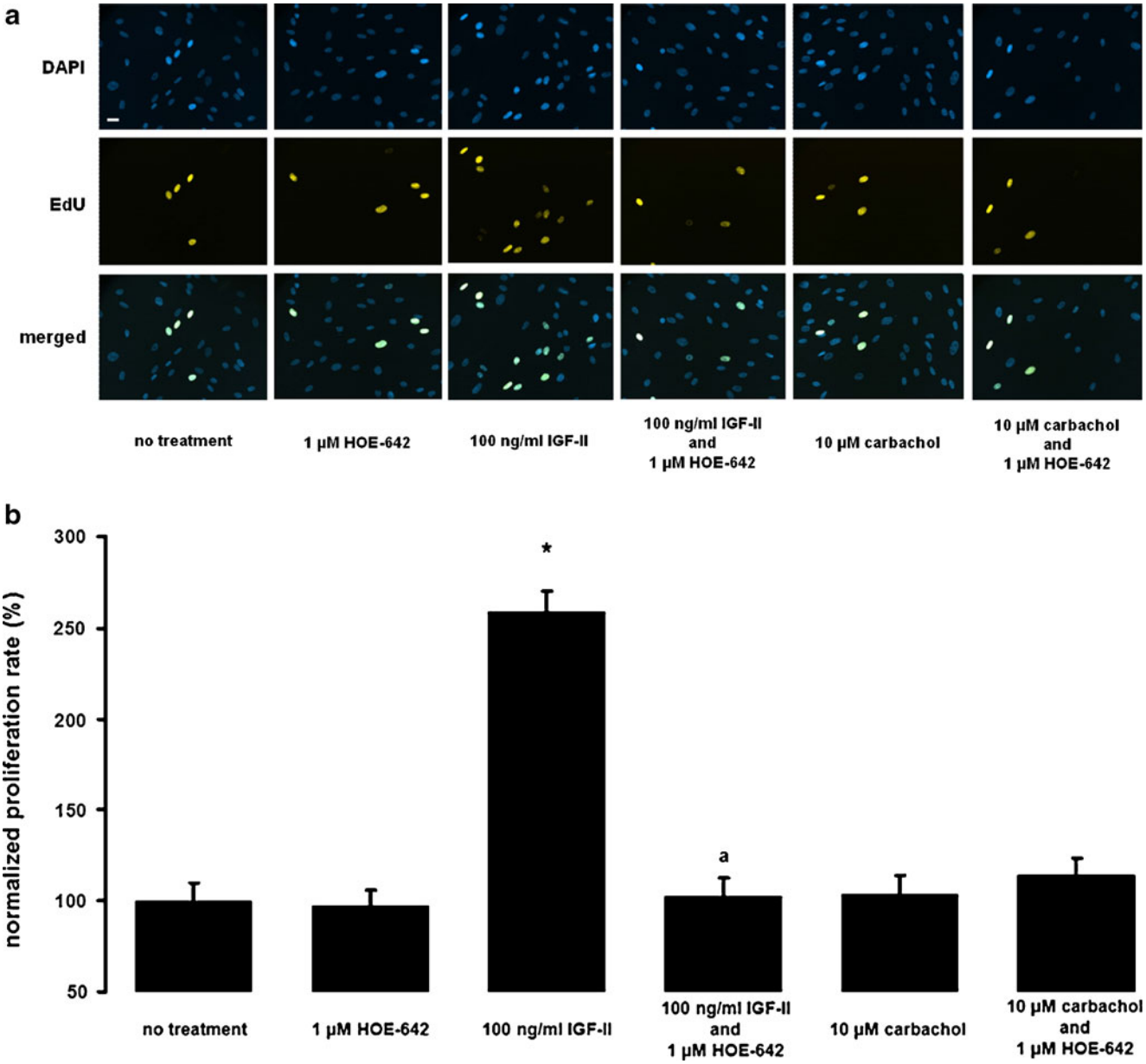

Fig. 8 IGF-II stimulates the proliferation of HGMs in a NHE1-dependent manner. **a** Representative images showing EdU localisation after treatment with 1 μM HOE-642, 100 ng/ml IGF-II and/or 10 μM carbachol compared to control. HOE-642 (1 μM) did not affect proliferation either on its own, or in a combination with 10 μM carbachol. IGF-II (100 ng/ml) increased the rate of proliferation. Furthermore, the inhibition of NHE1 suppressed the IGF-II stimulatory response. Nuclei were counterstained with DAPI (*blue staining*). The *scale bar* on the first picture represents 50 μm. **b** The *bar chart* shows the proliferation rates of *a* normalized to the basal proliferation rate; *$p<0.05$, *a* $p<0.05$ vs 100 ng/ml IGF-II ($n=5/1–2$)

[36, 52], also stimulated NHE activity. It is known that IGF-II exerts its effects through the tyrosine kinase receptor IGF-IR and it is also well known that NHE1 is mainly regulated by phosphorylation. Meima et al. reported that IGF-IR activates Ser/Thr kinases in the Akt signalling pathway and increases myofibroblast migration, growth and NHE activity by phosphorylating intracellular NHE regulatory domains thus enhancing transporter activity [37]. The distal region of the cytoplasmic tail of NHE corresponding to amino acids 700–815, is enriched in serine and threonin residues that are phosphorylated by different protein kinases in response to hormones and/or growth factors [51]. It has also been suggested that Ser/Thr kinases not only stimulate NHE1 activity, but also increase NHE1 promoter transcription [5]. ERK1/2 regulates gene expression via the MAPK cascade [40] after NHE1 phosphorylation/activation through $p90^{RSK}$ (a downstream substrate of ERK1/2) [56]. $p90^{RSK}$ directly phosphorylates NHE1 at position 703(Ser) in vascular

smooth muscle cells after growth hormone treatment and the exchanger activity was found to be increased [56]. Another important factor in the regulation of NHE is protein 14-3-3, which binds to position 703(Ser) after its phosphorylation and limits dephosphorylation by protein phosphatases [33]. Additional Ser/Thr phosphorylation sites have been recently identified in the ERK pathway, but their importance must be confirmed [35].

Our experiments demonstrate that reagents increasing NHE activity also increase HGM migration and proliferation, so the question arises whether in turn NHE inhibition may inhibit cell migration and proliferation. The effects of parasympathomimetics on cell migration are conflicting, though they are thought to stimulate NHE activity in general. In HaCaT cells, carbachol did not alter single random cell locomotion compared to non-treated cultures [38]. Epidermal keratinocytes showed enhanced migration after long-term muscarinic stimulation with acetylcholine in an agarose gel outgrowth system [18], whereas carbachol treatment arrested wound healing in epidermal keratinocytes [9]. Besides the differences between species and tissues, it seems that various muscarinic receptors can mediate different migration responses even in the same cell [63]. Our experiments clearly showed that 10 μM carbachol stimulated migration of HGMs, at least partly in a NHE1-dependent manner, but higher or lower doses had no further effect on migration (data not shown). It is known that protein kinase C (PKC) might mediate M3 receptor signals causing PLC to cleave membrane phospholipids. PIP2 is cleaved into diacyl glycerol and IP3 which is released into the cytosol and binds to IP3 receptors localised at the ER (or SR) causing consequent increase of the cytosolic calcium concentration and a cascade of activity including locomotion of contractile cells [1]. M3 receptors, through PLC, may also activate PI3K/Akt cascade. In the context of gastric cancer, it is worth mentioning that apoptosis can be suppressed through the PI3K/Akt/mTOR pathway allowing vigorous proliferation and better survival [68]. PKC modulates gene regulation via NF-κB and by joining Raf/MAPK cascade. It has been shown recently that PKC may phosphorylate the potent activation transcription factor-2, which controls c-Jun-mediated activation of transcription [66]. The observed increase in migration in our studies suggests, however, a permissive or supporting role of NHE1 in enabling migratory mechanisms to take effect in response to bioactive compounds. Others have found that not only NHE1 activity, but also intact NHE1 protein structure is required for locomotion, since mutations/modifications of protein structure or inhibition of the exchanger activity also inhibits migration [30]. Notably, NHE1 is a scaffolding-organizing protein functioning as a transmembrane signal transducer for various agents modulating cell volume, cell migration and growth through NHE1 activity [27]. Muscarinic agonists have also been shown to evoke differential effects on proliferation depending on the type of the muscarinic receptor [63]. We found that the M3 agonist carbachol does not induce proliferation of HGMs.

IGF-II stimulates the proliferation of many cell types, including myofibroblasts [19, 36]. NHE1 may act as an organizer of different cell growth inducing signals through modulation of transporter activity via receptor tyrosine kinases and joint pathways. Denker et al. reported that NHE1 protein contains an intracellular esrin/radixin/moesin (ERM) motif close to the plasma membrane, which anchors the protein to the subcortical actin filament network and serves as a host to actin polymerization [14]. In a wound healing assay, migration was impaired when mutations disrupted the ERM site. Not only ERM site mutations, but also mutations of the transporter sequence (resulting in diminished NHE1 activity), impair de-adhesion resulting in failure to retract lamellipodia. Besides this membrane anchoring, NHE1 is important in regulating cell volume and local pH at changing membrane sites of a moving cell; it is known that in fibroblasts NHE1 is most abundant at the rear and front pole of a spatially polarized migrating cell [14].

We showed that inhibition of NHE1 blocks migration and proliferation of HGMs. Since stromal cells play an important role in cancer initiation and progression [6, 13, 31], our results may have both physiological and therapeutic relevance. It is well documented that proliferation is reduced by NHE1 inhibition in human cancer cells [20, 49]. However, it is also possible that intracellular alkalization simply promotes or permits proliferative responses, because as the pH_i becomes more alkaline, cellular metabolism becomes more rapid mainly due to the more effective energy producing mechanisms [20]. For example, in tumour cells, acid/base conditions are of particular importance, because cancer cells share an aberrant intracellular alkalization facilitating their malignant behavior, whereas the microenvironment becomes more acidic [8]. Nevertheless, as mentioned before, NHE1 is highly regulated by phosphorylation and Akt kinases that phosphorylate NHE1 increasing its activity also stimulate proliferation at the same time [17, 34, 54].

In conclusion, we have demonstrated that HGMs express functionally active NHE, NBC and AE transporters which regulate pH_i. Furthermore, we have shown that NHE1 contributes to IGF-II- and carbachol-stimulated migration, and that it is obligatory for IGF-II-induced proliferation.

Acknowledgements We would like to thank Graham Dockray, professor at the Department of Physiology, University of Liverpool (Liverpool, UK) for his kind help and supervision of the molecular biology experiments. We would also like to thank Drs. László Tiszlavicz and István Balázs Németh, pathologists at the Department of Pathology, University of Szeged (Szeged, Hungary) for their continuous technical support and accurate histological evaluations of our gastric tissue specimens. Cariporide was a generous gift from Sanofi-Aventis,

(Frankfurt, Germany). Our funding sources were Hungarian Scientific Research Fund K76844, K73141, National Development Agency (TÁMOP) 4.2.1.B-09/1/KONV, 4.2.2-08/1/2008-0002 and 4.2.2-08/1/2008-0013, Hungarian Academy of Sciences BO/00334/08/5 and BO/00174/10/5, NIH PHS398/2590 and NIHR L115931.

Conflict of interest statement The authors hereby declare that there is no conflict of interest to disclose.

References

1. Alberts B, Alexander J, Julian L, Martin R, Keith R, Peter W (2002) Molecular Biology of the Cell, 4th edn. Garland Science, New York, US
2. Alexandratou E, Dido Y, Panagiotis H, Dimitris K, Spyros L (2002) Human fibroblast alterations induced by low power laser irradiation at the single cell level using confocal microscopy. Photochem Photobiol Sci 8:547–552
3. Bachmann O, Sonnentag T, Siegel WK, Lamprecht G, Weichert A, Gregor M, Seidler U (1998) Different acid secretagogues activate different Na+/H+ exchanger isoforms in rabbit parietal cells. Am J Physiol 275:G1085–G1093
4. Bachmann O, Reichelt D, Tuo B, Manns MP, Seidler U (2006) Carbachol increases Na+−HCO3- cotransport activity in murine colonic crypts in a M3-, Ca2+/calmodulin-, and PKC-dependent manner. Am J Physiol Gastrointest Liver Physiol 291:G650–G657
5. Besson P, Fernandez-Rachubinski F, Yang W, Fliegel L (1998) Regulation of Na+/H+ exchanger gene expression: mitogenic stimulation increases NHE1 promoter activity. Am J Physiol 274: C831–C839
6. Bhowmick NA, Neilson EG, Moses HL (2004) Stromal fibroblasts in cancer initiation and progression. Nature 432:332–337
7. Cala PM, Anderson SE, Cragoe EJ (1988) Na/H exchange-dependent cell volume and pH regulation and disturbances. Comp Biochem Physiol 90:551–555
8. Cardone RA, Casavola V, Reshkin SJ (2005) The role of disturbed pH dynamics and the Na+/H+ exchanger in metastasis. Nat Rev Cancer 5:786–795
9. Chernyavsky AI, Arredondo J, Wess J, Karlsson E, Grando SA (2004) Novel signaling pathways mediating reciprocal control of keratinocyte migration and wound epithelialization through M3 and M4 muscarinic receptors. J Cell Biol 166:261–272
10. Chung MK, Kim HC (2002) Volume-activated chloride currents from human fibroblasts: blockade by nimodipine. Gen Physiol Biophys 21:85–101
11. Damkier HH, Aalkjaer A, Praetorius J (2010) Na+-dependent HCO3- import by the slc4a10 gene product involves Cl- export. J Biol Chem 285:26998–27007
12. Davies JE, Ng LL, Kofoed-Enevoldsen A, Li LK, Earle KA, Trevisan R, Viberti G (1992) Intracellular pH and Na+/H+ antiport activity of cultured skin fibroblasts from diabetics. Kidney Int 42:1184–1190
13. De Wever O, Demetter P, Mareel M, Bracke M (2008) Stromal myofibroblasts are drivers of invasive cancer growth. Int J Cancer 123:2229–2238
14. Denker SP, Barber DL (2002) Cell migration requires both ion translocation and cytoskeletal anchoring by the Na-H exchanger NHE1. J Cell Biol 159:1087–1096
15. Duquette RA, Wray S (2001) pH regulation and buffering power in gastric smooth muscle. Eur J Physiol 442:459–466
16. Gleeson D (1992) Acid–base transport systems in gastrointestinal epithelia. Gut 33:1134–1145
17. Goss GG, Woodside M, Wakabayashi S, Pouyssegur J, Waddell T, Downey GP, Grinstein S (1994) ATP dependence of NHE-1, the ubiquitous isoform of the Na+/H+ antiporter. Analysis of phosphorylation and subcellular localization. J Biol Chem 269:8741–8748
18. Grando SA, Crosby AM, Zelickson BD, Dahl MW (1999) Agarose gel keratinocyte outgrowth system as a model of skin re-epithelization: requirement of endogenous acetylcholine for outgrowth initiation. J Invest Dermatol 101:804–810
19. Grotendorst GR, Rahmanie H, Duncan MR (2004) Combinatorial signaling pathways determine fibroblast proliferation and myofibroblast differentiation. FASEB 18:469–479
20. Harguindey S, Orive G, Pedraz JL, Paradiso A, Reshkin SJ (2005) The role of pH dynamics and the Na+/H+ antiporter in the etiopathogenesis and treatment of cancer. Two faces of the same coin—one single nature. Biochim Biophys Acta 1756:1–24
21. Hayashi H, Aharonovitz O, Alexander RT, Touret N, Furuya W, Orlowski J, Grinstein S (2008) Na+/H+ exchange and pH regulation in the control of neutrophil hemokinesis and chemotaxis. Am J Physiol Cell Physiol 294:C526–C534
22. Hegyi P, Rakonczay Z, Gray MA, Argent BE (2004) Measurement of intracellular pH in pancreatic duct cells: a new method for calibrating the fluorescence data. Pancreas 28:427–434
23. Hinz B (2010) The myofibroblast: paradigm for a mechanically active cell. J Biom 43:146–155
24. Hinz B, Phan SH, Thannickal VJ, Galli A, Bochaton-Piallat M-L, Gabbiani G (2007) The myofibroblast: one function, multiple origins. Am J Pathol 170:1807–1816
25. Iida M, Nakamura N, Kamouchi M, Kitazono K, Kuroda J, Matsuo R, Hagiwara N, Ishikawa E, Ooboshi H, Ibayashi S (2008) Role of NHE1 in calcium signaling and cell proliferation in human CNS pericytes. Am J Physiol Heart Circ Physiol 294: H1700–H1707
26. Kapus A, Grinstein S, Wasan S, Kandasamy R, Orlowski J (1994) Functional characterization of three isoforms of the Na+/H+ exchanger stably expressed in Chinese hamster ovary cells. ATP dependence, osmotic sensitivity, and role in cell proliferation. J Biol Chem 269:23544–23552
27. Koliakos G, Paletas K, Kaloyianni M (2008) NHE-1: a molecular target for signalling and cell matrix interactions. Connect Tissue Res 49:157–161
28. L'Allemain G, Paris S, Pouysségur J (1984) Growth factor action and intracellular pH regulation in fibroblasts. Evidence for a major role of the Na+/H+ antiport. J Biol Chem 259:5809–5815
29. L'Allemain G, Paris S, Pouysségur J (1985) Role of a Na+-dependent Cl-/HCO3- exchange in regulation of intracellular pH in fibroblasts. J Biol Chem 260:4877–4883
30. Lagana A, Vadnais J, Le PU, Nguyen TN, Laprade R, Nabi IR, Noël J (2000) Regulation of the formation of tumor cell pseudopodia by the Na(+)/H(+) exchanger NHE1. J Cell Sci 113:3649–3662
31. LaPointe MS, Batlle DC (1994) Na+/H+ exchange and vascular smooth muscle proliferation. Am J Med Sci 307:S9–S16
32. Lee SH, Kim T, Park E-S, Yang S, Jeong D, Choi Y, Rho J (2008) NHE10, an osteoclast-specific member of the Na+/H+ exchanger family, regulates osteoclast differentiation and survival. Biochem Biophys Res Commun 369:320–326
33. Lehoux S, Ji A, Florian JA, Berk BC (2001) 14-3-3 Binding to Na+/H+ exchanger isoform-1 is associated with serum-dependent activation of Na+/H+ exchange. J Biol Chem 276:15794–15800
34. Luo J, Sun D (2007) Physiology and pathophysiology of Na(+)/H(+) exchange isoform 1 in the central nervous system. Curr Neurovasc Res 4:205–215
35. Malo ME, Fliegel L (2006) Physiological role and regulation of the Na+/H+ exchanger. Can J Physiol Pharmacol 84:1081–1095
36. McCaig C, Duval C, Hemers E, Steele I, Pritchard DM, Przemeck S, Dimaline R, Ahmed S, Bodger K, Kerrigan DD, Wang TC, Dockray GJ, Varro A (2006) The role of matrix metalloproteinase-7

in redefining the gastric microenvironment in response to Helicobacter pylori. Gastroenterology 130:1754–1763
37. Meima ME, Webb BA, Witkowska HE, Barber DL (2009) The sodium-hydrogen exchanger NHE1 is an Akt substrate necessary for actin filament reorganization by growth factors. J Biol Chem 284:26666–26675
38. Metzger M, Just L, Boss A, Drews U (2005) Identification and functional characterization of the muscarinic receptor M3 in the human keratinocyte cell line HaCaT. Cells Tissues Organs 180:96–105
39. Moolenaar WH, Tsien RY, van der Saag PV, de Laat SW (1983) Na+/H+ exchange and cytoplasmic pH in the action of growth factors in human fibroblasts. Nature 304:645–648
40. Moor AN, Fliegel L (1999) Protein kinase-mediated regulation of the Na(+)/H(+) exchanger in the rat myocardium by mitogen-activated protein kinase-dependent pathways. J Biol Chem 274:22985–22992
41. Mutoh H, Sashikawa M, Hayakawa H, Sugano K (2010) Monocyte chemoattractant protein-1 is generated via TGF-beta by myofibroblasts in gastric intestinal metaplasia and carcinoma without H. pylori infection. Cancer Sci 101:1783–1789
42. Nakayama H, Enzan H, Miyazaki E, Toi M (2002) Alpha smooth muscle actin positive stromal cells in gastric carcinoma. J Clin Pathol 55:741–744
43. Noble A, Towne C, Chopin L, Leavesley D, Upton Z (2003) Insulin-like growth factor-II bound to vitronectin enhances MCF-7 breast cancer cell migration. Endocrinology 144:2417–2424
44. Orlowski J, Grinstein S (2004) Diversity of the mammalian sodium/proton exchanger SLC9 gene family. Eur J Physiol 447:549–565
45. Pedersen SF (2006) The Na+/H+ exchanger NHE1 in stress-induced signal transduction: implications for cell proliferation and cell death. Eur J Physiol 452:249–259
46. Perona R, Portillo F, Giraldez F, Serrano R (1990) Transformation and pH homeostasis of fibroblasts expressing yeast H(+)-ATPase containing site-directed mutations. Mol Cell Biol 10:4110–4115
47. Radhakrishnan J, Kolarova JD, Ayoub IM, Gazmuri RJ (2011) AVE4454B-a novel sodium-hydrogen exchanger isoform-1 inhibitor-compared less effective than cariporide for resuscitation from cardiac arrest. J Lab Clin Med 157:71–80
48. Rentsch ML, Ossum CG, Hoffmann EK, Pedersen SF (2007) Roles of Na+/H+ exchange in regulation of p38 mitogen-activated protein kinase activity and cell death after chemical anoxia in NIH3T3 fibroblasts. Eur J Physiol 454:649–662
49. Ritter M, Fuerst J, Wöll E, Chwatal S, Gschwentner M, Lang F, Deetjen P, Paulmichl M (2001) Na(+)/H(+)exchangers: linking osmotic dysequilibrium to modified cell function. Cell Physiol Biochem 11:1–18
50. Salic A, Mitchison TJ (2008) A chemical method for fast and sensitive detection of DNA synthesis in vivo. Proc Natl Acad Sci 105:2415–2420
51. Sardet C, Fafournoux P, Pouysségur J (1991) Alpha-thrombin, epidermal growth factor, and okadaic acid activate the Na+/H+ exchanger, NHE-1, by phosphorylating a set of common sites. J Biol Chem 266:19166–19171
52. Schmid C (1995) Insulin-like growth factors. Cell Biol Int 19:445–457
53. Schneider L, Stock C-M, Dieterich P, Jensen BH, Pedersen LB, Satir P, Schwab A, Christensen ST, Pedersen SF (2009) The Na+/H+ exchanger NHE1 is required for directional migration stimulated via PDGFR-alpha in the primary cilium. J Cell Biol 185:163–176
54. Slepkov ER, Rainey JK, Sykes BD, Fliegel L (2007) Structural and functional analysis of the Na+/H+ exchanger. Biochem J 401:623–633
55. Stock C, Gassner B, Hauck CR, Arnold H, Mally S, Eble JA, Dieterich P, Schwab A (2005) Migration of human melanoma cells depends on extracellular pH and Na+/H+ exchange. J Physiol 567:225–238
56. Takahashi E, Abe J, Gallis B, Aebersold R, Spring DJ, Krebs EG, Berk BC (1990) p90(RSK) is a serum-stimulated Na+/H+ exchanger isoform-1 kinase. Regulatory phosphorylation of serine 703 of Na+/H+ exchanger isoform-1. J Biol Chem 274:20206–20214
57. Taves J, Rastedt D, Canine J, Mork D, Wallert MA, Provost JJ (2008) Sodium hydrogen exchanger and phospholipase D are required for alpha1-adrenergic receptor stimulation of metalloproteinase-9 and cellular invasion in CCL39 fibroblasts. Arch Biochem Biophys 477:60–66
58. Thomas JA, Buchsbaum RN, Zimniak A, Racker E (1979) Intracellular pH measurements in Ehrlich ascites tumor cells utilizing spectroscopic probes generated in situ. Biochemistry 18:2210–2218
59. Tóth-Molnár E, Venglovecz V, Ózsvári B, Rakonczay Z, Varró A, Papp JG, Tóth A, Lonovics J, Takács T, Ignáth I, Iványi B, Hegyi P (2007) New experimental method to study acid/base transporters and their regulation in lacrimal gland ductal epithelia. Investig Ophthalmol Vis Sci 48:3746–3755
60. Vereninov AA, Vassilieva IO, Yurinskaya VE, Matveev VV, Glushankova LN, Lang F, Matskevitch JA (2001) Differential transcription of ion transporters, NHE1, ATP1B1, NKCC1 in human peripheral blood lymphocytes activated to proliferation. Int J Exp Cell Physiol Biochem Pharmacol 11:19–26
61. Watanabe M, Hirano T, Asano G (1995) Roles of myofibroblasts in the stroma of human gastric carcinoma. Nippon Geka Gakkai Zasshi 96:10–18
62. Weintraub WH, Machen TE (1989) pH regulation in hepatoma cells: roles for Na-H exchange, Cl-HCO3 exchange, and Na-HCO3 cotransport. Am J Physiol 257:G317–G327
63. Wessler I, Kirkpatrick CJ (2008) Acetylcholine beyond neurons: the non-neuronal cholinergic system in humans. Br J Pharmacol 154:1558–1571
64. Wray S (1988) Smooth muscle intracellular pH: measurement, regulation, and function. Am J Physiol Cell Physiol 254: C213–C225
65. Wu S, Song T, Zhou S, Liu Y, Chen G, Huang N, Liu L (2008) Involvement of Na+/H+ exchanger 1 in advanced glycation end products-induced proliferation of vascular smooth muscle cell. Biochem Biophys Res Commun 375:384–389
66. Yamasaki T, Takahashi A, Pan J, Yamaguchi N, Yokoyama KK (2009) Phosphorylation of activation transcription factor-2 at serine 121 by protein kinase C controls c-Jun-mediated activation of transcription. J Biol Chem 284:8567–8581
67. Yang X, Wang D, Dong W, Song Z, Dou K (2011) Suppression of Na(+)/H (+) exchanger 1 by RNA interference or amiloride inhibits human hepatoma cell line SMMC-7721 cell invasion. Med Oncol 28:385–390
68. Yap TA, Garrett MD, Walton MI, Raynaud F, de Bono JS, Workman P (2008) Targeting the PI3K-AKT-mTOR pathway: progress, pitfalls, and promises. Curr Opin Pharmacol 8:393–412
69. Yeruva S, Farkas K, Hubricht J, Rode K, Riederer B, Bachmann O, Cinar A, Rakonczay Z, Molnár T, Nagy F, Wedemayer J, Manns M, Raddatz D, Musch MW, Chang EB, Hegyi P, Seidler U (2010) Preserved Na(+)/H(+) exchanger isoform 3 expression and localization, but decreased NHE3 function indicate regulatory sodium transport defect in ulcerative colitis. Inflamm Bow Dis 16:1149–1161

II.

Carcinogenesis vol.33 no.8 pp.1553–1562, 2012
doi:10.1093/carcin/bgs180
Advance Access Publication May 18, 2012

Release of TGFβig-h3 by gastric myofibroblasts slows tumor growth and is decreased with cancer progression

Chris Holmberg[1], Michael Quante[2], Islay Steele[1], Jothi Dinesh Kumar[1], Silviya Balabanova[1], Cedric Duval[1], Matyas Czepan[3], Zoltan Rakonczay Jr[3], Laszlo Tiszlavicz[4], Istvan Nemeth[4], Gyorgy Lazar[5], Zsolt Simonka[5], Rosalind Jenkins[6], Peter Hegyi[3], Timothy C.Wang[7], Graham J.Dockray[1] and Andrea Varro[1,8,*]

[1]Department of Cellular & Molecular Physiology, Institute of Translational Medicine, University of Liverpool, Liverpool, UK, [2]II. Medizinische Klinik, Klinikum rechts der Isar, Technische Universität München, München, Germany, [3]First Department of Medicine, [4]First Department of Pathology and [5]First Department of Surgery, University of Szeged, Szeged, Hungary, [6]Department of Molecular & Clinical Pharmacology, Institute of Translational Medicine, University of Liverpool, Liverpool, UK, [7]Department of Medicine, Columbia University, New York, NY, USA and [8]Department of Molecular & Clinical Cancer Medicine, Institute of Translational Medicine, University of Liverpool, Liverpool, UK

[*]To whom correspondence should be addressed. Tel: +44 (0) 151 794 5331; Fax: +44 (0) 151 794 5315;
Email: avarro@liv.ac.uk

Tumor progression has been linked to changes in the stromal environment. Myofibroblasts are stromal cells that are often increased in tumors but their contribution to cancer progression is not well understood. Here, we show that the secretomes of myofibroblasts derived from gastric cancers [cancer-associated myofibroblasts (CAMs)] differ in a functionally significant manner from those derived from adjacent tissue [adjacent tissue myofibroblasts (ATMs)]. CAMs showed increased rates of migration and proliferation compared with ATMs or normal tissue myofibroblasts (NTMs). Moreover, conditioned medium (CM) from CAMs significantly stimulated migration, invasion and proliferation of gastric cancer cells compared with CM from ATMs or NTMs. Proteomic analysis of myofibroblast secretomes revealed decreased abundance of the extracellular matrix (ECM) adaptor protein like transforming growth factor-β-induced gene-h3 (TGFβig-h3) in CAMs, which was correlated with lymph node involvement and shorter survival. TGFβig-h3 inhibited IGF-II-stimulated migration and proliferation of both cancer cells and myofibroblasts, and suppressed IGF-II activation of p42/44 MAPkinase; TGFβig-h3 knockdown increased IGF-II- and CM-stimulated migration. Furthermore, administration of TGFβig-h3 inhibited myofibroblast-stimulated growth of gastric cancer xenografts. We conclude that stromal cells exert inhibitory as well as stimulatory effects on tumor cells; TGFβig-h3 is a stromal inhibitory factor that is decreased with progression of gastric cancers.

Introduction

Stromal cells are well recognized to play influential roles in determining tumor progression (1–4). Cancer-associated fibroblasts (CAFs) are an important stromal cell type with distinct properties (5–7) and recent work indicates that differences in gene expression in the stromal compartment predict clinical outcome and response to therapy (8–10). Many different stromal cell factors may contribute to the tumor microenvironment (6,11–14), but the changes that occur in stromal cell function with cancer progression remain poorly understood.

Abbreviations: ATM, adjacent tissue myofibroblasts; CAF, cancer-associated fibroblasts; CAM, cancer-associated myofibroblasts; IGF-II, insulin-like growth factor-II; NTM, normal tissue myofibroblasts; TGFβig-h3, transforming growth factor-β-induced gene-h3.

Myofibroblasts, also sometimes called activated fibroblasts, are considered to be a subclass of CAFs. They are present in normal tissue in low density, increase with inflammation, infection or tissue damage (15) and are responsible for secretion of extracellular matrix (ECM) proteins, matrix metalloproteinases, protease inhibitors, growth factors, cytokines and chemokines as well as cyclo-oxygenase products. Epigenetic changes have been detected in cancer-associated myofibroblasts (CAMs) from gastric adenocarcinoma compared with myofibroblasts derived from adjacent tissue (ATMs) providing a basis for understanding how gastric CAMs might differ from other myofibroblasts (16).

Gastric cancer is the second most frequent cause of cancer-related mortality in males worldwide, and is frequently associated with *Helicobacter pylori* infection of the gastric corpus (17,18). The progression to cancer occurs over many decades and is characterized by preneoplastic changes including gastritis, atrophy, intestinal metaplasia and spasmolytic peptide-expressing metaplasia, and dysplasia (19,20). Infection is also associated with increases in gastric myofibroblasts that may reflect increased insulin-like growth factor (IGF) activity through matrix metalloproteinase-7 degradation of IGF-binding protein-5 (21–23), as well as recruitment of bone marrow-derived cells (24,25).

Recent studies suggest a role in cancer progression for the ECM adaptor protein transforming growth factor-β-induced gene-h3 (TGFβig-h3; also known as βig-h3, TGFBI, βIGH3, keratoepithelin and MP78/70). The latter is a 68 kDa protein with four fasciclin-like domains and an RGD domain in the C-terminal region; it binds ECM proteins including collagen, fibronectin and laminin (26,27). TGFβig-h3 suppresses the growth of Chinese hamster ovary cells in nude mice (28) and mice null for TGFβig-h3 develop spontaneous tumors in a variety of organs (29); loss of TGFβig-h3 in ovarian cancer is associated with resistance to taxanes (30). However, the role of TGFβig-h3 in cancer remains uncertain since expression has been associated with increased aggressiveness of liver and colon cancer cells (31,32). In this study, we have characterized a panel of CAMs from gastric cancers and compared their secretomes with those of myofibroblasts from adjacent tissue. We report here that decreased secretion of TGFβig-h3 in CAMs is associated with lymph node involvement and shorter survival, and we show that TGFβig-h3 suppresses cancer cell migration and inhibits growth in a model of stroma-stimulated cancer growth *in vivo*.

Materials and methods

Materials

Human recombinant TGFβig-h3 and IGF-II were obtained from R&D Systems (Abingdon, Oxon, UK); siRNA for TGFβig-h3, and control scrambled sequences were purchased from Ambion (Austin, TX). Antibodies for alpha-smooth muscle actin (α-SMA), vimentin and desmin were purchased from RDI (Flanders, NJ); antibody for pancytokeratin was used from Dako (Ely, Cambridgeshire, UK). Antibodies for TGFβig-h3, and GAPDH were obtained from R&D Systems and Biodesign (Saco, ME), respectively. Cleaved caspase-3 antibody was purchased from New England Biolabs (Hertfordshire, UK). Antibodies for Bax, Bim and Bcl-2 were purchased from Santa Cruz Biotechnology (Santa Cruz, CA), Abcam (Cambridge, UK) and Dako, respectively. Antibodies for total and phosphorylated p42/44 were obtained from Cell Signaling (Beverly, MA). All other chemicals were purchased from Sigma (Poole, Dorset, UK).

Generation of human primary myofibroblasts

Human primary myofibroblasts were derived from resected gastric cancers (CAM) and adjacent tissue (ATM) obtained from patients undergoing surgery for gastric cancer (Supplementary Table 1, available at *Carcinogenesis* Online (16,23)). Tumor and adjacent tissues were characterized using the TNM classification (Supplementary Methods, available at *Carcinogenesis* Online)

© The Author 2012. Published by Oxford University Press. All rights reserved. For Permissions, please email: journals.permissions@oup.com

Downloaded from http://carcin.oxfordjournals.org/ at Sydney Jones Library, University of Liverpool on November 14, 2012

for gastric cancer (33). Normal myofibroblasts (NTM) were generated from deceased transplant donors with normal gastric morphology. Tumor and normal tissues were characterized using a scoring system for myofibroblast morphology, architecture and number (Supplementary Methods, available at *Carcinogenesis* Online). For histopathological assessments, myofibroblasts were defined as stellate/spindle-shaped cells with consistent α-SMA and vimentin co-expression. Smooth muscle fibers were excluded based on their characteristic morphology. This study was approved by the Ethics Committee of the University of Szeged, Hungary. Myofibroblasts were cultured as described previously (23) and were used between passages 3 and 10. Conditioned medium (CM) was prepared from 1×10^6 myofibroblasts plated in 10 cm diameter dishes to give 80–90% confluency and collected after 24 h in 10 ml serum-free media.

Human gastric carcinoma cell lines

AGS cells (ATCC, Manassas, VA) and MKN45 gastric carcinoma cells (RIKEN, Ibaraki, Japan) were cultured as described previously (34).

Immunohistochemistry

Formalin-fixed, paraffin-embedded, tissue sections were processed for detection of α-SMA, vimentin and desmin after antigen recovery using Multivision Polymer Detection System (Thermo Scientific). For immunocytochemistry, cells were cultured in chamber slides, stained with α-SMA, vimentin, desmin and pancytokeratin followed by incubation with the appropriate fluorescein or Texas Red-labeled secondary antibodies raised in donkey (Jackson Immunoresearch, Soham, UK), and mounted with Vectashield containing 4′,6-diamidino-2-phenylindole (Vector Laboratories, Peterborough, UK). For visualization of F-actin, the primary antibody was substituted with 50 µg/ml tetramethyl rhodamine iso-thiocyanate-conjugated phalloidin. Slides were viewed using a Zeiss Axioplan-2 microscope (Zeiss Vision, Welwyn Garden City, UK). Images were captured using a JVC-3 charge-coupled device camera at ×40 magnification with KS300 software (Imaging Associates, Bicester, Oxfordshire, UK).

Migration, invasion, proliferation and apoptosis assays

Migration and invasion of primary human gastric myofibroblasts or cancer cells were studied in 8 µm pore chambers (BD Control Cell Culture Inserts or BD BioCoat Matrigel Invasion Chambers, respectively; BD Biosciences, Oxford, UK) as described previously (23,35). Incorporation of [^{3}H]-thymidine by human gastric myofibroblasts or AGS cells was studied using methods described previously (34). Additionally, proliferation was assessed by incorporation of BrdU (3 ng/ml) as described previously (23), or EdU (10 µM) according to the manufacturer's instruction (Invitrogen, Paisley, UK). Apoptosis was studied using cleaved caspase-3 antibody (New England Biolabs (Hertfordshire, UK).

Isobaric tagging for relative and absolute quantitation

Myofibroblast CM was concentrated to 500 µl, acetone precipitated and resuspended in 0.5 M triethylammonium bicarbonate (TEAB) in 0.1% sodium dodecyl sulfate. Myofibroblasts were lysed directly in TEAB/sodium dodecyl sulfate. Samples (100 µg) were labeled using the 4-plex iTRAQ® kit (AB SCIEX, Foster City, CA) according to manufacturer's instructions. Labeled samples were pre-fractionated using a PolyLC PolySULFOETHYL A (4.6 × 200 mm i.d.) cation exchange column using an Agilent 1100 HPLC system (Agilent Technologies, Santa Clara, CA). Samples were then analyzed using an LC Packings Ultimate nano-LC system run in-line with a QStar Pulsar i mass spectrometer (AB Sciex). Protein identification and quantification were performed using the ProteinPilot™ v3.0.1 software (AB Sciex). The Paragon algorithm was selected as the default search program, with the digestion agent set as trypsin and cysteine modification as methyl methanethiosulfonate. Proteins were reported based on the assignment of at least two tryptic peptides with a confidence >95%, or on the assignment of one tryptic peptide with a confidence >99% and a local false discovery rate calculated using the PSPEP algorithm of <1%. Proteins exhibiting a differential abundance in CAMs versus ATMs were calculated only on the assignment of at least two tryptic peptides using a Pro Group™ algorithm of ProteinPilot™. When comparing groups of patients, proteins that were identified in >80% in one of the groups were used in the analysis. Pathway analysis was performed using MetaCore® (GeneGo, St Joseph, MI).

Western blotting

Myofibroblast cell extracts were prepared in RIPA buffer containing protease and phosphatase inhibitors and proteins resolved by sodium dodecyl sulfate–polyacrylamide gel electrophoresis and processed for western blotting as described previously (22).

Knockdown of TGFβig-h3

Knockdown of TGFβig-h3 was performed using 35 µM of TGFβig-h3 siRNA, and negative control scrambled RNA, for 72 h by nucleofection using the NHDF transfection kit (Amaxa; Köln, Germany). The efficiency of the knockdown was verified by western blotting.

Xenograft studies in SCID mice

To study the effect of TGFβig-h3 on xenograft growth, 6- to 8-week-old immunocompromised mice (SCID, Jackson Laboratories, Bar Harbor, ME) were used for subcutaneous injection of tumor cells with or without CAMs. Gastric cancer cells (MKN45, 5×10^5) were injected alone, alone on the left flank and together with 2×10^5 myofibroblasts on the right flank (groups 1 and 2, respectively), or with TGFβig-h3 (1 µg per mouse per day) from day 0 by Alzet pump (groups 3 and 4, respectively). In a subset of the co-injected group, tumors were allowed to grow for 2 weeks before treatment with TGFβig-h3. Tumor size was monitored every 3 days for 4 weeks. Tumors were dissected, measured, fixed in 10% formalin or 4% paraformaldehyde (PFA), embedded in paraffin or OTC for frozen sections, and processed for hematoxylin/eosin staining or localization of α-SMA, using ABC avidin–biotin–DAB detection kit (Vector Labs) according to the supplied protocol.

Statistics

Results are expressed as mean ± standard error of the mean, unless otherwise stated. Student's *t*-test or analysis of variance (ANOVA; Systat Software Inc., Hounslow, London, UK) as appropriate was used to determine statistical significance of results and considered significant at $P < 0.05$, unless otherwise stated (see above for the statistical analysis of the proteomic data).

Results

Increased migration and proliferation of gastric cancer-derived myofibroblasts

The primary gastric tumors employed in this study exhibited increased numbers of myofibroblasts typically with disordered architecture and morphology compared with adjacent tissue or normal tissue (Supplementary Figure 1, available at *Carcinogenesis* Online). Tissues adjacent to the tumor resection margin exhibited a range of morphologies including chronic gastritis (7), intestinal metaplasia (2) and intestinal metaplasia with atrophy (3) (Supplementary Table 1, available at *Carcinogenesis* Online).

Cultured myofibroblasts derived from normal tissue, cancer or tissue adjacent to gastric tumors all expressed α-SMA and vimentin but not desmin, and they were negative for pancytokeratin (Figure 1A). Basal rates of CAM migration in Boyden chambers were consistently greater than those of NTMs or their ATM counterparts (Figure 1B). Moreover, compared with their respective ATMs, CAMs also exhibited increased BrdU incorporation (Figure 1C), which was attributable to shorter G_1 phase of the cell cycle (Figure 1D). There was no difference in rates of apoptosis determined by cleaved caspase-3 staining (Figure 1C and E).

Stimulation of cancer cell proliferation and migration by cancer-derived myofibroblasts

Interestingly, CM from both CAMs and ATMs, but not NTMs, resulted in epithelial–mesenchymal transition of gastric cancer AGS cells characterized by increased cell scattering (Figure 2A) and α-SMA expression (Figure 2B). Moreover, there was increased AGS cell migration (Figure 2C) and proliferation (Figure 2D) in response to CAM-CM and ATM-CM. The migration, invasion and proliferation responses to CAM-CM were consistently greater than those to their ATM counterparts. When CAMs were divided into groups based on tumor depth (pT1-2 versus pT3-4) there was no difference in the effect of CM on AGS cell proliferation (not shown). However, when CAMs were separated into groups based on lymph node involvement (pN0-1 versus pN2-4) the stimulation of [^{3}H]-thymidine incorporation was greater in response to CM from CAMs of patients with high lymph node involvement (Figure 2E).

Myofibroblast proteomes change during cancer progression

To identify proteins that might account for the different properties of CAMs compared with ATMs, we first examined the cellular proteomes of 11 pairs of cells using isobaric tagging for relative and absolute quantitation (iTRAQ) labeling followed by liquid chromatography–mass spectrometry/mass spectrometry (LC-MS/MS) identification of labeled tryptic peptides (Supplementary Table 2, available at *Carcinogenesis* Online). A total of 768 proteins were identified in at least 3 pairs of samples and a core set of 241 proteins were identified in all 11 pairs which included proteins

Downloaded from http://carcin.oxfordjournals.org/ at Sydney Jones Library, University of Liverpool on November 14, 2012

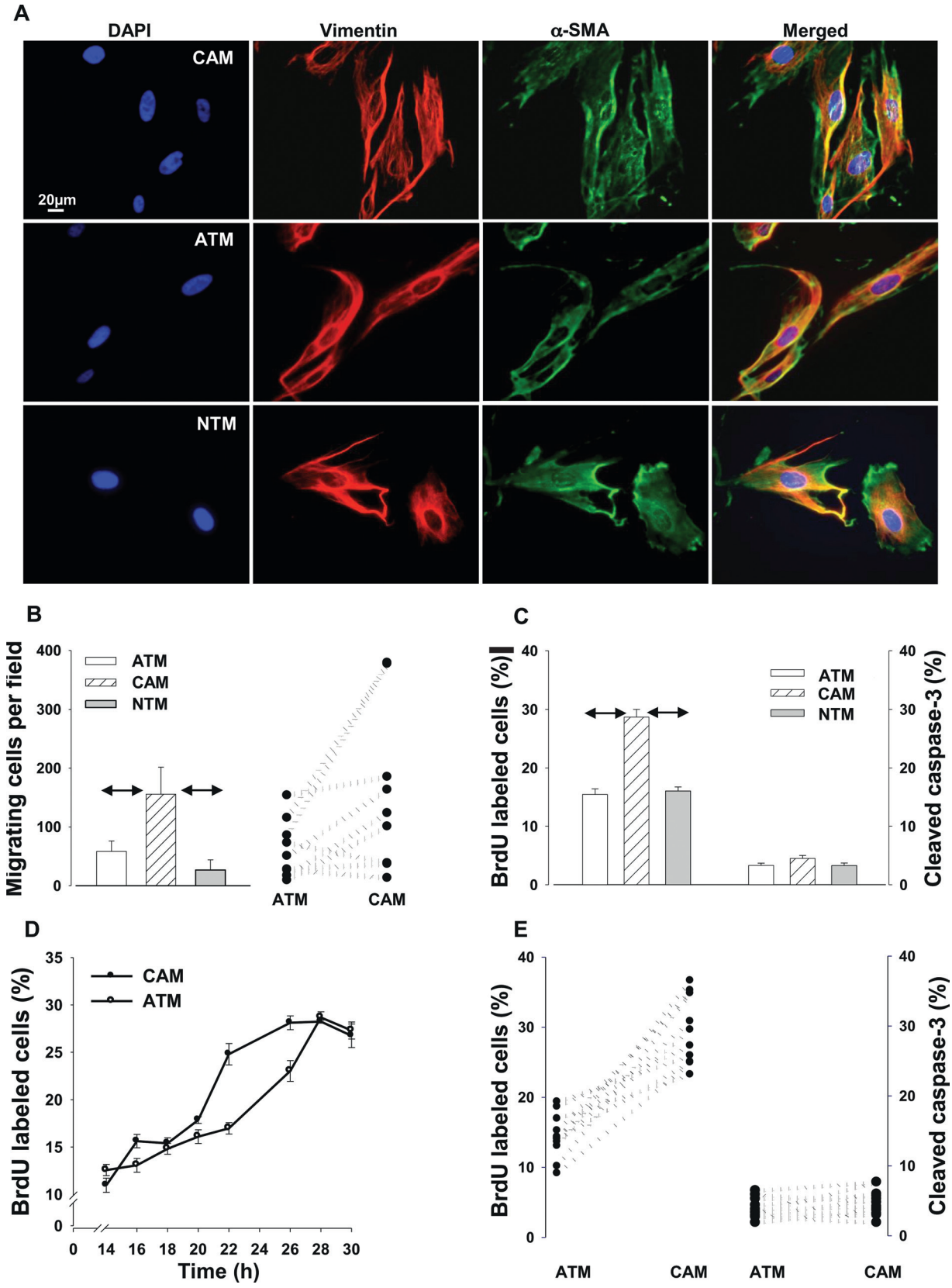

Fig. 1. Increased migration and proliferation of cultured gastric cancer-associated myofibroblasts. (**A**) Positive α-SMA (green) and vimentin (red) staining in cultured myofibroblasts (nuclear staining with 4′,6-diamidino-2-phenylindole, blue); top, CAMs; middle, ATMs; bottom, NTMs. (**B**) Increased migration of CAMs compared with ATMs and NTMs (left) in Boyden chambers, and individual pair-wise comparisons of CAMs versus their corresponding ATMs (right). (**C**) Increased BrdU labeling (left), but not apoptosis indicated by cleaved caspase-3 staining (right), in CAMs compared with ATMs and NTMs. (**D**) Shorter G_1 phase in CAMs compared with ATMs. (**E**) Individual pair-wise comparison of BrdU labeling and cleaved caspase-3 staining in CAMs versus their corresponding ATMs. Horizontal arrows, $P < 0.05$, ANOVA and $n = 10–14$.

Downloaded from http://carcin.oxfordjournals.org/ at Sydney Jones Library, University of Liverpool on November 14, 2012

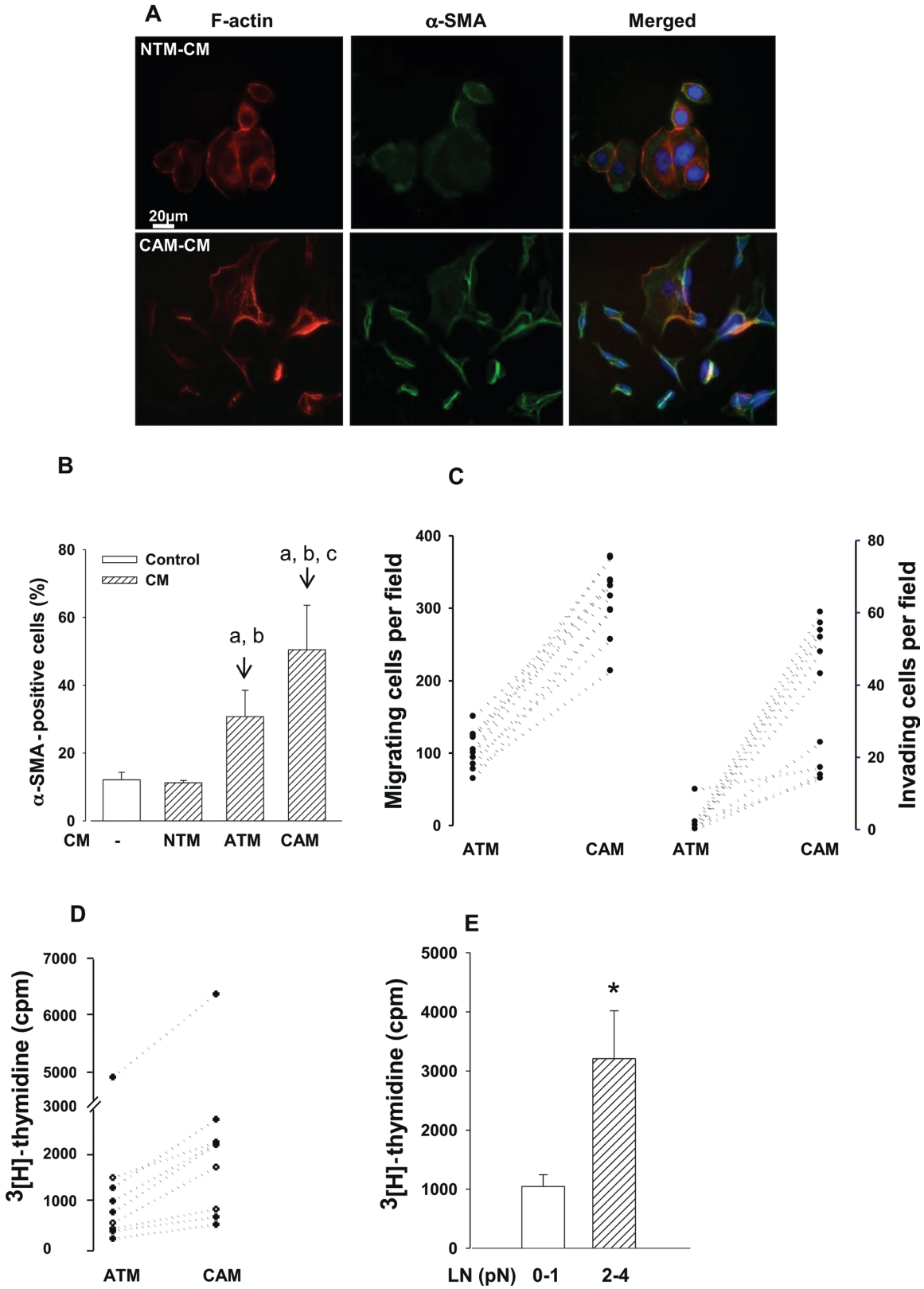

Fig. 2. Increased epithelial–mesenchymal transition, migration, invasion and proliferation of AGS cancer cells treated with CM from CAMs compared with ATMs. (**A**) Example of epithelial–mesenchymal transition characterized by scattering, α-SMA (green) and phalloidin staining (f-actin, red; nuclear staining with 4′,6-diamidino-2-phenylindole, blue) in AGS cells treated with CM from NTMs (top) compared with CAMs (bottom). (**B**) Quantification of α-SMA-positive AGS cells treated with CM from CAMs compared with ATMs and NTMs; a: $P < 0.05$ versus control, b: $P < 0.05$ versus NTM, c: $P < 0.05$ versus ATM (ANOVA). (**C**) Comparison of AGS cell migration (left) and invasion (right) in response to CM from paired samples of CAMs and ATMs. (**D**) ^{3}[H]-thymidine incorporation in AGS cells treated with CM from CAMs compared with their matched ATMs. (**E**) ^{3}[H]-thymidine incorporation in CAMs from patients with high (pN2-4) versus low or no (pN0-1) lymph node involvement; see Supplementary Methods, available at *Carcinogenesis* Online for details of the TNM classification. Horizontal arrows, ANOVA or *t*-test, $^{*}P < 0.05$ and $n = 10–14$.

Downloaded from http://carcin.oxfordjournals.org/ at Sydney Jones Library, University of Liverpool on November 14, 2012

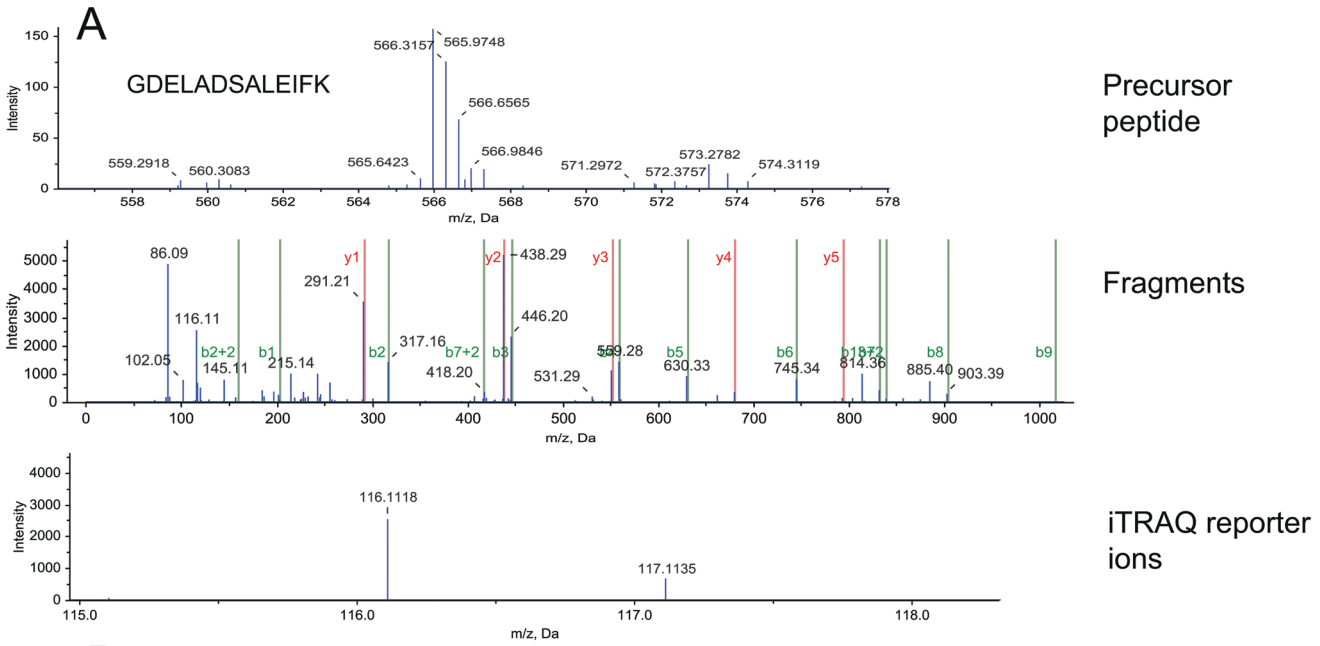

B

MALFVRLLAL ALALALGPAA TLAGPAKSPY QLVLQHSRLR GRQHGPNVCA VQKVIGTNRK YFTNCKQWYQ RKICGKSTVI
SYECCPGYEK VPGEKGCPAA LPLSNLYETL GVVGSTTTQL YTDRTEKLRP EMEGPGSFTI FAPSNEAWAS LPAEVLDSLV
SNVNIELLNA LRYHMVGRRV LTDELKHGMT LTSMYQNSNI QIHHYPNGIV TVNCARLLKA DHHATNGVVH LIDKVISTIT
NNIQQIIEIE DTFETLRAAV AASGLNTMLE GNGQYTLLAP TNEAFEKIPS ETLNRILGDP EALRDLLNNH ILKSAMCAEA
IVAGLSVETL EGTTLEVGCS GDMLTINGKA IISNKDILAT NGVIHYIDEL LIPDSAKTLF ELAAESDVST AIDLFRQAGL
GNHLSGSERL TLLAPLNSVF KDGTPPIDAH TRNLLRNHII KDQLASKYLY HGQTLETLGG KKLRVFVYRN SLCIENSCIA
AHDKRGRYGT LFTMDRVLTP PMGTVMDVLK GDNRFSMLVA AIQSAGLTET LNREGVYTVF APTNEAFRAL PPRERSRLLG
DAKELANILK YHIGDEILVS GGIGALVRLK SLQGDKLEVS LKNNVVSVNK EPVAEPDIMA TNGVVHVITN VLQPPANRPQ
ERGDELADSA LEIFKQASAF SRASQRSVRL APVYQKLLER MKH

C

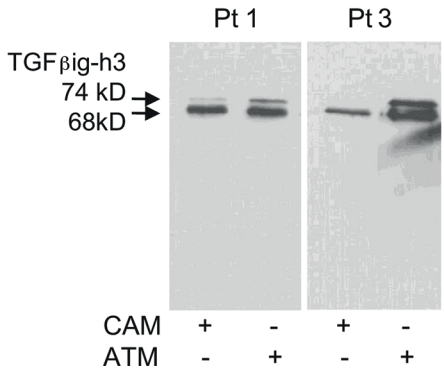

Fig. 3. Identification of TGFβig-h3 as differentially expressed in CAMs. (**A**) Representative spectra showing, top, identification of one of the precursor peptides for a typical tryptic fragment (GDELADSALEIFK); middle, identification of fragments of the precursor peptide; bottom, isobaric tagging for relative and absolute quantitation reporter ions for this identification. (**B**) The sequence of TGFβig-h3 showing in red the coverage of tryptic peptides identified in a representative sample; functional domains of the protein are underlined. (**C**) Representative western blots of TGFβig-h3 in media of CAMs and ATMs from patients with high (pN2-4) (right side) versus low or no (pN0-1) (left side) lymph node involvement showing depressed abundance in CAMs from the former.

that are putative myofibroblast markers including vimentin, cofilin and fibroblast activation protein-alpha (Supplementary Figure 2, available at *Carcinogenesis* Online) (36,37). Proteins exhibiting a significant difference in relative abundance were then analyzed by Metacore® (GeneGo) to identify *Process Networks* of differentially regulated interactions. Of 168 possible *Process Networks*, 39 were identified as significantly influenced. However, only one of these was significant in all 11 pairs of CAMs and ATMs (Supplementary Figure 3 and Supplementary Table 3, available at *Carcinogenesis* Online), namely the involvement of actin filaments, which is consistent with the observed differences between CAMs and ATMs in cell migration assays.

Downloaded from http://carcin.oxfordjournals.org/ at Sydney Jones Library, University of Liverpool on November 14, 2012

The contribution of myofibroblast secretomes to the tumor microenvironment

In order to identify directly the secreted proteins that might account for the properties of CAM CM, we then applied iTRAQ labeling followed by LC-MS/MS to myofibroblast media. Taking the secretomes of 11 pairs of CAMs and ATMs together, we identified 167 proteins that were expressed in three or more pairs of cells. Of these, 76 were considered secreted proteins using UniProt as the main database of which the largest categories were ECM proteins, proteases, binding proteins and ligands (Supplementary Figure 4, available at *Carcinogenesis* Online). Proteins exhibiting a differential abundance in CAMs versus ATMs varied between 12 and 42% of the total (Supplementary Table 4, available at *Carcinogenesis* Online). Interestingly, many of the differentially abundant proteins were decreased in CAMs, and included protease inhibitors and ECM-related proteins (Supplementary Table 4, available at *Carcinogenesis* Online). We then used Metacore® (with an MKN45 cell transcriptome as background) to identify candidate responses in cancer cells as a consequence of the differences in myofibroblast secretomes. Significant differences were found in 17 of 168 possible networks, of which 3 were significant in all 11 pairs of CAMs and ATMs (Supplementary Figure 5, available at *Carcinogenesis* Online). Importantly, given the biological properties of CM from CAMs in stimulating cancer cell invasion and migration, the three networks were associated with cell–matrix interactions, ECM remodeling and ECM degradation.

Secreted TGFβig-h3 from myofibroblast is linked to lymph node involvement and survival

We next analyzed the secretome data to identify candidate proteins exhibiting differences in abundance in CAMs from patients divided on the basis of low or no lymph node involvement (pN0-1) versus high lymph node involvement (pN2-4). The patients with high lymph node involvement had significantly shorter survival (9.6 ± 3.1 months) compared with patients with low or no lymph node involvement (44.0 ± 5.5 months, $P < 0.05$). Strikingly, in the dataset as a whole only a single protein, TGFβig-h3, exhibited a robust difference between the two groups (Fisher exact test with false discovery rate correction for multiple comparisons). Furthermore, TGFβig-h3 was one of the nodes in the cell–matrix interactions network, and also had interactions with nodes from the ECM remodeling and ECM degradation networks; thus, changes in TGFβig-h3 potentially influence all three of these signaling networks. The demonstration of TGFβig-h3 as decreased in CAMs from patients with high lymph node involvement was made on the basis of identification in all media samples with similar coverage in CAM and ATM samples (Figure 3B; Supplementary Table 5, available at *Carcinogenesis* Online). The finding was confirmed by western blot of media which revealed bands of approximately 68 and 72 kDa with decreased abundance in CAM media from patients with high lymph node involvement (Figure 3C).

TGFβig-h3 inhibits myofibroblast and cancer cell migration

To examine the consequence of TGFβig-h3 secretion by myofibroblasts, we then studied effects on cell migration and proliferation. Thus, TGFβig-h3 produced a concentration-dependent inhibition of IGF-II-stimulated migration of both myofibroblasts and AGS cells in Boyden chambers (Figure 4A). Similarly, IGF-II-stimulated myofibroblast and cancer cell proliferation was inhibited by TGFβig-h3 (1 µg/ml; Figure 4B). There was also increased cleaved caspase-3 in both myofibroblasts and cancer cells in response to TGFβig-h3 (Figure 4C); in the former, we showed associated increases in Bax and Bim, and decreased Bcl2, by western blot (Figure 4D).

To test whether TGFβig-h3 in myofibroblast media restrained IGF-II-stimulated migration, we examined the effects of siRNA knockdown. Treatment of myofibroblasts with TGFβig-h3 siRNA reduced the abundance of TGFβig-h3 detected by western blot of cell extracts by 64%, but did not change the abundance of another ECM protein, decorin, used as a negative control (Supplementary Figure 6, available at *Carcinogenesis* Online). In siRNA-treated cells, the stimulation of migration by IGF-II was enhanced indicative of an autocrine stimulatory role for IG-II (Figure 5A). To determine whether TGFβig-h3 released from myofibroblasts influenced cancer cell migration, we then examined CM from ATMs after prior treatment with TGFβig-h3 siRNA or control oligonucleotides. The stimulatory effect of myofibroblast CM on AGS cell migration was increased after TGFβig-h3 knockdown (Figure 5B), indicating that release of TGFβig-h3 inhibits growth factor-stimulated migration of both cancer cells and myofibroblasts. To elucidate the signaling pathways involved, we looked at the involvement of kinases downstream of the IGF-I receptor. Inhibition of p42/44 (U0126) activation significantly reduced IGF-II-stimulated myofibroblast migration and there was a smaller inhibition by a p38 kinase inhibitor (SB202190; Figure 5C), whereas the PI3-kinase (LY294002) and Jun-kinase (JNK-II) inhibitors had no or little effect; similar results were obtained in AGS cells (Supplementary Figure 7, available at *Carcinogenesis* Online). TGFβig-h3 inhibited IGF-II-stimulated phosphorylation of p42/44 kinase (Figure 5D).

TGFβig-h3 inhibits tumor growth in vivo

Finally, we asked whether TGFβig-h3 inhibited tumor growth *in vivo* using a xenograft model. For these studies, we used MKN45 cells that reproducibly establish tumors in a xenograft model and selected a CAM line (patient 3) that in preliminary studies stimulated MKN45 cell growth when coinjected in xenografts. Tumor growth after 4 weeks of MKN45 cells co-injected with CAMs (right side) was completely inhibited when TGFβig-h3 was administered for the duration of the experiment (Figure 6A and B). Moreover, there was even a reduction of approximately 85% of increased tumor mass when TGFβig-h3 was administered 2 weeks after the start of the experiment. There was no effect of TGFβig-h3 on tumor growth when MKN45 cells were injected in the absence of myofibroblasts, indicating that TGFβig-h3 prevents stromal cell-stimulated tumor growth even in established tumors. Interestingly, the TGFβig-h3-treated tumors exhibited more necrosis and less α-SMA-positive cells than their untreated counterparts (Figure 6A).

Discussion

Stromal cells drive tumor growth by multiple mechanisms influencing angiogenesis, inflammation and immune responses, as well as direct effects on tumor cells (12,14,37). We show here that gastric CAMs, which are a subset of CAFs, stimulate migration, proliferation and invasion of tumor cells compared with ATMs or NTMs; there are differences in the cellular proteomes and secretomes of CAMs and ATMs and we identify decreased secretion of the ECM protein TGFβig-h3 in CAMs from patients with high lymph node involvement and shorter survival. Cell migration and proliferation in response to IGF stimulation are inhibited by TGFβig-h3. Moreover, in a xenograft model, administration of TGFβig-h3 slows stroma-stimulated tumor growth. Thus, stromal cell secretion of an ECM protein provides a mechanism to inhibit tumor growth which is lost with tumor progression, indicating that stromal cells exhibit protective as well as aggressive properties.

There are differences in number, architecture and morphology of gastric CAMs compared with ATMs and NTMs; there are also functional differences when these cells are cultured. In principle, it is possible that cultured myofibroblasts might be unstable, but at least up to 10 passages we have found both the functional properties and molecular profiles of these cells to be stable. It becomes possible, then, to perform both functional studies and molecular profiling of secreted proteins in the same cells and to relate the findings to clinical data on cancer status. Although studies of stromal cell transcriptomes and proteomes can be carried out on microdissected tumor tissue, this approach does not lend itself to either concomitant functional studies in the same cells or kinetic analysis of the secreted proteins which determine the tumor microenvironment. These data indicate that in both cellular proteomes and in secretomes, there are differences between gastric CAMs and their corresponding ATMs consistent with observed functional differences, notably increased migration and inva-

Downloaded from http://carcin.oxfordjournals.org/ at Sydney Jones Library, University of Liverpool on November 14, 2012

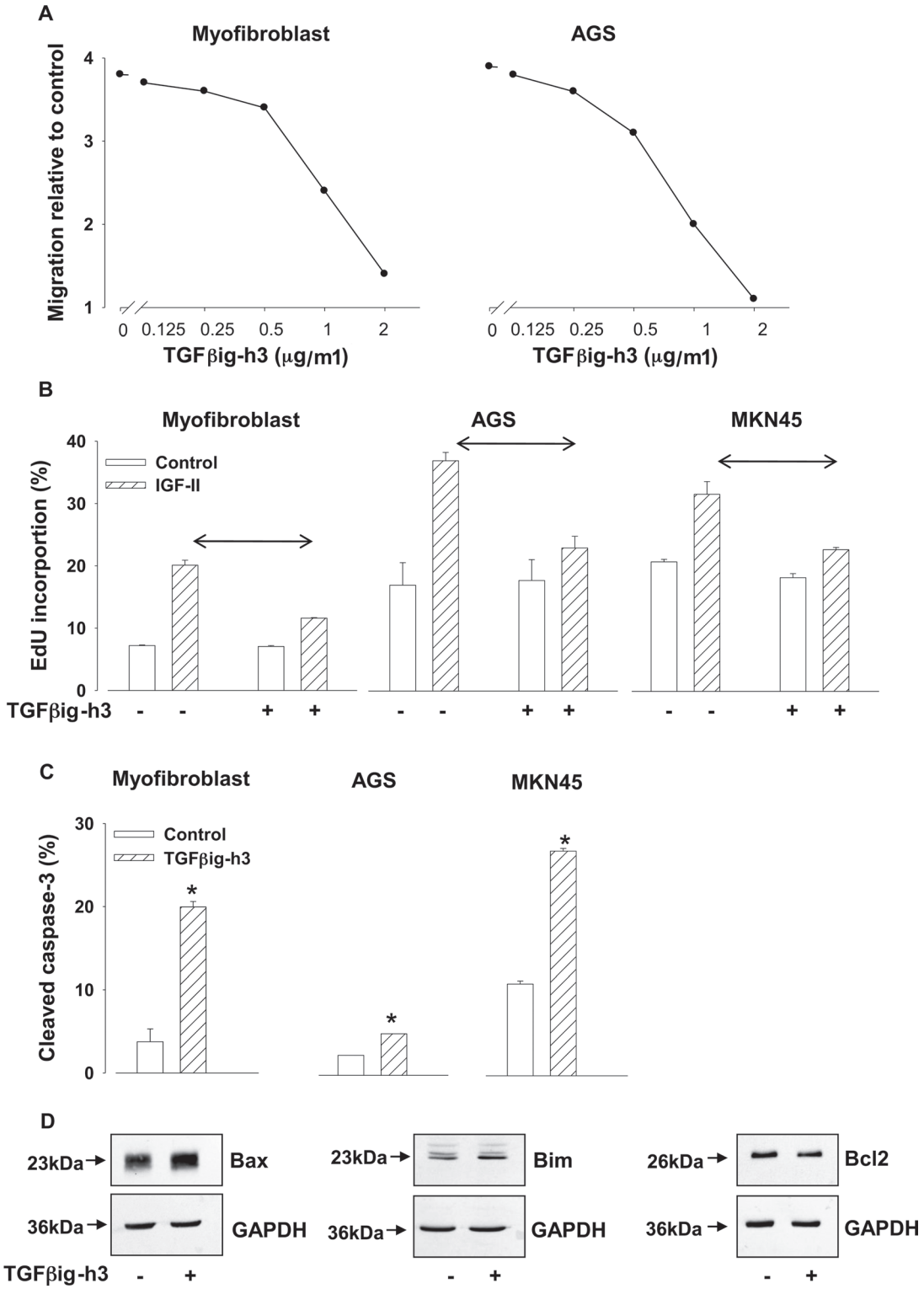

Fig. 4. Inhibition of myofibroblast and cancer cell proliferation and migration by TGFβig-h3 and stimulation of apoptosis. (**A**) Concentration-dependent inhibition of IGF-II (100 ng/ml)-stimulated myofibroblast and AGS cell migration by TGFβig-h3. (**B**) TGFβig-h3 (1 μg/ml) inhibition of IGF-II-stimulated myofibroblast, AGS and MKN45 cell proliferation determined by EdU incorporation. (**C**) TGFβig-h3 increased caspase-3 staining of myofibroblast, AGS and MKN45 cells. (**D**) TGFβig-h3 increased Bax and Bim in myofibroblasts detected by western blot and decreased Bcl-2. Horizontal arrows, ANOVA or *t*-test, $^*P < 0.05$ and $n = 3$.

sion by CAMs and by CAM CM applied to tumor cells. Moreover, a comparison of myofibroblast secretomes in patients with high versus low or no lymph node involvement revealed decreases in the ECM adaptor protein TGFβig-h3 in CAMs from advanced gastric tumors. The mechanism underlying loss of TGFβig-h3 remains uncertain, although examination of a microarray dataset indicates that mRNA abundance is unchanged (data not shown). This study was not designed to address differences in myofibroblast biology with respect to either tumor type (e.g. intestinal versus diffuse), or in preneoplastic changes (e.g. chronic gastritis, intestinal metaplasia and atrophy); nevertheless,

Downloaded from http://carcin.oxfordjournals.org/ at Sydney Jones Library, University of Liverpool on November 14, 2012

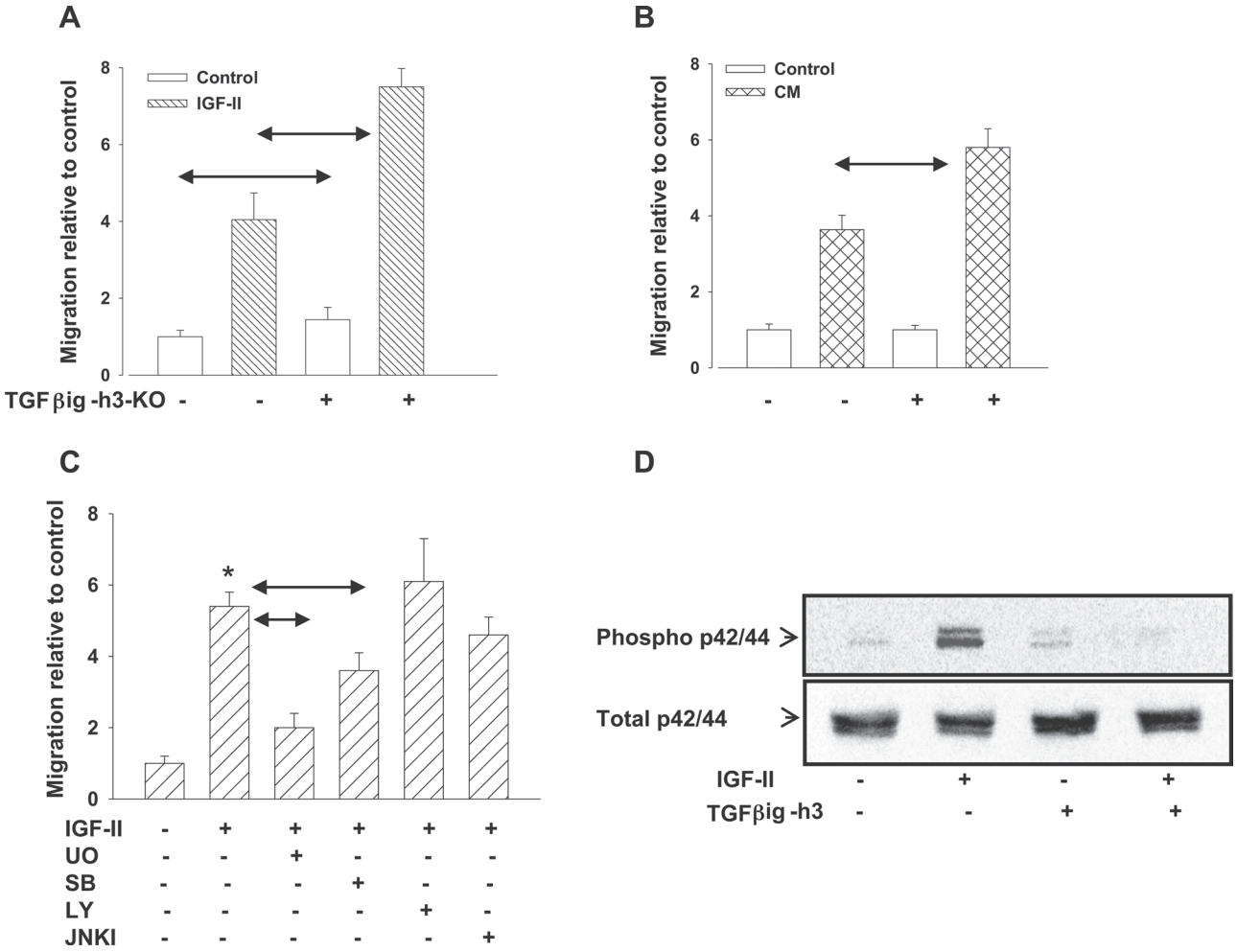

Fig. 5. Enhanced migration of myofibroblasts and AGS cells after knockdown of TGFβig-h3. (**A**) TGFβig-h3 siRNA knockdown (TGFβig-h3-KO) increased IGF-II (100 ng/ml)-stimulated myofibroblast migration. (**B**) CM from TGFβig-h3 siRNA-treated myofibroblasts increased AGS cell migration compared with CM from cells treated with control oligonucleotides. (**C**) IGF-II-stimulated myofibroblast migration is inhibited by U0126 (UO, 10 μM) and SB202190 (SB, 3 μM) but not LY294002 (LY, 50 μM) and JNK-II (JNK, 50 μM). (**D**) Representative western blot showing phosphorylation of p42/44 kinase was inhibited by TGFβig-h3. Horizontal arrows, $^*P < 0.05$ and $n = 3$.

our findings suggest that it is now both feasible and worthwhile to address these issues.

Myofibroblasts are well known to contribute to the deposition of ECM (38,39). These studies of myofibroblast secretomes indicate, however, that while some ECM proteins are increased in CAMs, others are decreased. Moreover, these differences are exaggerated in CAMs from patients with high lymph node involvement and poor survival, suggesting changes in CAM function as the disease progresses. In particular, there is an overall loss of diversity in the secretome with cancer progression and analysis of interaction networks indicates that these predict changes in cell behavior corresponding to functional changes observed *in vivo* notably with respect to cell migration and invasion.

It is only quite recently that proteomic approaches have been applied to the analysis of stromal cell secretomes (40). The identification of TGFβig-h3 as significantly decreased in the secretome of CAMs from patients with high lymph node involvement and short survival suggests a new dimension to the role of this protein in cancer. TGFβig-h3 was originally identified as a TGFβ-induced gene in the lung adenocarcinoma cell line A549 (26). There is accumulation of TGFβig-h3 at sites of inflammation and wound healing and it is thought to play a role in adhesion as a ligand of several integrins and by binding to collagen and other ECM proteins (27). Mutations of TGFβig-h3 are associated with corneal dystrophies (41,42), but its role in cancer is still unclear. Over-expression of TGFβig-h3 in Chinese hamster ovary cells decreased their tumor-forming capacity in nude mice (28), and a tumor suppressor function is indicated by the observation that mice null for TGFβig-h3 exhibit spontaneous tumors in a number of organs (29). Similarly, expression of TGFβig-h3 in ovarian cancer cells and in non-small cell lung cancer cells is associated with sensitivity to chemotherapy (30,43), and expression in neuroblastoma (44), lung and breast cancer cells (45,46) has been associated with decreased tumorigenicity. Conversely, however, TGFβig-h3 has been reported to promote invasion of colon and ovarian cancer cells (31,32,47). These studies have focused on the expression of TGFβig-h3 in tumor cells, and present finding of changes in stromal cell production of TGFβig-h3 indicates a more complex role than supposed previously.

These data show that TGFβig-h3 alone had little or no effect on myofibroblast or cancer cell proliferation and migration, although there was some stimulation of apoptosis. However, TGFβig-h3 strongly inhibited IGF-II-stimulated migration and proliferation of both cell types; knockdown of TGFβig-h3 expression increased the stimulatory effect of myofibroblast CM on cell migration; and in a xenograft model of myofibroblast-stimulated tumor growth, TGFβig-h3 had an inhibitory effect. The latter experiments employed SCID mice which have deficiencies in T- and B-cell maturation, making it unlikely that an immune response to TGFβig-h3 was involved. Moreover, the response to TGFβig-h3 is distinct from that to other proteins used in the same model (25). Previous work has established that gastric myofibroblasts produce IGF-II that can act as both an autocrine growth factor and a

Downloaded from http://carcin.oxfordjournals.org/ at Sydney Jones Library, University of Liverpool on November 14, 2012

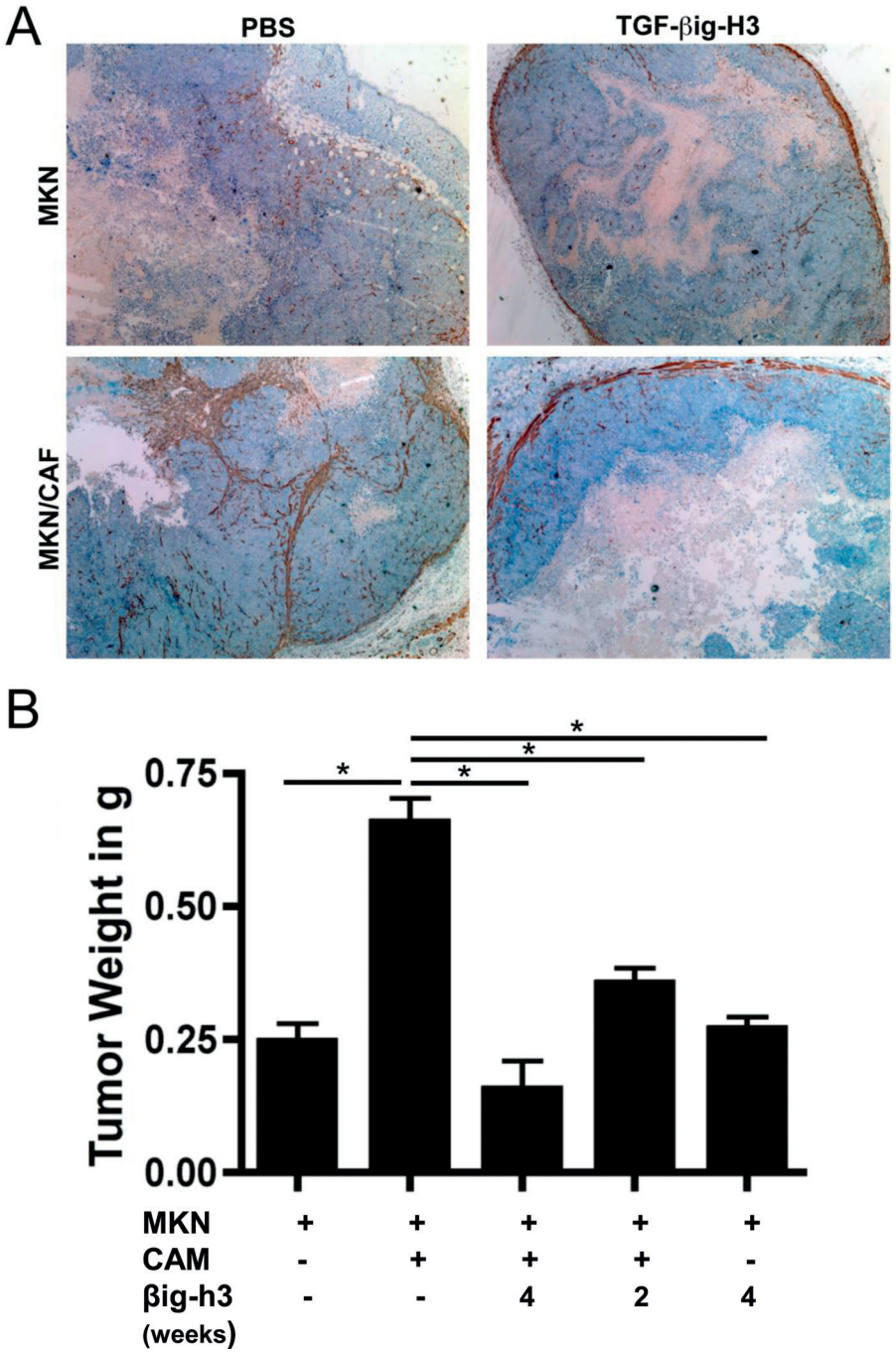

Fig. 6. Inhibitory effects of TGFβig-h3 in a xenograft model of stromal-stimulated tumor growth. (**A**) Representative images of α-SMA localization in xenografts and (**B**) quantification and statistical analysis of tumor volume. Mice were treated with TGFβig-h3 (1 μg per mouse per day) either for the whole duration of the experiment (4 weeks) or after 2 weeks of tumor growth. Treated xenografts were compared with untreated xenografts with and without co-injection of CAMs with MKN45 cells as appropriate. $n = 5$ per group, $^*P < 0.05$ and Dunnett for multiple comparisons; all data are represented as mean ± standard error of the mean.

paracrine stimulant of gastric epithelial cell proliferation and migration (23). The present findings extend this by showing that there are functional differences between CAMs and ATMs, and between CAMs based on tumor stage, in response to IGF-II. Moreover, inhibition of these effects by exogenous and endogenously generated TGFβig-h3 indicates that there is a dynamic equilibrium between stimulatory effects of IGF-II and inhibitory effects of TGFβig-h3 generated by stromal cells, that is lost in cancer progression. Interactions between TGFβig-h3 and IGF-II appear to occur proximal to activation of p42/44 MAPkinase which mediates the effects of IGF-II. There are RGB and FAS1 domains in TGFβig-h3 that mediate integrin binding; since there are well-recognized interactions between ECM proteins, integrins and IGF-receptor signaling (48), we suggest that the inhibitory action of TGFβig-h3 is exerted at this level.

Taken together, these data show myofibroblasts from gastric cancer differ from those from adjacent tissue in stimulating cancer cell proliferation, migration and invasion. By focusing on CAM secretomes, we have identified an unexpected role for myofibroblasts in restraining tumor migration and proliferation in early disease through secretion of TGFβig-h3. Depression of TGFβig-h3 secretion by myofibroblasts occurs with tumor progression and could provide a novel functional biomarker for stromal cell properties in cancer. Since TGFβig-h3 had

Downloaded from http://carcin.oxfordjournals.org/ at Sydney Jones Library, University of Liverpool on November 14, 2012

a suppressive effect in a xenograft model of stroma-stimulated cancer growth, we suggest that it may also be possible to develop novel therapeutic strategies based on the observation that stromal cell-stimulated tumor growth *in vivo* is prevented by restoration of TGFβig-h3.

Supplementary material

Supplementary methods and Supplementary Tables 1–5 and Figures 1–7 can be found at http://carcin.oxfordjournals.org/.

Funding

National Institute of Health (TMEM, 5 U54 CA126513-04/1); North West Cancer Research Fund (CR793); Deutsche Krebshilfe to M.Q.

Acknowledgements

We thank Dr Victoria Elliot for help with HPLC and acknowledge the technical assistance of Charlotte Woodcock with BrdU labeling and Fuksz Zoltanne with myofibroblast cultures.

Conflict of Interest Statement: None declared.

References

1. Bissell,M.J. *et al.* (2001) Putting tumours in context. *Nat. Rev. Cancer*, **1**, 46–54.
2. Tlsty,T.D. *et al.* (2006) Tumor stroma and regulation of cancer development. *Annu. Rev. Pathol.*, **1**, 119–150.
3. Saadi,A. *et al.* (2010) Stromal genes discriminate preinvasive from invasive disease, predict outcome, and highlight inflammatory pathways in digestive cancers. *Proc. Natl. Acad. Sci. U.S.A.*, **107**, 2177–2182.
4. Tuxhorn,J.A. *et al.* (2002) Reactive stroma in human prostate cancer: induction of myofibroblast phenotype and extracellular matrix remodeling. *Clin. Cancer Res.*, **8**, 2912–2923.
5. Kalluri,R. *et al.* (2006) Fibroblasts in cancer. *Nat. Rev. Cancer*, **6**, 392–401.
6. Bhowmick,N.A. *et al.* (2004) Stromal fibroblasts in cancer initiation and progression. *Nature*, **432**, 332–337.
7. Allinen,M. *et al.* (2004) Molecular characterization of the tumor microenvironment in breast cancer. *Cancer Cell*, **6**, 17–32.
8. Finak,G. *et al.* (2008) Stromal gene expression predicts clinical outcome in breast cancer. *Nat. Med.*, **14**, 518–527.
9. Farmer,P. *et al.* (2009) A stroma-related gene signature predicts resistance to neoadjuvant chemotherapy in breast cancer. *Nat. Med.*, **15**, 68–74.
10. Hagglof,C. *et al.* (2010) Stromal PDGFRbeta expression in prostate tumors and non-malignant prostate tissue predicts prostate cancer survival. *PLoS One*, **5**, e10747.
11. Coussens,L.M. *et al.* (2002) Inflammation and cancer. *Nature*, **420**, 860–867.
12. Erez,N. *et al.* (2010) Cancer-associated fibroblasts are activated in incipient neoplasia to orchestrate tumor-promoting inflammation in an NF-kappaB-dependent manner. *Cancer Cell*, **17**, 135–147.
13. Crawford,Y. *et al.* (2009) PDGF-C mediates the angiogenic and tumorigenic properties of fibroblasts associated with tumors refractory to anti-VEGF treatment. *Cancer Cell*, **15**, 21–34.
14. Orimo,A. *et al.* (2005) Stromal fibroblasts present in invasive human breast carcinomas promote tumor growth and angiogenesis through elevated SDF-1/CXCL12 secretion. *Cell*, **121**, 335–348.
15. Powell,D.W. *et al.* (2005) Epithelial cells and their neighbors I. Role of intestinal myofibroblasts in development, repair, and cancer. *Am. J. Physiol. Gastrointest. Liver Physiol.*, **289**, G2–G7.
16. Jiang,L. *et al.* (2008) Global hypomethylation of genomic DNA in cancer-associated myofibroblasts. *Cancer Res.*, **68**, 9900–9908.
17. Peek,R.M., Jr. *et al.* (2002) Helicobacter pylori and gastrointestinal tract adenocarcinomas. *Nat. Rev. Cancer*, **2**, 28–37.
18. Kamangar,F. *et al.* (2006) Patterns of cancer incidence, mortality, and prevalence across five continents: defining priorities to reduce cancer disparities in different geographic regions of the world. *J. Clin. Oncol.*, **24**, 2137–2150.
19. Correa,P. *et al.* (1994) Gastric cancer. *Cancer Surv.*, **19–20**, 55–76.
20. Weis,V.G. *et al.* (2009) Current understanding of SPEM and its standing in the preneoplastic process. *Gastric Cancer*, **12**, 189–197.
21. Wroblewski,L.E. *et al.* (2003) Stimulation of MMP-7 (matrilysin) by Helicobacter pylori in human gastric epithelial cells: role in epithelial cell migration. *J. Cell Sci.*, **116**, 3017–3026.
22. Hemers,E. *et al.* (2005) Insulin-like growth factor binding protein-5 is a target of matrix metalloproteinase-7: implications for epithelial-mesenchymal signaling. *Cancer Res.*, **65**, 7363–7369.
23. McCaig,C. *et al.* (2006) The role of matrix metalloproteinase-7 in redefining the gastric microenvironment in response to Helicobacter pylori. *Gastroenterology*, **130**, 1754–1763.
24. Houghton,J. *et al.* (2004) Gastric cancer originating from bone marrow-derived cells. *Science*, **306**, 1568–1571.
25. Quante,M. *et al.* (2011) Bone marrow-derived myofibroblasts contribute to the mesenchymal stem cell niche and promote tumor growth. *Cancer Cell*, **19**, 257–272.
26. Skonier,J. *et al.* (1992) cDNA cloning and sequence analysis of beta ig-h3, a novel gene induced in a human adenocarcinoma cell line after treatment with transforming growth factor-beta. *DNA Cell Biol.*, **11**, 511–522.
27. Billings,P.C. *et al.* (2002) The transforming growth factor-beta-inducible matrix protein (beta)ig-h3 interacts with fibronectin. *J. Biol. Chem.*, **277**, 28003–28009.
28. Skonier,J. *et al.* (1994) beta ig-h3: a transforming growth factor-beta-responsive gene encoding a secreted protein that inhibits cell attachment in vitro and suppresses the growth of CHO cells in nude mice. *DNA Cell Biol.*, **13**, 571–584.
29. Zhang,Y. *et al.* (2009) TGFBI deficiency predisposes mice to spontaneous tumor development. *Cancer Res.*, **69**, 37–44.
30. Ahmed,A.A. *et al.* (2007) The extracellular matrix protein TGFBI induces microtubule stabilization and sensitizes ovarian cancers to paclitaxel. *Cancer Cell*, **12**, 514–527.
31. Tang,J. *et al.* (2007) BetaIg-h3 is involved in the HAb18G/CD147-mediated metastasis process in human hepatoma cells. *Exp. Biol. Med. (Maywood)*, **232**, 344–352.
32. Ma,C. *et al.* (2008) Extracellular matrix protein betaig-h3/TGFBI promotes metastasis of colon cancer by enhancing cell extravasation. *Genes Dev.*, **22**, 308–321.
33. Sobin,L.H. *et al.* (2009) *TNM Classification of Malignant Tumours*. Wiley-Blackwell, Chichester.
34. Varro,A. *et al.* (2002) Gastrin-cholecystokinin(B) receptor expression in AGS cells is associated with direct inhibition and indirect stimulation of cell proliferation via paracrine activation of the epidermal growth factor receptor. *Gut*, **50**, 827–833.
35. Varro,A. *et al.* (2004) Helicobacter pylori induces plasminogen activator inhibitor 2 in gastric epithelial cells through nuclear factor-kappaB and RhoA: implications for invasion and apoptosis. *Cancer Res.*, **64**, 1695–702.
36. Pho,M. *et al.* (2008) Cofilin is a marker of myofibroblast differentiation in cells from porcine aortic cardiac valves. *Am. J. Physiol. Heart Circ. Physiol.*, **294**, H1767–H1778.
37. Kraman,M. *et al.* (2010) Suppression of antitumor immunity by stromal cells expressing fibroblast activation protein-alpha. *Science*, **330**, 827–830.
38. Desmouliere,A. *et al.* (2004) The stroma reaction myofibroblast: a key player in the control of tumor cell behavior. *Int. J. Dev. Biol.*, **48**, 509–517.
39. Bissell,M.J. *et al.* (2011) Why don't we get more cancer? A proposed role of the microenvironment in restraining cancer progression. *Nat. Med.*, **17**, 320–329.
40. Xu,B.J. *et al.* (2010) Quantitative analysis of the secretome of TGF-beta signaling-deficient mammary fibroblasts. *Proteomics*, **10**, 2458–2470.
41. Kannabiran,C. *et al.* (2006) TGFBI gene mutations in corneal dystrophies. *Hum. Mutat.*, **27**, 615–625.
42. Thapa,N. *et al.* (2007) TGFBIp/betaig-h3 protein: a versatile matrix molecule induced by TGF-beta. *Int. J. Biochem. Cell Biol.*, **39**, 2183–2194.
43. Irigoyen,M. *et al.* (2010) TGFBI expression is associated with a better response to chemotherapy in NSCLC. *Mol. Cancer*, **9**, 130.
44. Becker,J. *et al.* (2006) Keratoepithelin suppresses the progression of experimental human neuroblastomas. *Cancer Res.*, **66**, 5314–5321.
45. Wen,G. *et al.* (2011) TGFBI expression reduces in vitro and in vivo metastatic potential of lung and breast tumor cells. *Cancer Lett.*, **308**, 23–32.
46. Zhao,Y. *et al.* (2006) Loss of Betaig-h3 protein is frequent in primary lung carcinoma and related to tumorigenic phenotype in lung cancer cells. *Mol. Carcinog.*, **45**, 84–92.
47. Ween,M.P. *et al.* (2011) Transforming growth factor-beta-induced protein secreted by peritoneal cells increases the metastatic potential of ovarian cancer cells. *Int. J. Cancer*, **128**, 1570–1584.
48. Beattie,J. *et al.* (2010) Cross-talk between the insulin-like growth factor (IGF) axis and membrane integrins to regulate cell physiology. *J. Cell Physiol.*, **224**, 605–611.

Received March 8, 2012; revised April 26, 2012; accepted May 2, 2012

Downloaded from http://carcin.oxfordjournals.org/ at Sydney Jones Library, University of Liverpool on November 14, 2012

Humán, gyomor eredetű myofibroblasztok alapvető funkcióinak vizsgálata

Ph. D. tézis kivonat

Bevezetés

A myofibroblasztok fontos szerepet játszanak az egyedfejlődésben, a sebgyógyulásban, az extracelluláris mátrix termelésében és – neurohumorális úton kommunikálva az epitélsejtekkel – azok funkciójában, valamint a carcinogenesisben is. Az eddigi tanulmányok szerint a malignus transzformációban és az áttétképződésben fontos szerep jut az epitélsejtek mikrokörnyezetében található sejteknek, többek között a myofibroblasztoknak, amelyekre vonatkozóan kevés az irodalmi adat. Funkciójukat a subepitheliális térben látják el, ahol aktívan migrálnak és osztódnak a körülményeknek megfelelően és eközben intracellulárisan nagy mennyiségű savas metabolitot halmoznak fel. A felfokozott anyagcsereutak következtében felhalmozódott protonokat sav/bázis transzporterek segítségével távolítják el, hogy fenntartsák az intracelluláris pH-t (pH_i). A közelmúltbéli kutatások azt mutatták, hogy a sav/bázis transzporterek kulcsfontosságú szerepet töltenek be a sejtfunkcióban és fontos szerepük van a carcinogenesisben, az epitélsejtek malignus elfajulásában. A rákbetegség kutatásában egy új irányvonal jelent meg, amely sejtek anyagcseréjével, a rákbetegség thermodinamikai megközelítésével foglalkozik. A kutatási eredmények szerint a malignus sejtek anyagcseréjében jelentős változások következnek be a sav/bázis transzporterek szintjén, amely új lehetőségeket nyithat meg a rákos betegek kezelésében. Az eddigi vizsgálatok az epitélsejtekre fókuszáltak, a myofibroblasztok vonatkozásában nincs humán adat a sav/bázis háztartás szabályozását illetően.

Cél

Célunk volt a humán, gyomor eredetű myofibroblasztok sav/bázis transzportereinek kísérletes vizsgálata valamint kapcsolat keresése a sejtfunkció és ezen transzporterek működése között.

Betegek és módszerek

Gyomorrák miatt műtött betegek rezekciós műtétjénél etikai engedély birtokában és a betegek beleegyezését követően intraoperatívan vettünk szövetmintákat (n=3). Két további gyomor szövetmintát szintén etikai engedély birtokában cadaver donorokból vettünk. A

szövetmintákból humán, gyomor eredetű myofibroblasztokat (HGM) izoláltunk és tenyésztettünk steril laboratóriumban, majd kísérleteinkhez az amplifikált, passzált sejttenyészeteket használtuk. Sejttenyészeteink közel 100 % tisztaságúnak bizonyultak. A szövetmintákból patológiai vizsgálatot is végeztünk. Kísérleteinkhez immuncitokémiát, mikrofluoreszcens módszert, RT-PCR-t és Western-blot analízist használtunk.

Eredmények

A gyomorrákból származó hisztológiai blokkokban a myofibroblasztok száma jelentős emelkedést mutatott a stromában, cytomorfológiailag súlyos károsodást szenvednek és a cytoarchitektura elveszíti orientált jellegét az egészséges szövetből származó hisztológiai preparátumokban észlelt myofibroblasztokhoz viszonyítva.

A szakirodalomban elsőként vizsgáltuk a HGM sejtek sav/bázis háztartását, meghatároztuk nyugalmi pH-jukat és a sejtek pufferkapacitását élettani körülmények között *in vitro*. Többféle technika kombinációjával karakterizáltuk a plazmamembránon elhelyezkedő Na^+/H^+ exchanger (NHE) 1, 2 és 3-as izoformájának, a Na^+/HCO_3^- cotransporternek (NBC) és az anion exchangernek (AE) a funkcionális aktivitását egészséges szövetből származó HGM sejtekben.

A mikrofluoreszcens adatok szerint a HGM sejtekben az NHE 1-3, az NBC és az AE transzporterek funkcionálisan aktívak. Vizsgálataink szerint nagy aktivitást mutat az NBC és az NHE-ek közül az NHE1 a legaktívabb izoforma. Az NHE-ek jelenlétét mRNS és fehérje szinten is igazoltuk.

A neurohumoralis kommunikációban fontos kolinerg rendszer agonista, carbacholt és a korábban a myofibroblasztok funkciójában már bizonyítottan serkentő hatású inzulinszerű növekedési faktor II-t (IGF-II) használtuk a HGM sejtek stimulálására.

Kimutattuk karc-sebzéses technikával, specifikus NHE1 inhibitor (HOE-642) segítségével, hogy a carbachol és az IGF-II fokozzák a HGM sejtek migrációját és ezt – legalábbis részben – NHE1-dependens úton teszik. Ethynil-deoxi-uridin (EdU) inkorporációs vizsgálattal értékeltük a HGM sejtek osztódását. Az EdU vizsgálattal bizonyítottuk, hogy az IGF-II jelentősen fokozza a HGM sejtek osztódását és ezen hatás felfüggeszthető HOE-642-vel.

Eredményeink szerint az NHE1 funkcionális aktivitása szükséges az IGF-II által indukált proliferációs válaszhoz. Ezen eredmények is bizonyítják a sav/bázis állapot fontosságát a

stroma sejtek funkciójában és kiemelik a transzporterek jelentőségét, potenciális lehetőségeinket új irányvonalban tervezett kezelési stratégiák felé.

Következtetések

Összegezve, elsőként karakterizáltuk a HGM-ok pH_i szabályozását. Megállapítottuk, hogy az NHE1 funkcionális aktivitása szükséges a carbachol- és IGF-II-indukálta migrációs válaszhoz és elengedhetetlen az IGF-II által kiváltott proliferációs válaszhoz HGM sejtekben *in vitro*.

UNIVERSITY OF LIVERPOOL

Professor Andrea Varro
Professor of Physiology
Director of Postgraduate Studies

Institute of Translational Medicine
Faculty of Health & Life Sciences
The Sherrington Buildings
Ashton Street
Liverpool L69 3BX

T 0151 794 5331
E avarro@liverpool.ac.uk
W http://www.liv.ac.uk/translational-medicine/

12/11/2012

Kedves Matyas

Nagyon szivesen igazolom, hogy a "**Release of TGFβig-h3 by gastric myofibroblasts slows tumor growth and is decreased with cancer progression."** cikkunkhoz a kiserletekben hasznalt sejtvonalak megszerzeset, izolalasat, tenyeszteset vegezted. Ezenkivul meg nagy vonalban hozzajarultal a betegek adatainak gyujtesehez es a betegek tulelesenek kovetesehez. Reszveteled a munkahoz hozzajarult a cikk elfogadasahoz.

Udvozlettel

Andrea

Andrea Varro